CBM Progress Report

2006

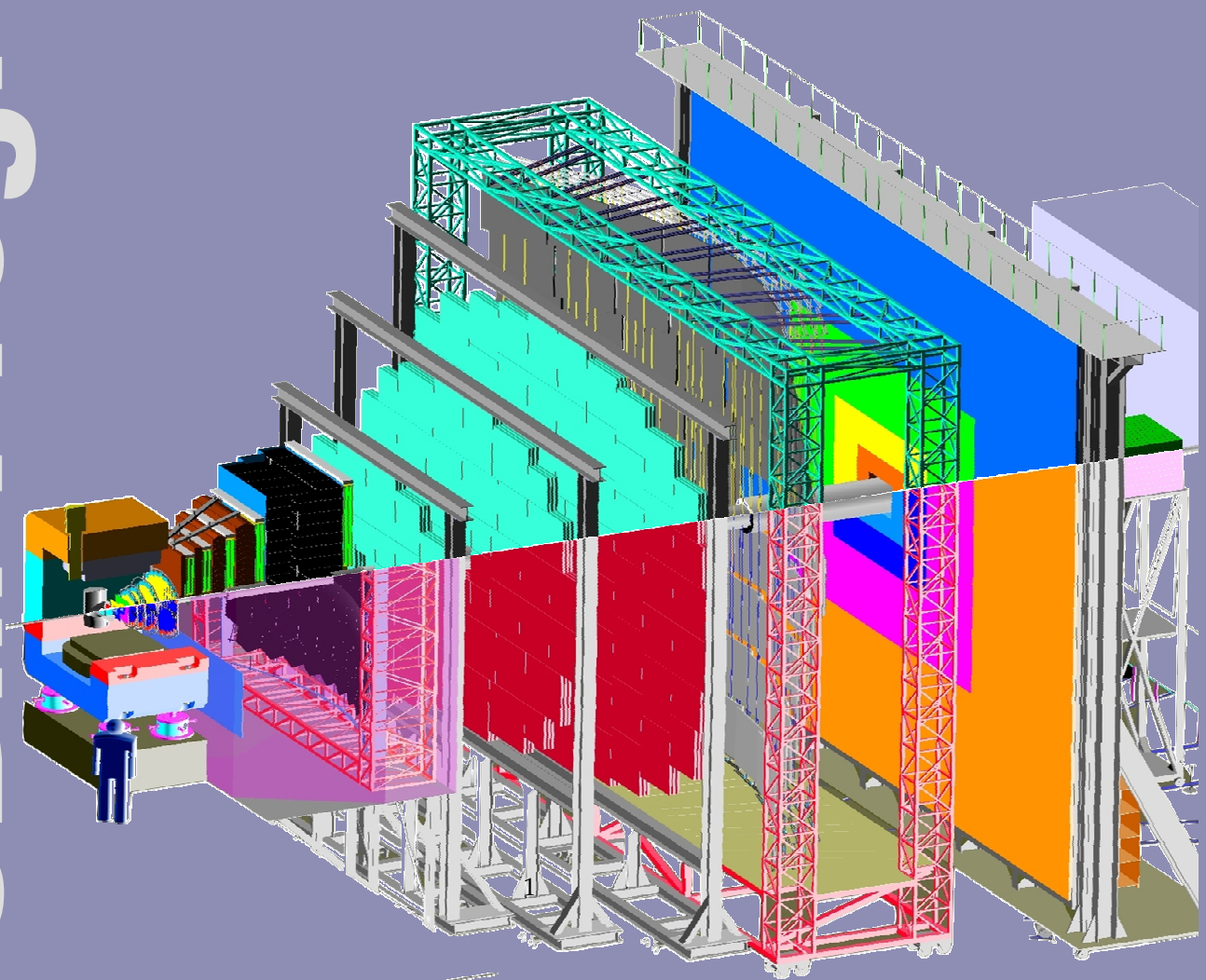

Preface

In 2006 the CBM project has made important steps towards realisation. This includes progress in the design and development of simulation software, detector components, front-end electronics, and concepts for data acquisition.

The continuous improvements of the software framework (CBMroot) and of the event reconstruction algorithms permitted to optimize the layout of the Silicon Tracking System (STS). Track reconstruction based on a realistic STS design is now routinely used in the feasibility studies for open charm measurements, for the identification of hadrons (including multi-strange hyperons), and for the reconstruction of vector mesons via their dileptonic decays. The identification of electrons is based now on the realistic response of the Ring Imaging Cherenkov (RICH) detector using ring recognition algorithms, and on the analysis of the energy loss signals in the Transition Radiation Detector (TRD). For muon identification a compact absorber/detector system has been developed with promising performance. Full track reconstruction is available for particle identification taking into account the hits in the STS, in the 12 TRD layers, and in the timing Resistive Plate Chamber (RPC) wall.

Hardware R&D concentrated on the design, construction and test of various prototype detectors: radiation tolerant Monolithic Active Pixel Sensors, thin double-sided Silicon Microstrip sensors, TRDs with high rate capability, high-rate timing RPCs, and modules for the Projectile Spectator Detector. Concerning the development of front-end electronics we made a big step forward with the first prototype of a self-triggered fast readout chip for Silicon Strip and GEM detectors which is available now and being tested. Moreover, building blocks for the front-end electronics of TRD and RPC have been designed. Last but not least the framework of a future data acquisition system is under development.

The status of the ongoing CBM activities is documented in this Report. There is also progress in the development of the collaboration: six groups from Indian universities and institutes have joined CBM in 2006. They will concentrate on the development of the muon detection system. Beyond the efforts devoted to the design and construction of the experimental setup there is ongoing work – mainly by many colleagues from theory - to write-up the CBM Physics Book. The first draft of the book has been completed and is being discussed within the theory working groups.

Many thanks to the colleagues who have contributed to this report.

February 2007 Peter Senger

Contents

The CBM experiment at FAIR

V. Friese, W.F.J. Müller, P. Senger, GSI Darmstadt

CBM physics and detector setup

The planned Compressed Baryonic Matter (CBM) experiment at FAIR offers unique possibilities to investigate baryonic matter at highest densities in the laboratory. The most promising observables from nucleus-nucleus collisions in the FAIR energy range are particles containing charm quarks (D-mesons and charmonium), low-mass vector mesons decaying into dilepton pairs (ρ, ω and ϕ mesons), and hyperons (Λ, Ξ, Ω and their antiparticles). This includes the measurement of (event-by-event) fluctuations, correlations, and collective flow of hadrons. A systematic and comprehensive investigation of these observables, in particular their excitation functions, will permit to extract information on the equation-of-state of baryonic matter at high densities, on the location of the phase boundary between hadronic and partonic matter (including the QCD critical endpoint), and on the restoration of chiral symmetry at high net-baryon densities.

The experimental task is to identify hadrons and leptons in collisions with up to 1000 charged particles at event rates of up to 10 MHz. A particular experimental challenge is the identification of D-mesons which is based on the selection of secondary vertices with high accuracy. The measurements require a high-speed data acquisition (DAQ) architecture and an appropriate high-level event-selection concept.

A schematic view of the proposed CBM detector concept is shown in figure 1. Inside a large aperture dipole magnet there is a Silicon Tracking and Vertexing System which consists of two parts: a Micro-Vertex Detector (MVD, 2 silicon pixel layers) and the Silicon Tracking System (STS, several layers of silicon microstrip detectors). The Silicon detector array has to provide the capabilities for track reconstruction, determination of primary and secondary vertices, and momentum determination. Electrons from low-mass vector-meson decays will be identified with a Ring Imaging Cherenkov (RICH) detector. The TRD detector will provide charged particle tracking and the identification of high energy electrons and positrons. The ECAL will be used for the identification of electrons and photons. As an alternative to the RICH detector a muon detection/hadron absorber system is under investigation. If the RICH will be replaced by a muon detector the TRD will be converted into a tracking detector for hadron measurements together with the timing RPC. Then the TOF-RPC detector serves for two purposes: for background suppression during muon measurements with absorbers, and for hadron identification with muon absorbers removed.

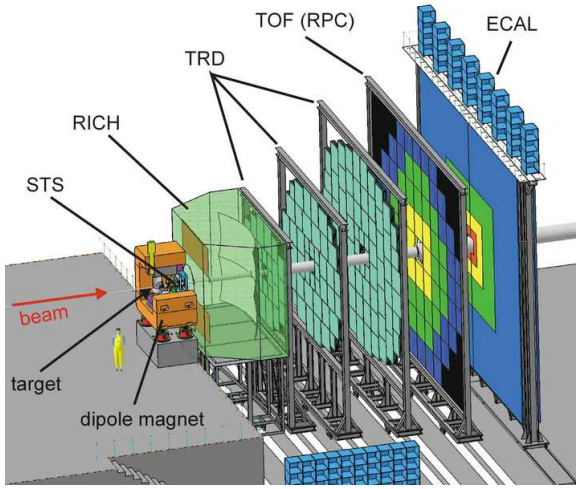

Figure 1: Schematic view of the Compressed Baryonic Matter (CBM) experiment planned at FAIR. The setup consists of a high resolution Silicon Tracking System (STS), a Ring Imaging Cherenkov detector (RICH), three stations of Transition Radiation Detectors (TRD), a time-of-flight (TOF) system made of Resistive Plate Chambers (RPC) and an Electromagnetic Calorimeter (ECAL).

Track reconstruction and STS development

The feasibility studies were performed within the CBM software framework which has been developed further. The routines for track and vertex reconstruction have been improved and used for optimization of the layout of the Silicon Tracking System. Track reconstruction efficiencies of above 95% can be obtained with a fast and radiation-hard detector system which consists either of two Silicon hybrid pixel detector stations together with 4 double-sided Silicon Strip detector layers, or of 6 Strip-sensor layers only. The STS can be used as a stand-alone tracker for high-rate measurements and for the identification of hyperons. The Micro-Vertex Detector (MVD) - which is close to the target and has limitations in radiation hardness and read-out speed - will be installed only for open charm measurements which requires high-precision vertexing.

Detector R&D concentrates on the design of a prototype STS which includes double-sided sensors, the low-mass micro-cables, the read-out chip and the mechanical structure. First prototype sensors have been designed and are being fabricated. Moreover, a fast self-triggered read-out chip has been developed within EU FP-6 NMI3 for neutron applications. It was fabricated and is under tests in cooperation with CBM, where it will serve as a prototype for the CBM-dedicated front-end development and addi-

tionally for current detector prototyping R&D efforts.

Hadron identification via TOF

Hadron identification in the CBM experiment is performed using the time-of-flight measurement in the RPC detector wall located about 10 m downstream of the target. This requires track reconstruction and momentum determination in the Silicon Tracking System, track following through the TRD stations, and matching of reconstructed tracks to the hits in the RPCs. The total reconstruction efficiency for hadrons (STS-TRD-RPC) is well above 80 %. This result is based on realistic detector layouts and performances. The R&D on prototype timing RPCs concentrates on high rate capability, low resistivity material, long term stability and the realization of large arrays with overall excellent timing performance.

D meson identification and vertex detector

D mesons will be identified via their hadronic decay into one or two charged pions and a kaon. In order to suppress the overwhelming combinatorial background of promptly emitted pions and kaons one has to determine the D meson decay vertex with an accuracy of about 50 μm ($\tau(D^0)$ = 123 μm/c, $\tau(D^{\pm})$ = 312 μm/c). This measurement requires an extremely thin and highly granulated pixel detector. We are developing a Micro-Vertex Detector (MVD) consisting of two layers of Monolithic Active Pixel Sensors (MAPS) with a pixel size between 25x25 μm^2 and 40x40 μm^2 and a thickness of 100 μm. Both vertex resolution and radiation damage increase with decreasing distance from the target. Simulations have been performed in order to optimize signal-to-background, efficiency, distance and detector lifetime. According to these studies it is possible to record 3.6×10^5 D mesons in 10^{12} minimum bias Au+Au collisions at 25 AGeV within the lifetime of a MAPS. With a collision rate of 100 kHz the first MAPS station would have to be replaced after 120 days of running. The R&D on the MVD concentrates on the improvement of radiation hardness and readout speed of the MAPS, and on system integration.

Electron identification with RICH and TRD

Electrons and positrons are identified with the RICH detector and with the TRD. The simulations include track reconstruction in STS and TRD, ring recognition in the RICH photon detector, ring-track matching, and the analysis of the energy loss signal in the TRD. With information only from RICH the pions can be suppressed by a factor of about 500 up to a momentum of about 9 GeV/c. Taking into account additional information from the TRD the total pion suppression factor is larger than 10^4 for momenta above 1 GeV/c in central Au+Au collisions at 25 AGeV. This value will be sufficient to discard misidentified pions from the combinatorial electron background in vector-meson measurements.

The major challenge in the identification of low-mass vector mesons via their di-electronic decay is to reject the physical background of electron-positron pairs from Dalitz decays and gamma conversion. The background rejection strategies are based on electron identification by RICH and TRD, and use an improved track reconstruction method for low momentum particles. The omega meson, for example, can be measured in central Au+Au collisions at 25 AGeV with a signal-to-background ratio of 0.2 and an efficiency of 8%. In the mass range of the J/ψ meson the combinatorial background can be dramatically reduced by the requirement of a high transverse momentum of the electrons. For example, when requiring electron transverse momenta of $p_t \geq 1.2$ GeV/c for central Au+Au collisions at 15 (25, 35) AGeV, signal-to-background ratios of S/B = 0.8 (1.7, 14.5) and efficiencies of ϵ = 0.09 (0.12, 0.14) can be achieved for J/ψ mesons. TRD R&D is focused on the improvement of the electron identification performance, and on the development of highly granular and fast gaseous detectors which can stand the high-rate environment of CBM. Prototype gas detectors (based on MWPC and GEM technology) have been built and tested with particle rates of up to 400 kHz/cm^2 without deterioration of performance.

Muon measurements with hadron absorbers

As an alternative approach to the dielectron measurement we have studied the possibility of detecting vector mesons (ρ, ω, ϕ, J/ψ) via their decay into $\mu^-\mu^+$ pairs. The idea is to suppress the hadrons with several iron absorber layers located behind the Silicon Tracking System. In order to match the muons which pass the absorber to the tracks measured by the Silicon tracker (which defines the momentum) one has to track all charged particles through the absorber. This is done by highly granulated and fast detectors which are located in each gap between the absorber layers.

The simulations are based on track reconstruction algorithms taking into account a realistic response of the STS. The high track density requires a position resolution in the order of σ = 100-300 μm for the first muon chambers. The studies demonstrate that for example the ω meson can be measured in central Au+Au collisions at 15 (25, 35) AGeV with a signal-to-background ratio of S/B = 0.4 and with an efficiency of ϵ = 0.01 (0.013, 0.015). J/ψ mesons can be identified with a signal-to-background ratio of about 100 and an efficiency of ϵ = 0.19 for central Au+Au collisions at 25 AGeV. Such a number would be sufficient for the identification of ψ' mesons in Au+Au collisions. For the charmonium experiments the total thickness of the hadron absorber has to be increased as compared to measurements of low-mass vector mesons.

The challenge for the muon chambers and for the track reconstruction algorithms is the huge particle density of up to 1 hit/cm^2 per event in the first detector layers. Therefore, detector R&D concentrates on the design of fast and highly granulated gaseous detectors based on GEM technology.

FairRoot/CbmRoot Simulation and Analysis framework

M. Al-Turany, D. Bertini, M. Dahlinger, V. Friese, I. Koenig, and F. Uhlig
GSI, Darmstadt, Germany

Introduction

The Virtual Monte Carlo concept allows performing simulations using Geant3, Geant4 or Fluka without changing the user code [1]. This concept was used as a base for developing the CbmRoot framework for the CBM collaboration [2]. In this concept, the same framework is used for simulation and data analysis. An oracle database with a build-in versioning management is available and can be used to efficiently store the detector geometry, materials and parameters.

As more experiments at the GSI where interested in using this framework, the framework was revised and the base packages of the framework where completely separated from the specific CBM implementation. Moreover, the framework got the new name FAIRROOT. On the Oracle server side, data bases for each experiment are running on a high availability cluster, new experiments can easily be added.

The Schematic design of the framework is shown in Fig.[1].

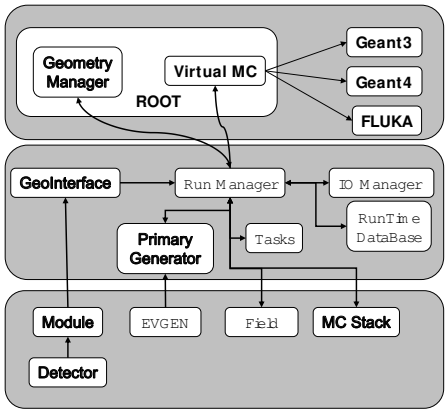

Figure 1: Schematic design of FairRoot.

New Developments

- Geane Interface:

  The Geane package allows the user to calculate the average trajectories of particles and to calculate the transport matrix as well as the propagated error covariance matrix. Geane is a set of routines worked out by the European Muon Collaboration [3, 4] and it is integrated to the GEANT3 system [5]. An interface for using Geane was developed in collaboration with the Pavia group from the PANDA collaboration. The modification to the VMC classes needed for Geane where also communicated to the ALICE collaboration at CERN and included in the VMC distribution.

- New detector geometry reader

  A new geometry reader for the framework was developed. The input of this reader is in form of TGeoVolumes (Root Geometry format). This reader is used by the PANDA collaboration to read the detector geometries which are converted from Step file format (CAD system) to Root format.

- CMake for configuration

  CMake is a cross-platform, open-source make system [6]. CMake is used to control the software compilation process using simple platform and compiler independent configuration files. CMake generates native makefiles and workspaces that can be used in the compiler environment of user choice. Now CMake and autoconf/automake are used in parallel.

- Subversion

  The frame work is now distributed via Subversion.

Summary

A VMC based framework for CBM has been implemented, the first release was in March 2004. The October 2004 release was used to produce and analyze data for the CBM technical status report[7]. Work on digitizers and full tracking in CBM and PANDA collaborations is going on.

References

[1] http://alisoft.cern.ch/

[2] M.Al-Turany, D. Bertini and I. Koenig , “CBM Simulation and Analyis Framework”, GSI scintific report 2004, FAIR-EXP-07.

[3] W.Wittek, EMC Internal Reports: (*EMC/80/15, EMCSW/80/39, EMCSW/81/13, EMCSW/81/18)*

[4] A.Haas, The EMC Utility Package: (UTIL42)

[5] R.Brun, F.Bruyant, M.Maire, A.C.McPherson, P.Zanarini (DD/EE/84-1), May 1986

[6] http://www.cmake.org/

[7] CBM Collaboration Technical Status Report (GSI, Darmstadt, 2005)

Event Reconstruction in the CBM Experiment

I. Kisel[1,2], S. Gorbunov[1,3], J. Heuser[3], V. Lindenstruth[1], and Iou. Vassiliev[3]
[1]KIP, Ruprecht-Karls University, Heidelberg, Germany; [2]LIT, Joint Institute for Nuclear Research, Dubna, Russia;
[3]GSI, Darmstadt, Germany

A track reconstruction procedure [1, 2, 3] has been improved and used for optimization of the layout of the Silicon Tracking System. Fig. 1 shows dependency of the efficiency of track reconstruction versus momentum in STS with 2 MAPS stations and 10 double-sided strip stations, which are grouped into pairs with 1 cm internal distance (geometry with doubled strip stations).

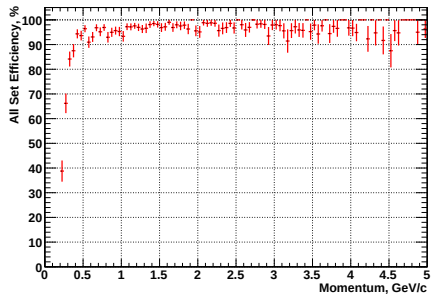

Figure 1: Efficiency of the Cellular Automaton track finder in STS with doubled strip stations.

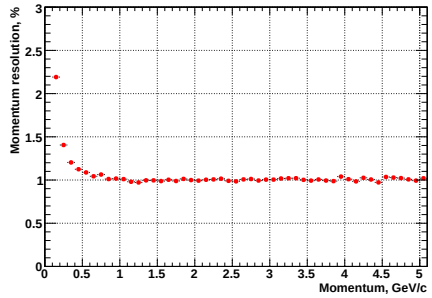

Figure 2: Momentum resolution for the standard STS geometry.

Momentum resolution is given in Fig. 2 for the standard STS geometry showing dominant influence of multiple scattering.

The track fitting algorithm based on the Kalman filter has been optimized with respect to the memory access when calculating the magnetic field. Being relatively smooth the magnetic field can be locally approximated by polynomials in planes of each station (see Fig. 3 for comparison of two alternative field representations) and along particle trajectories. Using such polynomial field representation the algorithm works within the cache thus significantly increasing the speed.

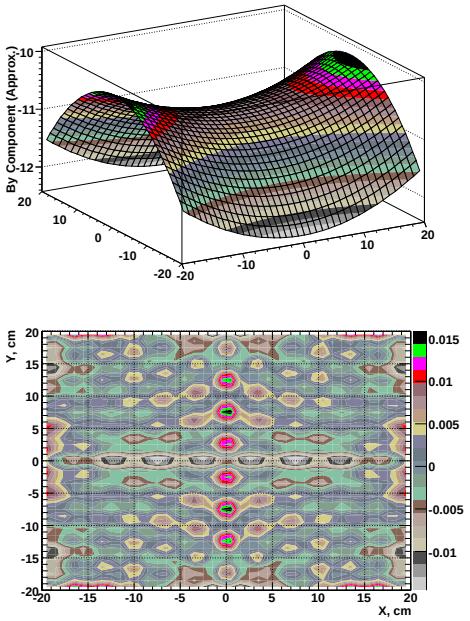

Figure 3: The most significant (B_y) component of the active magnetic field in the middle of the detector system ($z = 50$ cm) calculated using the polynomial approximation (top) and difference between two alternative field representations (bottom).

The routines for reconstruction of vertices [4, 5] have been significantly extended in order to estimate the decayed particle parameters.

References

[1] I. Kisel, Event reconstruction in the CBM experiment. Nucl. Instr. and Meth. A566 (2006) 85-88.

[2] S. Gorbunov and I. Kisel, Analytic formula for track extrapolation in non-homogeneous magnetic field. Nucl. Instr. and Meth. A559 (2006) 148-152.

[3] S. Gorbunov and I. Kisel, Elastic net for stand-alone RICH ring finding. Nucl. Instr. and Meth. A559 (2006) 139-142.

[4] S. Gorbunov and I. Kisel, Primary vertex fit based on the Kalman filter. CBM-SOFT-note-2006-001, 09 January 2006.

[5] S. Gorbunov and I. Kisel, Secondary vertex fit based on the Kalman filter. CBM-SOFT-note-2006-002, 14 September 2006.

Track reconstruction in the CBM-STS

O. Rogachevsky and A. Jerusalimov
JINR, Dubna, Russia

The goal of the CBM experiment is the investigation of the properties of compressed nuclear matter as produced in high-energy heavy-ion collisions. The main interest is the search for in-medium modifications of hadron properties and for the phase transition boundary between hadronic and quark-gluon matter at highest baryon densities.

In heavy-ion collisions at relativistic energies, a large number of particles is produced. In central Au+Au collisions at 25 GeV/n, about 800 tracks are within the acceptance of the Silicon Tracking System (STS) of CBM. The reconstruction of such events, strongly kinematically focussed due to the fixed-target setup, is very challenging. Several track finding algorithms are currently being developed to cope with the extreme environment.

In the Laboratory of High Energy (LHE) at JINR Dubna, a track finding algorithm based on the approximate solution of motion equation (ASME) for particles [1] has been developed with special focusing on the finding of secondary particles. This algorithm was tested for events of central Au+Au collisions at 25 GeV/n. The STS setup used consisted of two MAPS stations ($d = 150\ \mu$m) at z = 10 cm and 20 cm, two hybrid pixel stations ($d = 750\ \mu$m) at z = 30 cm and 40 cm, and four micro-strip stations ($d = 400\ \mu$m, z = 50, 60, 75 and 100 cm). The single-hit efficieny was 99 % in the first two stations and 100 % in the others. The fake hit rate in the MAPS stations was 3 %, while the projective geometry led to a large number (80 %) of fake hits in the strip stations. Due to these reasons we have restricted ourselves to finding tracks with at least four consecutive hits in stations 2 - 6. With this constraint, the algorithm reconstructs ~ 600 tracks per event for physics analyses.

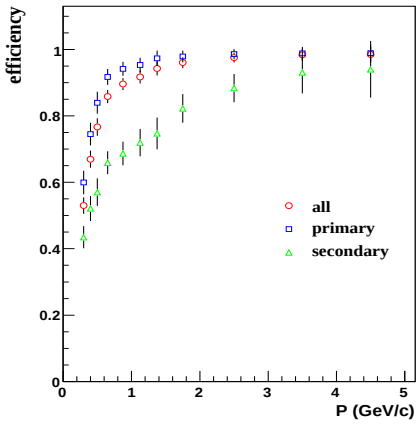

Figure 1: Track reconstruction efficiency as a function of momentum for all, primary and secondary particles

Figure 1 shows the track finding efficiency as a function of momentum. We obtain a good efficiency for primary particles with momenta above 0.5 GeV/c and a reasonable efficiency for secondary particles, allowing studies of long-lived decaying particles.

The relative momentum resolution obtained from the track fit is shown in Figure 2 as function of momentum. Its value is about 1.6 % roughly independent on momentum, thus demonstrating that it is dominated by multiple scattering in the STS detector material. A good resolution for the masses of decayed particle is achieved as well.

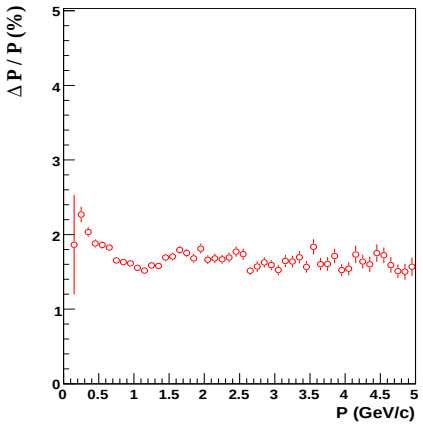

Figure 2: Relative momentum resolution for all reconstructed tracks as function of momentum

The algorithm is very fast ($5 - 8$ s per event) and the results obtained with it are promising. Further development of this algorithm is in progress.

References

[1] A. Jerusalimov: Reconstruction of track parameters in non-uniform magnetic field, http://www.gsi.de/Documents/DOC-2005-Jan-58.html

Implementation of a Hough Tracker for CBM*

C. Steinle[1], A. Kugel[1], and R. Männer[1] and the CBM Collaboration
[1]University of Mannheim, Department of Computer Engineering V, 68131 Mannheim, Germany

Abstract: In this report we describe an adaptation of the Hough Transform for the tracking of particles in the CBM STS detector, together with a possible implementation of the algorithm in hardware using FPGAs.

Hough Transform

The Hough transform is a global method for track finding. All STS detector hits have to be transformed into a parameter space according to the components of the track momentum p (θ, $-q/p_{xz}$, m). This leads to our 3D Hough transform [1].

The goal of the implementation is to process the tracking with maximum speed, e.g. to process one detector hit per clock cycle. Therefore the complicated calculations of the Hough transform according to the real detector geometry and the real magnetic field are implemented with look-up tables (LUTs). Since the calculation of the LUTs is done offline, any sufficiently precise algorithm can be used.

Unfortunately a direct implementation of the 3D Hough space requires a huge amount of memory. This can be avoided by the decomposition into several 2D layers, where the number of parallely computed layers can be adjusted to the existing hardware resources (see figure 1).

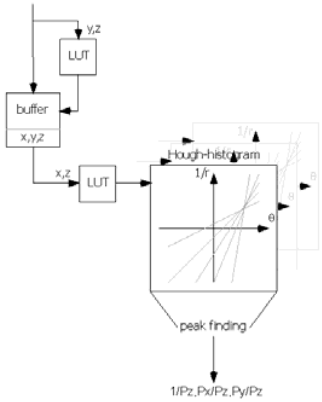

Figure 1: Hough Tracker algorithm structure

Figure 2 shows the realization of the buffer between the LUTs. The main elements are a dual-ported RAM (DP-RAM) and a register for each layer. The task of this unit is to store the information from the first LUT together with the information needed for the second LUT (see figure 1). Further on this data has to be stored in linked lists, while one list is needed for each layer. To this each entry of a list must have the ability to be moved to a list afterwards. Within this context the registers store the DP-RAM address of the actual processed entry of the list, while the DP-RAM stores the information combined with the address of the previous entry (link) of the list. So by processing the Hough entries one has just to modify the registers with addresses and to update the corresponding list addresses in the DP-RAM, if an entry has to be moved to a consecutive list. So the same Hough entry is prevented to occur more than once in the DP-RAM, even if it is used in more than one list and accordingly more than one layer.

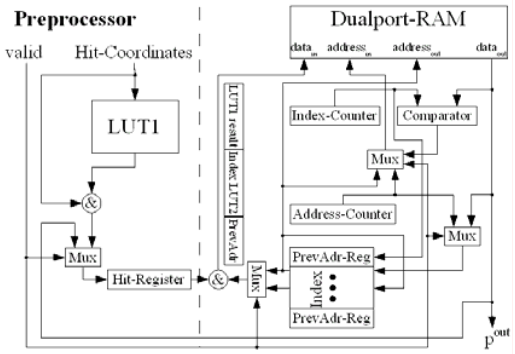

Figure 2: Hardware structure of the buffer

At present the Hough transform is further developed, in particular the adjustment of a good algorithm to produce the LUTs. We started with the formulas:

$$m = 100 \bullet 2 \frac{z\sin\gamma - y\cos\gamma}{\left(y\sin\gamma + z\cos\gamma\right)^2} \tag{1}$$

$$-\frac{q}{p_{xz}} = 10000 \bullet 0.3 \frac{2\left(z\sin\theta - x\cos\theta\right)}{B\left(x\sin\theta + z\cos\theta\right)^2} \tag{2}$$

Important is in Formula 2 the constant B which represents originally a homogenous magnetic field. Within the software framework we use instead of the correct inhomogeneous magnetic field an optimal constant factor for B at each detector plane. Our next step was to use the inhomogeneous field directly in the formula. This can be done by building the average of the integral of the magnetic field from the target to the actual plane. But surprisingly the algorithm's efficiency is decreased. So our next step is to use the 4th order Runge-Kutta method to improve the track model. This should end up in a better efficiency. We are able to use such a method because both sides of our transformation are digital and we are using LUTs.

References

[1] J. Gläss, C. Steinle, R. Männer, "Tracking in the Silicon Tracker System of the CBM Experiment using Hough Transform", 14th IEEE-NPSS REAL TIME Conference, June 2005, Stockholm, http://www.sysf.physto.se/RT2005/

* Work supported by EU/FP6 HADRONPHYSICS

Global tracking and hadron identification in the CBM experiment

D. Kresan and V. Friese
GSI, Darmstadt, Germany

The physics programme of the CBM experiment at FAIR includes a systematic investigation of hadron production in heavy-ion reactions as function of collision energy and system size. Of particular interest are event-by-event fluctuations in the particle ratios as well as directed and elliptic flow. For this purposes, excellent identification of pions, kaons and protons is indispensable. It will also help to reduce the background for the measurements of open charm and hyperons detected by their weak-decay topology.

Hadron identification in CBM will be performed by a time-of-flight (TOF) wall situated about 10 m downstream of the interaction target. It will consist of RPC chambers with pad and/or strip readout. A system time resolution of 80 ps at a maximal rate of 20 $\mathrm{kHz/cm^2}$ is aimed at.

The feasibility of the particle identification via TOF measurement relies on the matching of a hit in the TOF detector to the momentum measurement in the Silicon Tracking System (STS) of CBM, which is located directly after the target. Several layers of Transition Radiation Detectors (TRD) fill the space between STS and TOF and allow extrapolating a track found in the STS towards the TOF wall. Hadron identification in CBM thus requires track reconstruction in the STS, tracking through the TR detectors (either by track-following from the STS or by standalone TRD tracking plus merging with STS tracks), and matching of a TOF hit to the reconstructed global track.

In this study, we use a Cellular Automaton method for tracking in the STS (see I. Kisel et al., this report). The reconstruction efficiency for primary tracks in central Au+Au collision at 25 AGeV is about 96 %. A 3-D track following method based on a Kalman filter is employed to prolong the tracks throughout the TRD system. A TRD track reconstruction efficiency of about 94 % is obtained. The global track is then extrapolated towards the TOF wall, and the nearest TOF hit is attributed to it. Fig. 1 shows the efficiency of TOF hit matching (left) and the total TOF efficiency (right), including STS and TRD reconstruction efficiencies, as a function of momentum. These results were obtained with a realistic description of the RPC coordinate resolution, taking into account the single gap response also in case of mutiple hits and inclined tracks.

The losses in TOF-track matching of about 7 % are dominated by particle decays and double hits in the RPCs. The latter contribution amounts to some 2 % and can be reduced by resolving double hits in the RPC strip readout. Optimisation of the RPC pad/strip sizes is ongoing in order to reduce the number of electronic channels while roughly keeping the performances.

The global event reconstruction is completed by attaching reconstructed rings in the RICH to the global track, which enables electron identification. With these new reconstruction algorithms, developed in the course of the last year in the framework of CBMROOT, a complete reconstruction of simulated events is now available, giving path to feasibility studies of physics observables.

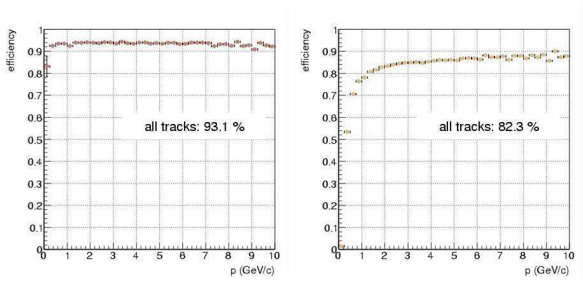

Figure 1: Efficiency of (left) matching a TOF hit with a global track and (right) total TOF reconstruction efficiency as function of momentum

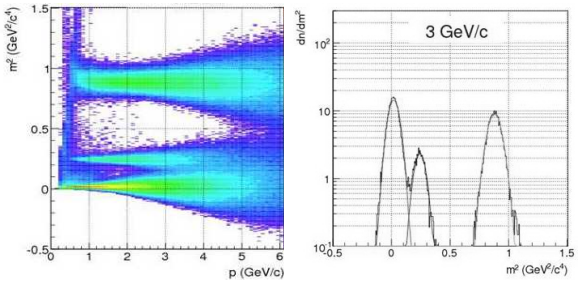

Figure 2: (Left) reconstructed particle mass from the TOF measurement as function of momentum; (right) mass spectrum derived from TOF at $p = 3\,\mathrm{GeV}$

As an example, fig. 2 (left) shows the reconstructed squared particle mass from the time-of-flight, track length and momentum, as a function of momentum, for an assumed time resolution of 80 ps. The reconstructed mass spectrum at $p = 3\,\mathrm{GeV}$ is shown on the right side of the figure. With an overall efficiency of 80 % to 90 %, separation of kaons and pions can be achieved up to laboratory momenta of about 3.5 GeV, while protons can be identified up to 7 GeV.

Tracking in the TRD

A. Lebedev and G. Ososkov
Laboratory of Information Technologies, Joint Institute for Nuclear Research, Dubna, Russia

For the problem of tracking in the CBM-TRD system, we developed two approaches: Track propagation from STS and standalone TRD tracking.

1. In the case of track following from the STS, already reconstructed STS tracks are propagated through the RICH detector to the first TRD layer. The information of the track direction in this layer is used for the intialisation of TRD track candidates. The momentum magnitude is used to properly take into account multiple scattering when propagating in the TRD system.

2. In the standalone case, only TRD information is available. Here, the problem is more complicated, since the momentum and direction of the particle are unknown. In order to initiate the search we have to create track candidates and roughly estimate the track parameters by a well-organized search through all admissible combinations.

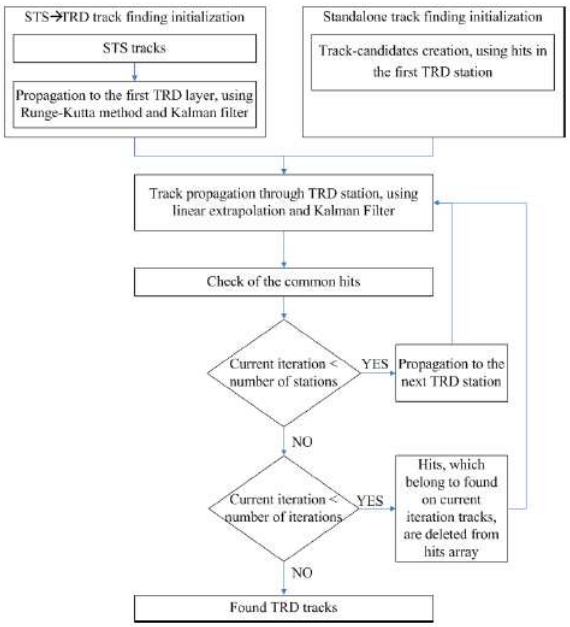

Figure 1: TRD tracking flowchart

After initialization, the created track candidates are propagated through the TRD as shown in the track-finding flow chart in fig. 1. For the track propagation from the STS, the Runge-Kutta method is used, taking into account the stray magnetic field. In the field-free region of the TRD system, a linear extrapolation is employed. After attaching hits in a TRD layer, the track is refitted using the Kalman filter technique [1] and propagated to the next layer.

Software implementing the proposed algorithms was implemented into the CBMROOT framework (release JUN06) and tested for 1,000 central Au+Au collisions at 25 AGeV. Three different TRD geometries with 9 layers (3+3+3), 10 layers (4+3+3) and 12 layers (4+4+4), respectively, were investigated. The first TRD station was located five meters upstream of the target. The obtained performances of TRD track finding are summarised in table 1.

Efficiency, %						
	STS to TRD			Standalone		
TRD layers	9	12	10	9	12	10
Reference	94,0	94,3	94,4	87,4	94,4	94,5
All	93,7	94,1	94,2	78,0	88,7	88,6
Vertex	93,7	94,1	94,3	84,8	94,1	94,1
Non-vertex	92,6	93,3	93,3	62,7	76,1	75,8
Ghost	4,2	4,2	2,3	12,8	6,6	4,3
Clone	0,0	0,0	0,0	0,0	0,0	0,0
Time, sec	2,3	3,7	3,2	10,7	6,1	3,8

Table 1: Track-finding efficiencies for different TRD geometries. Reference tracks are vertex tracks with $p > 1$ GeV.

We find the performance for the STS-TRD track finder almost independent of the TRD geometry, with exception of the ghost rate which is minimal for the 12-layer setup. The efficiency of the standalone track finder for vertex tracks in the 10 and 12 layer setups is similar to that obtained by the STS-TRD track finder, but is considerably lower for off-vertex particles. The ghost rate is higher in the standalone approach.

Summarising these results, we find that the 10 layer (4+3+3) TRD option appears as the optimal solution from the point of view of track finding performance and cost considerations. The 9 layer (3x3) setup seems not suitable for standalone TRD track finding.

References

[1] R. Frühwirth, Application of Kalman filtering to track and vertex fitting, Nucl. Instrum. Meth. A 262 (1987) 444

Standalone TRD tracking using the Cellular Automaton Algorithm

A. Bubak , M. Krauze , and W. Zipper
University of Silesia, Katowice, Poland

The extreme interaction rates foressen for the CBM experiment necessitate a high-speed data acquisition and online event selection. For high-level event selection, it is desirable to employ information from a selected detector subsystem only. Reconstruction algorithms operating on such data must be fast, efficient and reliable in order to allow trigger decisions on e. g. J/ψ signatures.

In this report, we describe a procedure for standalone track reconstruction in the CBM-TRD which is based on the Cellular Automaton method. The considered TRD detector is composed of three stations, each of them consisting of four layers. Each layer provides coordinates in a two-dimensional space, either the X-Z or the Y-Z plane, in an alternating way. It is assumed that every TRD plane has an ideal detection efficiency, i. e. every charged particle that crosses an active volume generates a signal. The registered and digitized signal is called a hit. Every hit owns information about its spatial coordinates and energy deposited by the particle. In a typical heavy-ion collision, the TRD detectors register about 700 hits in each sensitive plane.

The track reconstruction procedure is splitted into five parts. First. the data from two adjoining detector layers are combined to create a point in 3-D space. Combining two space points from two adjacent layer pairs, a segment is created. Every segment contains the information from all four layers of a single detector station.

After the simultaneous creation of segments for all three TRD stations, the Cellular Automaton merges the segments to tracks. To every created segment a number is attached signifying the number of other segements it is connected to. For instance, if a segment is connected to a set of two other ones from neighbouring stations, it has the value of 2 assigned, meaning it is the starting segment of a long track candidate, composed of three segments. For every long track candidate, the χ^2 value is calculated, which is a criterion of competition between tracks. In the next step the tracks are sorted in accordance with rising χ^2 value. The first track from the top of the stack (with lowest χ^2) is classified automatically as a "track candidate". After that, all hits attached to this track are marked as "used" and do not participate in further processing. If any of the next tracks in the stack uses one or more hits marked as "used", it is classified as "fake track". When all tracks candidates are processed, the procedure described above is repeated with less restrictive conditions and after exclusion of the hits already used.

In the present shape the described algorithm gives promising results with regard to speed and efficiency. As

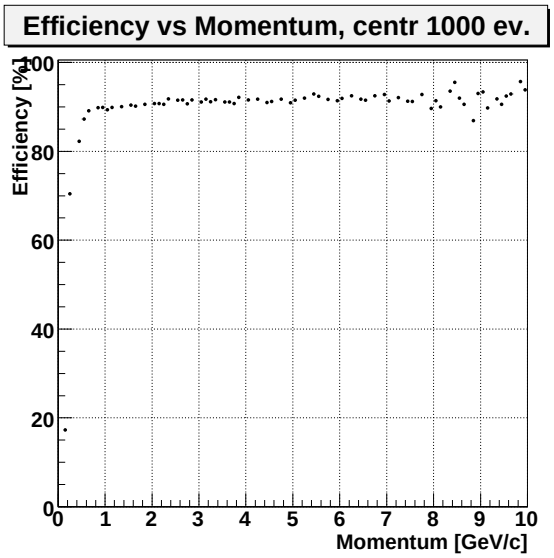

Figure 1: Track reconstruction efficiency as function of momentum in central Au+Au collisions at 25 AGeV

testing environment the particles produced from central Au+Au collision at 25 AGeV were taken. On average, 550 tracks per event were reconstructed. The efficiency of correctly reconstructed tracks is about 86% and 91% for particles with momentum below and above 1 GeV/c, respectively. Fig. 1 shows the efficiency as function of momentum. The average processing time per event is about 1.2 seconds on a standard PC with 2 multithread, 3 GHz processors and 1 GB RAM.

Ring recognition in the RICH detector of CBM

S. Lebedev[1], A. Ayriyan[1], C. Höhne[2], and G. Ososkov[1]
[1]LIT JINR, Dubna Russia; [2]Gesellschaft für Schwerionenforschung mbH, Darmstadt, Germany

Two algorithms for ring finding in RICH were developed: the first is based on information obtained by propagating tracks from the STS detector, and the second which is a standalone approach is based on the Hough Transform (HT) [1] combined with preliminary area clustering to decrease combinatorics.

Both ring-finders are working with good efficiency, however, there is a considerable number of fake rings present after ring finding. Routines have to be developed to reject them. A typical fake ring is formed by "stealing" hits from neighboring rings which seriously disturbs ring parameters. Our strategy was to develop cuts for a set of parameters which could be used to reject fake rings without a drop of the ring finding efficiency. Two approaches of fake ring rejection were developed: 2D cuts and a method based on an artificial neural network (ANN). 7 ring parameters were used for the fake rejection which were found to be essential: the number of hits in a narrow corridor around the ring; the number of hits in the ring; the distance between closest track projection and ring center; the biggest angle between neighboring hits; the χ^2 - criterion, and the radial position of the ring on the photodetector plane.

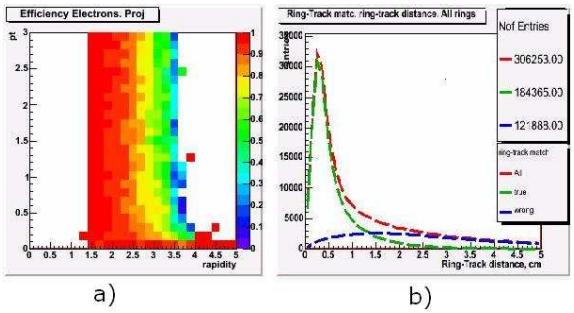

Figure 1: a) Ring finding efficiency for electrons in dependence on pt and rapidity (HT ring finder and ANN fake rejection), b) Distances between ring center and the closest track.

A table summarizing the efficiencies is presented below.

	HT	HT+ 2D cuts	HT+ ANN cut
Electrons, %	95.36	91.39	91.34
Fakes/event	15.41	2.59	0.91
Clones/event	7.07	2.23	1.24

Table 1: Efficiency of ring finding for electrons, number of fakes and clone rings per event.

HT+ANN for fake rejection showed very good results in terms of ring finding efficiency and fake and clone ring rates. As next step towards particle identification, robust algorithms for ring fitting of measured points were studied and optimized. We compared the currently used Crawford method [5] with methods known as COP (Chernov-Ososkov-Pratt) [2] and TAU (Taubin) [3]. To satisfy the robustness requirement we used both, the optimal and the Tukey's weight functions [4]. Testing algorithms on large statistics showed that the best performance was reached with the TAU method (see Fig.2).

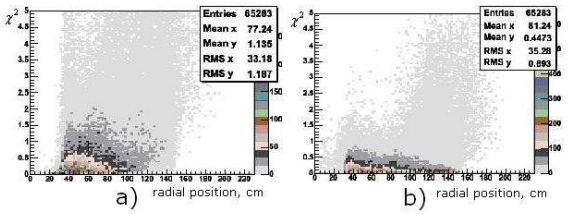

Figure 2: The chi-squared criterion χ^2 vs radial position on the photodetector plane. a) simple method b) TAU method

All results presented above were extracted for central Au+Au collisions at 25 AGeV with additionally added $5e^+$ and $5e^-$ at the main vertex in order to enhance electron statistics over the full phase space. The described methods were used in the event reconstruction chain for electron identification in RICH and proved a very good performance [6]. Next their optimization is planned as well as a further extension of ring fitting to ellipse fitting algorithms.

References

[1] Hough P.V. C. *Method and Means for Recognizing Complex Patterns*, U.S. Patent 3,069,654 1962.

[2] N. I. Chernov and G. A. Ososkov, *Effective algorithms for circle fitting*, Comp. Phys. Comm. 33 (1984) 329-333.

[3] G. Taubin, *Estimation Of Planar Curves, Surfaces And Nonplanar Space Curves Defined By Implicit Equations, With Applications to Edge And Range Image Segmentation*, IEEE Transactions on Pattern Analysis and Machine Intelligence 13, 1991, 1115-1138.

[4] G. Ososkov, I. Puzynin, A. Polyansky, *Modern methods of experimental data processing in high energy physics*, PEPAN, v.33, p. 3 (2002) 676-745.

[5] J. F. Crawford, *A non-iterative method for fitting circular arcs to measured points*, Nucl. Instr. and Meth. 211 (1983) 223-225.

[6] C. Höhne et al., *Electron identification with RICH and TRD*, this report.

Application of the ω_n^k test for J/ψ detection in the CBM experiment

E.P. Akishina[1], T.P. Akishina[1], V.V. Ivanov[1], A.I. Maevskaya[2], O.Yu. Denisova[1]
[1]LIT JINR, Dubna, Russia,[2]INR,Troitsk,Russia

The measurement of charmonium is one of the key goals of the CBM experiment. To detect J/ψ meson in its dielectron decay channel, the main task is the separation of electrons and pions. We present the electron/pion identification using energy losses in $n = 12$ layers of the CBM TRD detector applying the ω_n^k test.

The test criteria that check the correspondence of preassigned hypothesis (the null-hypothesis H_0) against all possible alternative hypotheses are called the *goodness-of-fit* criteria [1]. The most efficient criteria are based on a comparison of the distribution function $F(x)$ corresponding to the null-hypothesis H_0 with the empirical distribution function $S_n(x)$ [2]:

$$S_n(x) = \begin{cases} 0, & \text{if} \quad x < x_1; \\ i/n, & \text{if} \quad x_i \le x \le x_{i+1}, \quad i = 1, \ldots, n-1. \\ 1, & \text{if} \quad x_n \le x, \end{cases} \tag{1}$$

Here $x_1 \le x_2 \le \ldots \le x_n$ is the ordered sample (*variational series*) of the size n constructed on the basis of observations of the variable x.

The testing statistics is a measure of "distance" between the theoretical $F(x)$ and empirical $S_n(x)$ distribution functions. In [2] a new class of non-parametric statistics

$$\omega_n^k = n^{k/2} \int_{-\infty}^{\infty} [S_n(x) - F(x)]^k f(x) dx \tag{2}$$

has been proposed: $f(x)$ is the density function corresponding to H_0.

The distributions of energy losses by pions have a Landau distribution form, and it is resonable to use this distribution as H_0. First, we transfom the initial measurements to the set of a new variable λ (see details in [3]):

$$\lambda_i = \frac{\Delta E_i - \Delta E_{mp}^i}{\xi_i} - 0.225, \qquad \text{i = 1,2,...,n,} \tag{3}$$

where ΔE_i is the energy loss in the i-th absorber of the TRD, ΔE_{mp}^i – the most probable energy loss, $\xi_i = \frac{1}{4.02}$ FWHM of distribution of energy losses of pions in the i-th absorber [3], n – the number of layers in the TRD. In order to determine the value ΔE_{mp}^i and the value FWHM, the indicated distributions were approximated by the log-normal distribution.

The sample of obtained values λ_i, $i = 1, ..., n$ was ordered due to values (λ_j, $j = 1, ..., n$) and then used for ω_n^k calculation. The values of the Landau distribution function were calculated with the help of the DSTLAN function (from the CERNLIB library).

From Monte-Carlo simulation we exactly know which particle we deal with, and one can choose for combinatorial background only "real" electrons. For a good signal-to-background ratio, the electron identification purity is a crucial factor. The reconstructed track participates in a combinatorial background if it satisfies the following criteria: a) track vertex is inside the target; b) p_t is more than 1.2 GeV/c; c) RICH identifies track as electron: the ring radius is 5.9 to 7 cm; d) full energy loss in all TRD layers is larger than 70 keV.

Figure 1 shows the dielectron invariant mass spectra for background (top histogram) and J/ψ (bottom peak) after the above described ("abcd") cuts.

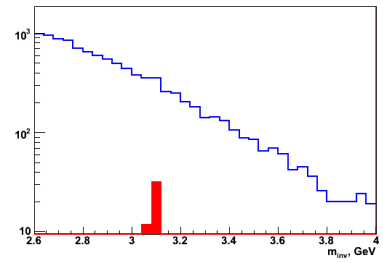

Figure 1: Dielectron invariant mass spectra for background (top histogram) and J/ψ (bottom peak) after application cuts "abcd"

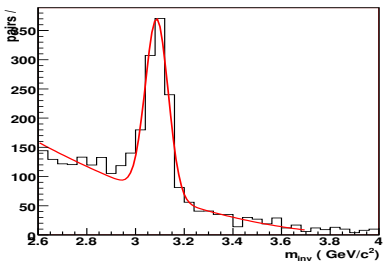

Figure 2: Invariant mass spectrum for particles identified as electrons by RICH and TRD for J/ψ and corresponding amount of central background events after "abcd" and $\omega_{12}^8 > 11$ cuts

Figure 2 presents an invariant mass spectrum for particles identified as electrons by RICH and TRD for J/ψ and corresponding amount of central background events after "abcd" and $\omega_{12}^8 > 11$ cuts: see Maevskaya et al., "J/ψ detection via electron-positron decay in CBM", this report.

References

[1] W.T. Eadie, D. Dryard, F.E. James, M. Roos and B. Sadoulet: *Statistical Methods in Experimental Physics*, North-Holland Pub.Comp., Amsterdam-London, 1971.

[2] V.V. Ivanov and P.V. Zrelov, Int. J. Comput. & Math. with Appl.,vol. **34**, No. 7/8, (1997)703-726; JINR Communication P10-92-461, 1992 (in Russian).

[3] P.V. Zrelov and V.V. Ivanov: NIM **A310**(1991)623-630.

Electron/pion identification in the CBM TRD using a multilayer perceptron

E.P. Akishina[1], T.P. Akishina[1], V.V. Ivanov[1], A.I. Maevskaya[2], O.A. Afanas'ev[1,3],
[1]LIT JINR, Dubna, Russia, [2]INR, Troitsk, Russia, [3]Kostroma State University, Kostroma, Russia

The measurement of charmonium is one of the key goals of the CBM experiment: see Maevskaya et al., "J/ψ detection via electron-positron decay in CBM", this report. To detect J/ψ meson in this decay channel, the main task is the separation of electrons and pions. Here we present the electron/pion identification using energy losses in $n = 12$ layers of the CBM TRD detector applying a multilayer perceptron (MLP).

A three-layered perceptron from the package JETNET3 [1] has been used for particle identification. The network included n input neurons (according to the number of the TRD layers), 35 neurons in the hidden layer and one output neuron. It was assumed that for pion events[1] the output signal has to be equal to -1, and for electron events – +1. To estimate the efficiency of the MLP training, we assumed that the network correctly recognized the sample given to the input, if the absolute error between the output signal and the target value did not exceed 0.05. An algorithm of the backward error propagation has been used for the error functional minimization at the stage of MLP training [2].

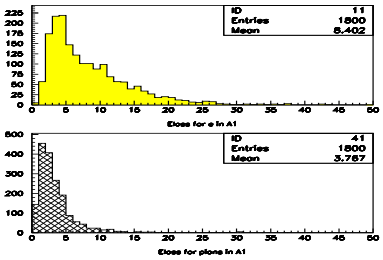

Figure 1: Distributions of energy losses (including transition radiation) by electrons (top plot) and energy losses by pions (bottom plot) in the first absorber of the TRD

Initially the events were formed using the set of energy losses $\Delta E_i,\ i = 1, ..., n$ corresponding to passage of pions or electrons through the TRD (Fig. 1). Although the distribution of energy losses by electrons, significantly differs from the character of the distribution of energy losses by pions, for such a choice of input data the training process was going on very slow (see bottom curve in Fig. 2). There were large fluctuations (against the trend) of the efficiency of events recognition by the network.

In this connection, the sets of a new variable λ were formed on the basis of the original samples:

$$\lambda_i = \frac{\Delta E_i - \Delta E^i_{mp}}{\xi_i} - 0.225, \qquad \text{i = 1,2,...,n}, \qquad (1)$$

where ΔE_i is the value of energy loss in the i-th TRD absorber, ΔE^i_{mp} is the most probable value of energy loss, $\xi_i = \frac{1}{4.02}$ FWHM of distribution of energy loss for pion in the i-th absorber (see details in [3]).

In order to determine the value of most probable energy loss ΔE^i_{mp} and the value FWHM of distribution of energy losses by pions in the i-th absorber, the indicated distributions were approximated by the density function of a log-normal distribution

[1]As event we define a data sample of the size n composed from energy losses of pion or electron detected by the TRD.

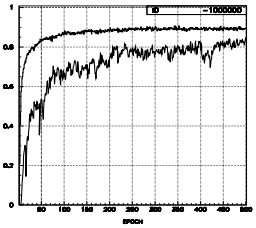

Figure 2: The efficiency of pion/electron identification by the MLP for original (bottom curve) and transformed (top curve) samples

$$f(x) = \frac{A}{\sqrt{2\pi}\sigma x} \exp^{-\frac{1}{2\sigma^2}(\ln x - \mu)^2}, \qquad (2)$$

where σ is the dispersion, μ is a mean value, and A is a normalizing factor [4]. The sample of obtained values $\lambda_i,\ i = 1, ..., n$ was ordered due to values ($\lambda_j,\ j = 1, ..., n$) and for each of them were calculated the values of Landau distribution function $\phi(\lambda)$ with the help of the DSTLAN function (CERNLIB, **G110** [5]), which were used to form the input pattern for the network.

In this case the reliable level of pion/electron identification by the network is reached after 10-20 training epoches in conditions of practical absence of fluctuations against the trend, and very quickly the needed level of pions suppression under the condition of a minimal loss of electrons is reached (see the behaviour of the top curve in Fig. 2).

At the stage of the MLP testing the event type was determined by the value of the output signal y: when it does not exceed the preassigned threshold y_t, then the event was assumed to belong to pion, in the opposite case – to electron.

Table 1 shows the results of comparison of the given methods MLP and ω^k_n (see E.P. Akishina et al., "Application of the ω^k_n test for J/ψ detection in the CBM experiment", this report): α is part of lost electrons, β is the fraction of pions identified as electrons, pion suppression factor equals to $100/\beta$.

Table 1: Comparison of the given methods MLP and ω^k_n

method	y_t	α,%	β, %	suppression of pions
MLP	0.84	9.4	0.6	167
ω^k_n	11.0	11.0	0.78	128

References

[1] C. Peterson, Th. Rögnvaldsson and L. Lönnblad: JETNET 3.0 package. Comp. Phys. Com. 81(1994)185.
[2] D.E. Rumelhart, G.E. Hinton, R.J. Williams: in D.E.Rumelhart, J.L.McClelland (Eds.), Parallel Distributed Processing: EMC.vol.1: Foundations. MIT Press, 1986.
[3] P.V. Zrelov and V.V. Ivanov:NIM A310 (1991) 623-630.
[4] W.T. Eadie, D. Dryard, F.E. James, M. Roos and B. Sadoulet: *SMEP*, North-Holland Pub. Comp., Amsterdam-London, 1971.
[5] K.S. Koelberg: CERN Computer Centre Program Library, **G110**.

Electron identification with RICH and TRD in CBM

C. Höhne[1], S. Das[1], S. Lebedev[2], A. Ayriyan[2], P. Stolpovsky[3], G. Ososkov[2], and V. Ivanov[2]
[1]GSI, Darmstadt, Germany; [2]JINR-LIT, Dubna, Russia; [3]IHEP Protvino, Russia

The observation of low-mass dilepton pairs and charmonium in the CBM experiment is one of the key measurements for the study of compressed baryonic matter in heavy ion collisions. The standard setup of CBM [1] foresees the measurement of electrons using particle identification with a ring imaging Cherenkov (RICH) detector and transition radiation detectors (TRD). In order to study the performance of the proposed setup with respect to electron identification and pion suppression capabilities, event reconstruction and particle identification routines have been developed. In this report first results on the performance of the CBM detector concerning electron identification including complete event reconstruction will be presented.

The simulations were performed for central Au+Au collisions at 25 AGeV beam energy generated by UrQMD [2]. These events were tracked through the CBM detector using GEANT, however, the transition radiation in the TRD was approximated by an external model still to be be improved. The event reconstruction starts with tracking in the STS, requiring a minimum of 4 STS hits. The tracks are then extrapolated to the RICH photodetector plane, to the TRD and with track following methods further on to TOF. Rings are found using ring reconstruction algorithms [3]. Ring-track as well as TOF hit-track matching were applied choosing pairs having the closest distance. This way fully reconstructed events with information on RICH, TRD, and TOF signals for each track are available.

For ring reconstruction in the RICH detector the most crucial parameter is the quantum efficiency of the photodetector, here existing MAPMTs from Hamamatsu were implemented (H8500-03) yielding about 21 hits per electron ring. Ring finding efficiencies are larger than 90% for midrapidity tracks and fall towards higher momenta [3]. High momentum tracks are located in the central region of the RICH detector where also high ring densities exist. This leads to dropping ring finding efficiencies and increasing rates of fake rings. The most central part is therefore excluded reducing only slightly the geometrical acceptance for rapidities larger than 4. In order to further reject fake rings a set of ring quality cuts was developed reducing ring finding efficiencies by $\sim$5% [3]. A more severe reduction of the electron identification efficiency is the requirement of a maximum distance between ring and track. The cut is currently placed at 1 cm which has to be compared to a ring radius of 6.17$\pm$0.14 cm for electron rings. This selection rejects $\geq$5% of good matches (depending on momentum), however, is important to reduce wrong ring-track matches, e.g. of a primary vertex pion track and an electron ring from a secondary electron for which no track could be reconstructed. Indeed, these wrong matches are the major source of electron misidentification for tracks with $p < 8$ GeV/c. Electrons are then selected choosing a range of radii of $\langle \mathrm{R} \rangle \pm 3\sigma$, with $\langle \mathrm{R} \rangle$ = 6.17 cm and σ = 0.14 cm. Pions leak into this band and will be identified as electrons only from 8-10 GeV/c on. Figure 1 shows the resulting pion suppression defined as $\frac{\pi \text{ identified as e}}{\pi \text{ in RICH acceptance}}$. Up to momenta of about 8 GeV/c the suppression factor lies between 500-1000 and pion misidentification is solely due to ring-track mismatches. From 8 GeV/c on pions leaking into the radius cut become dominant and lead to a continuous rise of the misidentification probability. Further sources of particle misidentification are mismatches of proton tracks to electron rings which can be fully eliminated using TOF information.

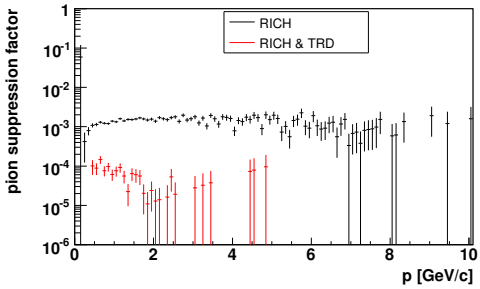

Figure 1: Pion suppression for electrons identified in RICH and in RICH & TRD for central Au+Au collisions at 25 AGeV.

Pions can be further rejected using energy loss information from the TRD. As first step a cut of 70 keV is placed on the summed energy loss in the 12 TRD layers rejecting already 90% of the remaining pions. For the final pion rejection shown in figure 1 electron/pion separation is improved using a statistical analysis of the energy loss spectra in each layer [4]. The combined pion suppression in RICH and TRD reaches values larger than 10^4 for $p > 1$ GeV/c. In future, these simulations will be improved taking into account the detector responses in more detail.

References

[1] V. Friese et al., *The CBM experiment at FAIR*, this report.

[2] S.A. Bass et al., Prog. Part. Nucl. Phys. 41 (1998) 255.

[3] S. Lebedev at al., *Ring recognition in the RICH detector of CBM*, this report.

[4] P.V. Zrelov, V. Ivanov, NIM A 310 (1991) 623.
E.P. Akishina et al., *Application of the ω_n^k test for J/ψ detection in the CBM experiment*, this report.

Feasibility of hyperon detection in the CBM experiment

E. Kryshen[1] and V. Friese[2]
[1]SPbSPU, St. Petersburg, Russia; [2]GSI, Darmstadt, Germany

The measurement of hyperons will enable the CBM experiment to characterise the strangeness content of the fireball created in high-energy nucleus-nucleus reactions, one of the key observables to access the collision dynamics. CBM aims at multi-differential measurements (spectra, flow) as function of collision energy and system size, which is a challenging task in particular for the rare Ω close to its elementary production threshold.

Hyperon detection is performed in the tracking system of CBM (STS) exploiting the topology of weak decays into charged hadrons. The feasibility studies are based on transport through the field and detector geometry, simulation of the anticipated detector response and reconstruction of tracks and secondary vertices in the STS, all inside the software framework CBMROOT.

Details about simulation and analysis can be found in [1]. The feasibility of hyperon measurements was studied for central Au+Au collisions at 25 AGeV using an improved STS layout without MAPS stations, new digitisation scheme and an advanced secondary track finding algorithm. In addition, the analysis was refined with respect to that presented in [1]. The main cut parameters to suppress the combinatorial background of uncorrelated pions and kaons are the track impact parameter in the target plane, the distance of closest approach of the track pair, the impact parameter of the reonstructed mother track, and the position of the fitted decay vertex along the beam axis.

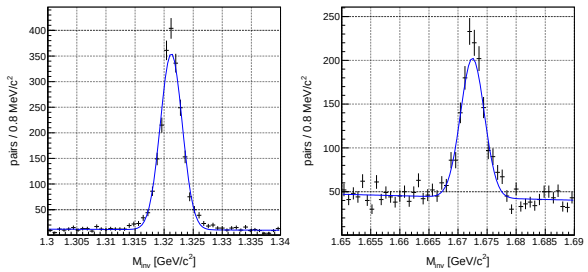

Figure 1: Invariant mass signals for (left) $\Xi^- \to \Lambda\pi^-$ and (right) $\Omega^- \to \Lambda K^-$ for central Au+Au collisions at 25 AGeV after acceptance and topological cuts

The invariant-mass signals for Ξ^- and Ω^- obtained after all topological cuts are shown in figure 1. The signal to background ratio is reduced compared to the previous analysis [1] due to more realistic setup. Table 1 shows the obtained results, including geometrical acceptance, efficiencies and signal-to-background ratio for Λ, Ξ^- and Ω^- after track reconstruction and all toplogical cuts.

Particle	$\Lambda + \Sigma^0$	Ξ^-	Ω^-
Yield/event	36.6	0.983	0.022
Statistics	10^5	10^5	$4.5 \cdot 10^6$
σ_m, MeV/c^2	1.34	1.87	2.04
Acceptance	28.5%	16.3%	14.6%
Rec. efficiency	62.5%	40.6%	46.2%
Cut efficiency	59.4%	32.2%	15.4%
Total efficiency	10.6%	2.1%	1.0%
S/B ratio	30.2	12.8	2.5
Significance	591	42	32.4

Table 1: Results on hyperon reconstruction in central Au+Au collisions at 25 AGeV. The hyperon multiplicities were taken from the UrQMD model.

Lately, it has been proposed that the CBM experiment could in addition be operated at SIS-100 for beam energies between 2 and 10 AGeV. Thus, the study has been extended towards smaller collision energies. Here, the measurement becomes tedious because of the extremely low hyperon multiplicities (about 10^{-3} for Ω^-). Results, obtained for central Au+Au collisions at 6 AGeV, are shown in table 2.

Particle	$\Lambda + \Sigma^0$	Ξ^-	Ω^-
Yield/event	12.8	0.118	$7.2 \cdot 10^{-4}$
Statistics	10^5	$9.4 \cdot 10^5$	$1.4 \cdot 10^8$
σ_m, MeV/c^2	1.31	2.21	1.96
Acceptance	25.1%	13.6%	13.9%
Rec. efficiency	73.4%	53.5%	64.9%
Cut efficiency	40.1%	35.1%	21.7%
Total efficiency	7.4%	2.6%	2.0%
S/B ratio	65	17.8	4.3
Significance	294	49.3	39

Table 2: Results on hyperon reconstruction in central Au+Au collisions at 6 AGeV. The hyperon multiplicities were taken from the UrQMD model.

Much higher cut efficiencies could be obtained with MAPS detectors installed, which provide significant improvement in the precision of track extrapolation and secondary vertex fitting. Besides, a measurement of the Ξ and Ω at sub-threshold energies can be improved significantly, provided the charged daughter particles can be identified by means of the CBM-TOF detector.

References

[1] E. Kryshen and Y. Berdnikov, CBM-PHYS-note-2005-002, http://www.gsi.de/documents/DOC-2005-Aug-35.html

Open charm measurement in the CBM experiment

I. Vassiliev[1], S. Gorbunov[1,2], and I. Kisel[2,3]

[1]GSI, Darmstadt, Germany; [2]KIP, Ruprecht-Karls University, Heidelberg, Germany; [3]LIT, Joint Institute for Nuclear Research, Dubna, Russia

One of the major experimental challenges of the CBM experiment is to trigger on the displaced vertex of the D-meson hadronic decay in the environment of a heavy-ion collision. This task requires fast and efficient track reconstruction algorithms and high resolution secondary vertex determination. Particular difficulties in recognizing the displaced vertex of the rare D meson decays are caused by weak K^0_S and hyperon decays which produce displaced vertices close to the target (the mean life time of the D^0 mesons is $c\tau = 122.9$ μm), very low multiplicity and branching ratio of the D meson production ($5.8 \cdot 10^{-6}$) for the central Au+Au collision at 25AGeV, and multiple scattering in the beam pipe and detectors.

To study the feasibility of open charm mesons measurement in the CBM experiment 10^4 central Au+Au UrQMD events at 25 AGeV have been simulated. K^- and π^+ pairs from D^0 decays have been added to each event in order to simulate a signal in the environment of background hadrons. A realistic STS geometry with 2 MAPS, one hybrid and 4 double-sided strip detectors has been used. The first MAPS detector have been placed at 10 cm downstream the target in order to reduce radiation damage. The primary vertex was reconstructed with high accuracy (5.7 μm in z direction, 1.0 μm in x and y) from about 450 tracks fitted in the STS with a non-homogeneous magnetic field by the Kalman filter procedure [1]. The resolution in the z distribution of the secondary vertex of 54 μm as achieved by the fitting procedure is sufficient to separate detached secondary vertices from the primary vertex.

Because of originating from a displaced decay vertex, the D^0 meson daughter tracks have a non-vanishing impact parameter at the target plane. Since the majority of the primary tracks have very small impact parameter, a significant part of the combinatorial background can be rejected using a cut on their χ^2 distance to the primary vertex. The combinatorial background is suppressed as well by the z-vertex cut to select detached vertices, the requirement for the D meson momentum to point to the primary vertex, the p_t-cut and the vertex χ^2 cut for good quality secondary vertices. After applying all cuts the D^0 reconstruction efficiency is 3.25% . The shape of the background in the signal IM region has been estimated using the event mixing technique. The resulting background plus D^0 and $\bar{D}^0$ signal spectrum is shown in Figure 1. The signal to background ratio is about 4.4 .

A novel algorithm has been developed to reconstruct the D^0's life time and the decay length together with their corresponding errors. The algorithm first finds the primary vertex using all reconstructed tracks, and then the D^0 meson is reconstructed from its two daughter particles K^- and π^+ using the primary vertex as the production point. The accuracy of the life time is 9.8 μm/c, only 8% of the nominal value 122.9 μm/c, showing that the reconstructed D^0 particles are well separated from the primary vertex. Figure 2 gives the life time distribution of all D^0 in the detector acceptance before applying reconstruction cuts with the fitted mean value of (122.8 ± 2.0) μm.

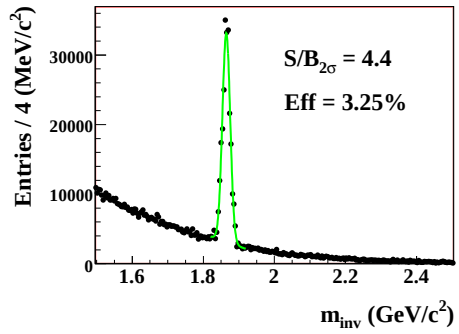

Figure 1: The D^0+$\bar{D}^0$ and combinatorial background invariant mass spectrum. The estimated spectrum corresponds to 10^{12} central events.

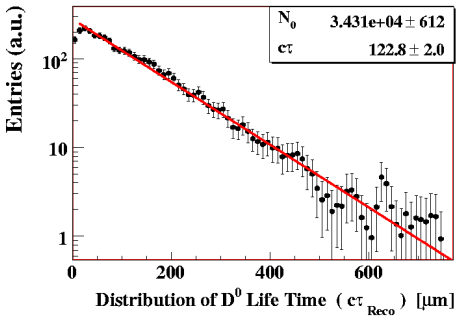

Figure 2: Distribution of the D^0 meson life time.

References

[1] S. Gorbunov, I. Kisel and Iouri Vassiliev, Analysis of D^0 Meson Detection in Au+Au Collisions at 25 AGeV, CBM-PHYS-note-2005-001, June 2005.

Full reconstruction of low-mass electron pairs in CBM

T. Galatyuk, S. Das, and C. Höhne
GSI, Darmstadt, Germany

The reconstruction of low-mass vector mesons (ρ, ω, ϕ) emitted out of the hot and dense phase of relativistic heavy ion collisions is one of the experimental goals of the CBM experiment. The status of simulations of an electron pair measurement will be summarized in this report.

Dominant background sources are random combinations of e^- and e^+ from π^0-Dalitz decay and γ conversion, the latter mostly in the target and to a smaller extent in the tracking stations, the beam pipe and the magnet yoke. In order to minimize electrons from conversions a single 25 μm gold target was assumed. A characteristic feature of conversion and π^0-Dalitz decays is the moderate decay momentum and small opening angle of the electron pair. A special challenge of the current concept is the fact that electron identification is not provided in front of the magnetic field. To increase the acceptance for low momentum particles the magnetic field was reduced to B_{max} = 0.7 T and the size of Silicon Tracking Stations 1 to 6 was increased.

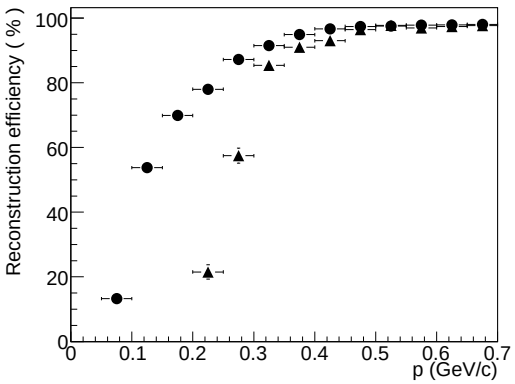

Figure 1: Track reconstruction efficiency as a function of momentum. Triangle: standard tracking algorithm, circle: improved tracking on low momentum tracks.

Considerable effort went into the problem of tracking in the STS for low momentum tracks because a large fraction of soft tracks suffers significantly from multiple scattering in the detector material. The track reconstruction efficiency is 90 % integrated over all momenta (see Figure 1). The reduction of the magnetic field to 70 % of its nominal value results in a momentum resolution still well below 2 %.

An important requirement for efficient background rejection is high efficiency and high purity of identified electrons. The electron identification includes the full CBM detector setup, ring recognition algorithms and ring-track matching algorithms. The pion suppression using only RICH information is about 500. A suppression factor of $\geq$ 1000 can be reached when including a cut on ToF information and a cut on the summed energy loss in 12 TRD layers for tracks with momenta above 1.5 GeV [1].

The strategy of background rejection described in [2] was applied. Invariant mass spectra of dielectron pairs including full event reconstruction and electron identification after applying all cuts are shown in Figure 2. The S/B ratio in a $\pm 1.4\ \sigma_m$ range around the vector meson peak is 0.2 for the ω meson with a signal efficiency of 8%. An optimization of the cuts will further reject background. A realistic concept how to suppress the magnetic field between the target and first Micro-Vertex Detector has to be worked out. The excellent two hit resolution in the MAPS detector ($< 100\mu$m) gives then a chance to reject close pairs. The rejection power of conversion pairs can even be improved by using energy loss information in the first MVD. The pion suppression factor will still increase considerably after applying the statistical analysis of the energy loss spectra in TRD [3].

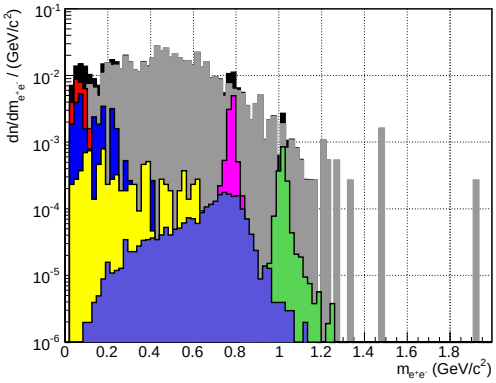

Figure 2: Di-electron invariant mass spectra for $Au + Au$ collisions at a beam energy of 25 AGeV, zero impact parameter. Black area: unlikesign combinations of e^+ and e^-, grey: combinatorial background. Red: π^0, dark blue: η, yellow: ω-Dalitz, magenta: ω, green: ϕ, violet: ρ^0. The simulated data sample is equal to 10 second of beam time.

References

[1] C. Höhne et al., *Electron identification with RICH and TRD in CBM*, this report.

[2] T.Galatyuk et al., see GSI Scientific Report 2005/FAIR-QCD-CBM-06.

[3] E.P. Akishina et al., *Application of the ω_n^k test for J/ψ detection in the CBM experiment*, this report.

Fast simulation of low-mass electron pair measurements with CBM

P. Staszel, R. Karabowicz, Z. Majka
Jagiellonian University, Poland

Investigation of the invariant mass spectrum of short lived neutral vector mesons (ρ, ω, ϕ) via detection of their electron-positron pairs is one of the major issue of the CBM physics. Besides of the electron-positron pairs that originate from the meson decays, there is a large number of electrons and positrons from π^0-Dalitz decays and the γ conversions in the target and the detector material budged. In addition, the charged pions misidentified as electrons contribute to the background.

Our study focus on Au+Au central reactions at 25 AGeV. The physics input was generated by the UrQMD event generator that accounts for the general event characteristics in terms of hadron production, and by PLUTO event generator that provides leptonic (e^+e^- pairs) and semi-leptonic decays of light vector mesons. The assumed multiplicities of mesonic "cocktail" together with the considered decay channels and their branching ratios can be found in [1]. The CBM analysis framework with embedded GEANT3 package [2] was used to transport primary particles through the CBM experimental set up geometry. The assumed STS geometry consists of enlarged first 6 STS stations to maximize the geometrical acceptance for low momentum particles. The magnetic field was set to 70% of its maximum value and the target thickness was set to 25μm. The reconstructed electrons are defined as these that passed through each of the 8 STS stations (tracking) and hit both RICH and TRD detector (high efficiency and purity of particle identification). The unlike sign pair invariant mass spectrum for the measured electrons is shown in Fig. 1 for uncorrelated (background, 10^5 events) and correlated (signal, 16×10^6 events) components by the solid line and the solid dots, respectively. It is seen that except of low mass region (gamma conversion and π^o-Dalitz) the combinatorial background exceeds signal by large factor that depends on invariant mass. In the range between 0.2 GeV and 0.6 GeV, specially interesting regarding the CBM physics, the signal

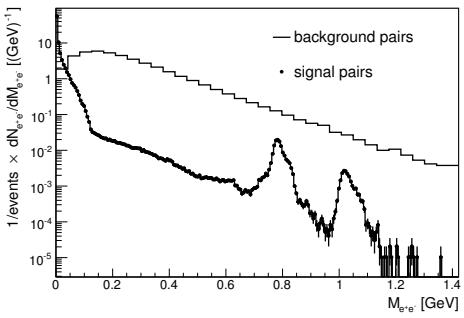

Figure 1: Combinatorial invariant mass spectrum for the measured electrons for uncorrelated pairs (background) and for correlated pairs (signal).

to background ratio is on the level of 3×10^{-3}. In order to suppress the combinatorial background, the following cuts have been applied: (a) cut on the invariant mass ($M_{inv} < 16MeV$) of the partially reconstructed unlike sign pairs (partially means that one track forming the pair is not identified), (b) cut on the invariant mass of fully reconstructed unlike sign pairs ($M_{inv} < 55MeV$) and (c) cut on the particle transverse momentum ($p_T < 0.3GeV$).

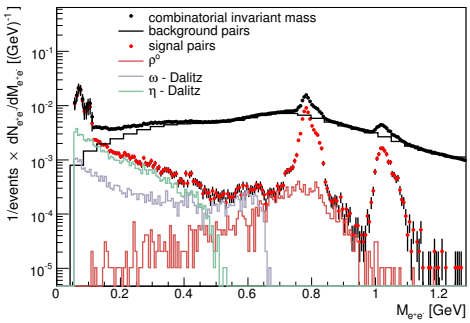

Figure 2: The combinatorial invariant mass spectrum of accepted tracks that survived all cuts. Realistic momentum resolution, track reconstruction efficiency and the pion suppression factor have been assumed.

The analysis is based on the Monte Carlo tracks and does not take into account the realistic performance of the detection system as well as the reconstruction ability of the existing reconstruction software. To obtain the more realistic results we took the momentum resolution, track reconstruction efficiency and the pion suppression factor determined from data digitization and reconstruction CBM procedures [3, 4]. The combinatorial invariant mass spectrum of accepted tracks that survived all cuts, together with the signal and background components are plotted in Fig. 2 as black symbols, red symbols and by the solid line, respectively.

The obtained result is very promising showing that the concept of the CBM detector geometry is well suited for the di-electron measurement in the low mass regime. This analysis, however, does not include realistic particle identification efficiency. This effect will be considered in the forthcoming studies.

References

[1] T. Galatyuk and J. Stroth, CBM-PHYS-note-2006-001.

[2] M. Al-Turany et al., *FairRoot/CbmRoot Simulation and Analysis Framework*, this report.

[3] C. Höhne et al., *Electron identification with RICH and TRD in CBM*, this report.

[4] T. Galatyuk et al., *Full reconstruction of low-mass electron pairs in CBM*, this report.

J/ψ detection via electron-positron decay in CBM

A. Maevskaya[1], V. Ivanov[1], and C. Höhne[2]
[1]Institut for Nuclear Research, Moscow, Russia; [2]GSI, Darmstadt, Germany

The measurement of charmonium production is one of the central aims of the CBM experiment. In order to study the feasibility of a charmonium measurement in the dielectron decay channel detailed simulations including for the first time full event reconstruction and particle identification have been performed and will be reported here. The major challenge is an efficient background suppression in order to detect the rarely produced J/ψ mesons as well as a high purity of identified electrons.

The simulations were performed with an implementation of the CBM detector layout as described in [1]. Decay electrons from J/ψ mesons were mixed into central Au+Au collisions generated by UrQMD [2]. Table 1 summarizes the multiplicities for J/ψ mesons at the different energies as they were taken from the HSD model [3]. The simulated

Table 1: Characteristic numbers for J/ψ production and reconstruction in CBM.

beam energy	$\langle J/\psi \rangle$**/central Au+Au coll.**	**efficiency [%]**	**S/B**
15 AGeV	$2.44 \cdot 10^{-6}$	9	0.8
25 AGeV	$1.92 \cdot 10^{-5}$	12	1.7
35 AGeV	$5.49 \cdot 10^{-5}$	14	14.5

events were then reconstructed using tracking algorithms in the STS requiring at least 4 STS stations to be crossed by the tracks, and track extrapolation towards the TRD. STS-TRD track matching, however, is still ideal in this simulation. Ring reconstruction algorithms were applied and ring-track matching was done selecting pairs with the closest distance.

Electron identification in the RICH detector was performed as described in more detail in [4]: The central part of the RICH detector was excluded as here highest track and ring densities lead to a number of fake rings as well as wrong ring-track matches, ring quality selection cuts were applied, a maximum distance of 1 cm was allowed for the ring-track matching, and finally electrons were selected requiring a ring radius between 5.9 cm and 7 cm. In the TRD electrons were identified by first selecting those tracks having an energy loss of more than 70 keV summing all TRD stations (12 layers). Furthermore, electron/pion separation is improved using a statistical analysis of the energy loss spectra in each layer [5]. A combined RICH & TRD pion suppression factor of more than 10^4 can be achieved for tracks with momenta larger than 1 GeV/c as has been shown in [4].

Figure 1(left) shows the invariant mass spectrum extracted after event reconstruction and electron identification as described above. In order to suppress the physical background, a cut on transverse momentum is applied ($p_t > 1.2$ GeV/c) on each track which shows only negligible effect on the J/ψ signal due to the high momenta of the decay electrons. The most crucial factor for a good signal-to-background ratio is the purity of the electron identification. Earlier simulations have shown that a factor 10^4 pion suppression is needed which is nicely fulfilled by this simulation. Reconstruction efficiencies including electron identification and geometrical acceptance of the CBM detector are given in table 1 for the different energies. Signal-to-background ratios (S/B) are given as well. Figure 1(right) illustrates that with the event reconstruction and electron identification introduced above a wide phase space coverage of J/ψ mesons is ensured covering in particular also midrapidity (y_{CM}=2 for 25 AGeV beam energy).

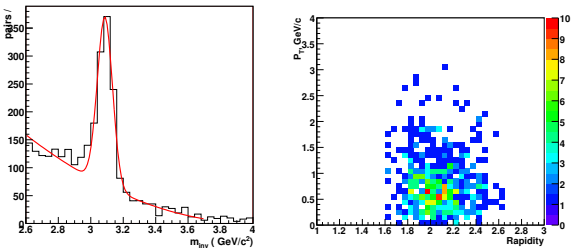

Figure 1: Invariant mass spectrum and $y - p_t$ distribution of reconstructed J/ψ mesons in central Au+Au collisions at 25 AGeV beam energy.

References

[1] V. Friese et al., *The CBM experiment at FAIR*, this report.

[2] S.A. Bass et al., Prog. Part. Nucl. Phys. 41 (1998) 255.

[3] W. Cassing, E.L. Bratkovskaya, S. Juchem, Nucl. Phys. A 674 (2000) 249.

[4] C. Höhne et al., *Electron identification with RICH and TRD in CBM*, this report.

[5] P.V. Zrelov, V. Ivanov, NIM A 310 (1991) 623.
E.P. Akishina et al., *Application of the ω_n^k test for J/ψ detection in the CBM experiment*, this report.

Vector meson detection via $\mu^+\mu^-$ decays in CBM

A. Kiseleva[1], R. Dzhigadlo[2], S. Gorbunov[3], I. Kisel[3], and I. Vassiliev[1]
[1]GSI, Darmstadt, Germany; [2]University, Kiev, Ukraine; [3]University, Heidelberg, Germany

As an alternative approach to the dielectron measurement we have investigated the possibility to detect vector mesons (ρ, ω, ϕ, J/ψ) via their decay into $\mu^+\mu^-$ pairs. The muon detection system is located downstream the STS. The actual design of the muon system consists of 5 hadron absorber layers made of iron of variable thickness, and of 15 detector layers with 100 μm position resolution. The first absorber is positioned inside of the magnet direct behind last STS, three sensitive layers are located in each gap between two absorbers, and three detectors are located behind the last absorber. For the muon simulation we take in to account not only STS and the muon system, but also two stations of the Transition Radiation Detectors (TRD) and the time-of-flight (TOF) system with 80 ps time resolution.

The vector meson decays were simulated with the PLUTO generator assuming a thermal source with a temperature of 130 MeV. The multiplicity of low-mass vector mesons and η for central $Au + Au$ collisions at 15, 25 and 35 AGeV beam energies is taken from the HSD transport code [1]. The background was calculated with the UrQMD event generator. All signals and background are transported through the detector setup using the transport code GEANT3 within the cbmroot simulation framework. The L1 tracking procedure [2] has been used for the track finding at STS and muon system, and for momentum reconstruction at STS. The time information from the TOF detector was used for suppression of punch-through protons and kaons.

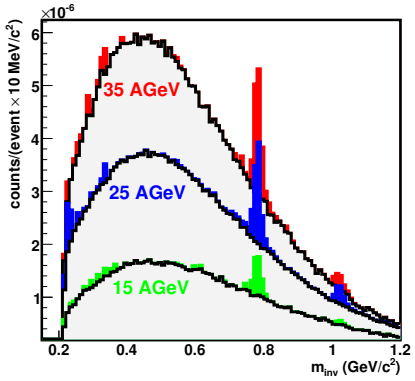

Figure 1: Dimuon invariant mass spectra for different beam energies. Black lines - only background includes, peaks of different colors - the spectra include the combinatorial background and signals (ρ, ω, ϕ, η and η_{Dalitz}).

Figure 1 shows the dimuon invariant mass spectra for central $Au + Au$ collisions at different beam energies. As signals the ρ, ω, ϕ, η and η_{Dalitz} were included. The signal-to-background ratio (calculated in a $\pm 2\sigma$ window around the signal peak) and the efficiency for ω meson detection is listed in table 1 for different beam energies.

beam energy (AGeV)	15	25	35
S/B ratio	0.4	0.4	0.4
efficiency (%)	1.0	1.3	1.5

Table 1: Signal-to-background ratio and efficiency for ω detection in central $Au + Au$ collisions at different beam energies.

For the J/ψ simulations 1 m of iron was added. Figure 2 shows the dimuon invariant mass spectrum in the region of the J/ψ peak for central $Au + Au$ collisions at 25 AGeV. The grey spectrum is invariant mass distribution after the tracking procedure without any cuts. The signal-to-background ratio is 44 and the efficiency is 20%. The red spectrum represents the invariant mass distribution after cuts on transverse momentum ($p_t \geq 1$ GeV/c) and opening angle ($\geq 12^\circ$).

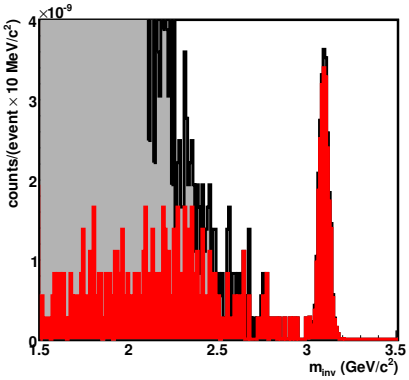

Figure 2: Dimuon invariant mass spectrum in the region of the J/ψ peak for central $Au + Au$ collisions at 25 AGeV: grey - without cuts and red - after cuts (see text).

The simulation results demonstrate the feasibility of dimuon measurements using hadron absorbers in $Au + Au$ collisions at FAIR beam energies. The next step will be the realistic design of the muon detector layout.

References

[1] W. Cassing, et al., Nucl. Phys. A 691 (2001) 74.

[2] S.Gorbunov, et al., CBM-PHYS-note-2005-001.

Study of J/Ψ measurements with distant muon detector arms

K. Piasecki, B. Sikora, K. Wisniewski, Warsaw University, Poland

One of the possible positions of a detector dedicated to the measurement of J/ψ mesons in the dimuon decay channel, is behind the basic CBM setup (STS, RICH, TRD and ECAL) [1]. The far location of the detector implies large dimensions (and costs) and asks for optimizing its geometry, aiming at largest reasonable reduction of detector area. As criteria were used the S_2 significance (defined as $S_2 = Signal/\sqrt{(Signal + Background)}$) and the signal to background ratio in a 100 MeV wide invariant mass window centered at $M_{J/\psi}$.

Charged muons originating from decays of $\pi^{\pm}$ mesons are the main source of background. As a first approximation, it is assumed that a thick absorber placed in front of the muon detector filters out 100% of pions and the remaining background is due to muons from $\pi \rightarrow \mu + \nu$ decays.

As the muons from J/ψ decays ("*signal*") are emitted into opposite hemispheres, the detector is designed in form of two symmetrically positioned (relatively to the beam axis) arms, i.e. planar areas of rectangular shape, each tangent to the sphere of radius 15 m, centered at the target. The center of each arm is initially fixed at ϑ=12.5°, the maximum emission angle of signal muons. This choice was confirmed by further fine tuning. The geometry is parametrized by: ϕ - azimuthal rotation angle of the set of arms, ϑ - polar angle of the centre of each arm, R=Y/X - aspect ratio, S=2·XY [m^2] - total area of the muon detector (X,Y - dimensions of arms). 1% resolution of the momentum reconstruction in the STS is assumed. The p_T >1 GeV cut is applied to all particles. The values of presented significance are obtained for 1 week of beam with with intensity 10^9 s^{-1} on a target of 1% interaction probability.

Fig. 1 shows the positions of hits of signal and background muon pairs in the detector, projected onto the plane perpendicular to the beam axis. The latter pattern is highly asymmetric with wings extending horizontally. This suggests avoiding the horizontal positioning of arms.

Indeed, as seen in Fig. 2a, the values of S_2 as function of ϕ and R (here for a fixed area S=40 m^2), show independently of *R* a clear preference for ϕ=90°, with a gain of factor 2 in comparison with ϕ=0°. The dependence of S_2 significance on *S* and *R* (see Fig. 2b) exhibits a steep rise in the region of S$\lesssim$25 m^2 and a flat hump at higher *S*. It demonstrates that with size reduced to 25 m^2, 85% of maximum significance is kept. Furthermore $S_2(R)$ has a broad maximum at $R \approx 1.8$. For such an optimum geometry, the J/ψ detection efficiency turns out to be 4.9%.

The efficiency is also studied in terms of Signal to Background ratio (S/B). For ϑ=12.5°, due to the larger exposition to background muons the *S/B* calculated as a function of *S* and *R* drops with increasing detector area. For the previously chosen geometry (S=25 m^2 and R=1.8), S/B reaches only 0.3.

In order to increase the S/B ratio, an improved *"kink"* filter [2] was applied. It aims at filtering out muons from $\pi \rightarrow \mu + \nu$ decays, using the hit positions in STS and TRD detectors. The kink at the decay vertex adds to the accumulated declination from the initial direction caused by multiple scattering. The filter follows the track and rejects trajectories missing the windows extrapolated from the corrected hit positions. A 250 mm position resolution of TRD's was assumed. By following correlations obtained in simulation, one can extrapolate more effectively the particle hit positions to next detectors, which makes the decay events more distinguishable from the "noise" produced by multiple scattering. For the selected optimum detector geometry (S=25 m^2, R=1.8, ϑ=12.5°, ϕ=90°), S/B reaches 0.9, without deteriorating the S_2 significance. Further work involves placing the detector closer to the target in order to decrease the background of decay muons.

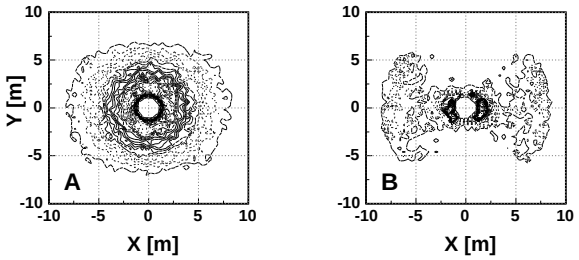

Figure 1: Hit patterns of A) signal and B) background muon pairs projected to the plane ⊥ to the beam axis.

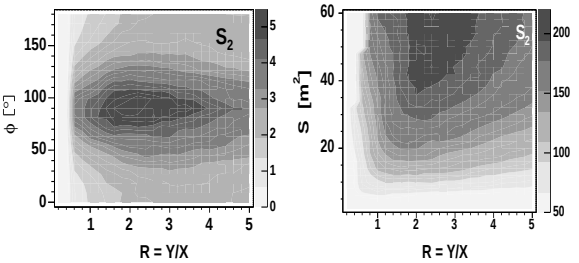

Figure 2: Significance S_2 of the J/ψ signal as a function of a) (ϕ, R) for fixed area S=40 m^2, and b) (S, R) for fixed ϕ=90°. In both cases the polar angle is fixed at ϑ=12.5°.

References

[1] CBM - Techn. Stat. Rep., GSI, Darmstadt , 2005, p.16

[2] K.Piasecki, B.Sikora, K.Wisniewski, CBM Coll. Meet., 19-22 Sep. 2006

Measurement of pion interaction in a lead absorber

S. Chattopadhyay
Variable Energy Cyclotron Centre, 1/AF Bidhan Nagar, Kolkata, India

In order to perform realistic simulations for muon detection in CBM, it is mandatory that the pion interaction in the absorbers is modelled correctly. A too narrow interaction profile in the simulations will result in underestimating the hit density in the muon chambers. In CBM, GEANT3.21 is currently being used for the simulation of the interaction of muons and hadrons throughout the absorber setup. To validate these simulations, we have performed a measurement of the interaction profile of pions in a lead absorber using a pion beam at CERN-PS, and compared the results with those obtained by a simulation with CBMROOT/GEANT3.

A high-granularity gas proportional chamber, consisting of cells of $0.23\,\mathrm{cm}^2$, has been exposed to a 6 GeV pion beam with and without a lead layer in front of the detector. These two configurations provide the comparison of interacting and non-interacting pions. Due to constraints of the experimental setup, the thickness of the lead layer was limited to 3 X_0. The test aimed at a comparison of the number of fired cells after the conversion of pions and their comparison with the results obtained from GEANT.

Fig. 1 shows the energy deposition spectrum, fig. 2 the spectrum of the number of fired cells with and without the lead converter. Without converter, the energy spectrum corresponds to the MIP spectrum, and mostly single cells are affected. The pion interaction in the converter is clearly seen in an increase in the number of fired cells and in an increase in the tail of the enrgy deposition spectrum.

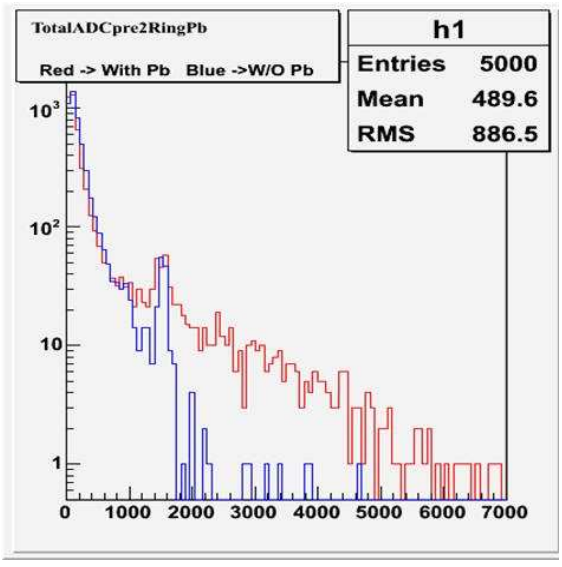

Figure 1: Energy deposition spectrum for pions with (red) and without (blue) converter expressed in terms of total ADC in the cluster. The spike in the spectrum is due to saturation in the read-out.

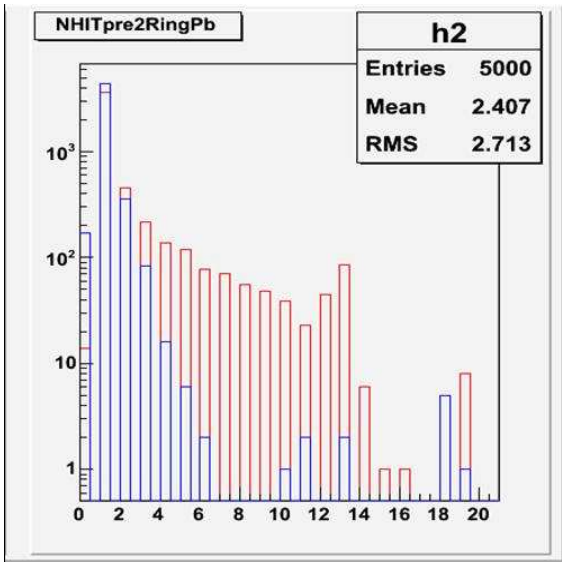

Figure 2: Spectrum of the number of affected cells with (red) and without (blue) converter

The corresponding analysis within GEANT3 was performed with exactly the same detector geometry implemented. As a final comparison, we have calculated the increase in the fraction of events above a certain energy threshold and above a threshold on the number of active cells for both experiment and simulation. Events above these threshold are considered to have interacted in the converter. It is found that the fraction of events signalling an interaction is 1.4 - 1.8 times higher in the experimental data than in the simulation. It can therefore be concluded that the number of interacting pions in the simulation must be increased by a factor of about two in order to obtain realistic results.

Feasibility studies for a muon detection system

Subhasis Chattopadhyay for the Indian CBM Muon Collaboration
Variable Energy Cyclotron Centre, Kolkata, India

The Indian CBM Muon Collaboration consists of the following Institutions:
Variable Energy Cyclotron Centre, Kolkata; Saha Institute of Nuclear Physics, Kolkata; Institute of Physics, Bhubaneswar; Bhabha Atomic Research Centre, Mumbai; Panjab University Chandigarh; University of Rajasthan, Jaipur; Aligarh Muslim University, Aligaarh; University of Calcutta, Kolkata; Banaras Hindu University, Varanasi; Indian Institute of Technology, Kharagpur; Kasmir University, Srinagar; Jammu University, Jammu

For CBM experiment Indian scientists propose to design and build muon stations for the measurement of vector mesons. India is involved along with collaborators at GSI and at other places in simulating the responses of muons in CBM. Simulations codes are installed and operational at VECC-Kolkata. Different types of geometries have been tried to optimize the performance. A version with absorber combination of W (tungsten) at the beginning and iron at the end of the chain of muon stations shows good performance. Currently we are trying to optimize the response of J/Ψ and Ψ' in CBM muon stations.

Fig. 1 shows some of the absorber-chamber design options tried in the simulation studies. One of the main aspects being investigated is the hit density at different chambers as this is an important parameter for the design of the chambers. Their number varies between 13-16.

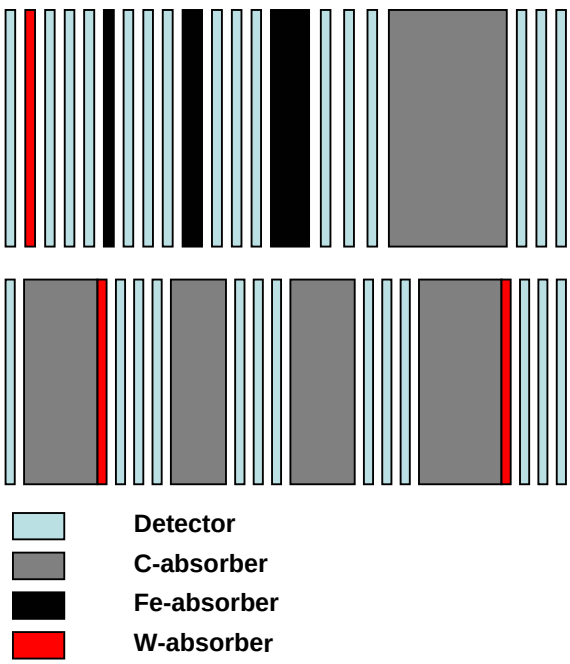

Fig. 1: Various detector-absorber combinations studied at VECC. Detector thickness = 1 cm. Top 2 figs correspond to following combinations,
(a) W5+Fe10+Fe20+Fe30+C120
(b) (C75+W6)+C60+C70+(C80+W6) e.g. Fe10 means 10cm thick Iron absorber

Fig. 2 shows the maximum hit density for different combinations shown above. Much_3st_geo and much_CW_V65.geo corresponds to configurations (a) and (b) respectively in fig.1. Much_CWFe04.geo represents another configuration where carbon is reduced and some more Fe is added in the middle.

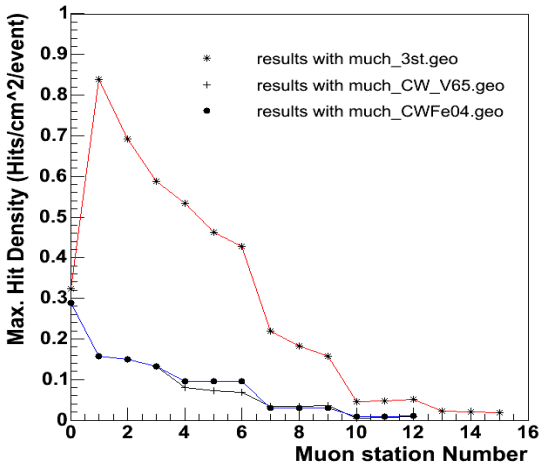

Fig. 2: Maximum hit densities at successive muon stations in different absorber-detector combinations.

We have made detailed studies on the design options available for the muon stations. According to the studies made so far, GEM-based gas detectors at first few stations and MWPC/Micromegas as other stations will satisfy the criteria for desired resolution and rate. Having good expertise in gas detector development, Indian collaborators are hopeful of building the chambers.

At VECC and at BHU, we have started testing small GEM-based chambers with radioactive sources. Readout being used is based on GASSIPLEX used in PMD of STAR experiment and in HMPID of ALICE experiment.

Muon detector simulations and choice of the RICH mirror shape *

V. Baublis, A. Khanzadeev, B. Komkov, V. Nikulin, V. Samsonov, O. Tarasenkova, and E. Vznuzdaev
PNPI, Gatchina, Russia

The PNPI team in 2006 participated in the CBM experiment in 3 main directions: the studies of the muon system absorber layout, estimations for the feasibility of modern tracking detectors for both MuCh designs and development of the mirror-adjusting mechanics for RICH.

1. The CBM muon identification system (MuCh) is supposed to be a set of absorbers interlaced with the tracking chambers. The GSI team works on the design optimized for the track-following Kalman filter procedure: a set of absorbers with subsequently increasing thickness. This design offers an optimal performance, but requires the expensive high resolution tracking detectors detectors that can work in very high hit density environment (up to $\sim$ 1 $hit\ per\ cm^2$). Somewhat different design is proposed by the members of the PNPI team. An ideal absorber should catch all hadrons, keeping the muons intact. The absorption power of the media is characterized by the "Interaction Length" (hereafter λ_I) - a mean distance between the hadron interaction, while the influence of the Coulomb interaction is reflected by the value X_0. In "classical" approach (NA50, NA60, ALICE...) the light-A absorbers (for example, made of carbon) are chosen because they offer the smallest value of X_0 for given λ_I: in other words they offer the smallest multiple scattering for given nuclear absorption.

The proposed MuCh layout consists of the 145 cm thick carbon absorber ($3.86\lambda_I$) followed by 60 cm thick iron ($3.58\lambda_I$). The total absorption length is the same as for the GSI option; at this thickness the ratio of the absorption powers for muons (due to the Coulomb scattering) and hadrons (due to hadron showers) reaches a plateau. Placing a thick carbon layer before iron one gives a possibility to reduce the hit density of secondary tracks in coordinate detectors. Thus the influence of the neighboring tracks is minimized.

The total thickness of carbon and iron layers has been fixed, but the number of iron layers and number of detectors was varied. The GEANT3-based CBMroot framework v.OKT04 was used for track transport through the detector. The background and the signal (decay muons from J/Psi and LMVM) tracks for 25 GeV Au+Au central and minimum bias events were simulated with UrQMD and Pluto generators respectively. The so-called cone method has been used for the track-finding: each STS track was considered as a muon one provided there is as minimum one hit within the multiple scattering cone around its extension in each tracking station.

The analysis demonstrated that the proposed layout of absorbers (with thick first carbon layer) allows to reach a pretty high signal to background ratio. For the minimum bias events the achieved values of the efficiency and signal-to-background ratio are quite close to the results of the GSI team (see Figure 1). For the case of central events the performance of the muon system is obviously degrades due to high hit density in tracking stations. Additional inefficiency is inherent to the cone method;the resulting efficiency drops to the level of $S/B \simeq 4 \times 10^{-3}$.

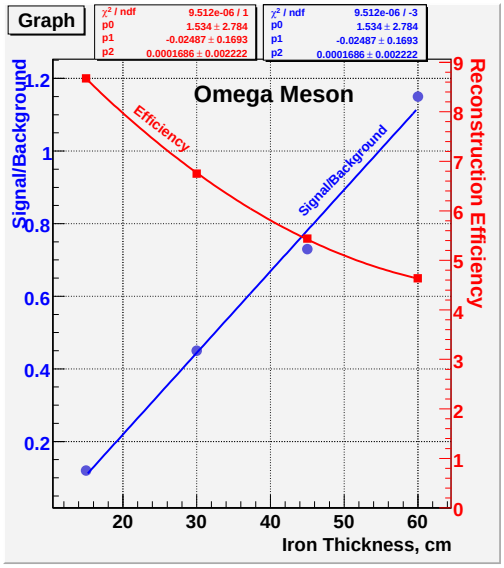

Figure 1: The signal-to-background ratio (blue line) and the selection efficiency (red curve) as a function of the number of 15 cm thick iron absorbers for the minimum bias events.

2. It has been demonstrated that the existing modern position-sensitive detectors (micromegas, GEM, even the cathode pad chambers in peripheral zone) could be used in case of MuCh. Even for the hottest zones with hit density of about 1 cm^{-2} the gas detectors could be built. However, the significant angular distribution implies the limitation on the spatial resolution of the detectors: according to our estimations one will not be able to achieve the resolution better than 0.25 mm, most likely the best resolution will be of order ~ 0.3 mm.

3. The designer team presented a conception of the design for RICH mirrors adjustment and fixation mechanics. Two prototypes were aso built: the first uses the mirror fixation at its center, in the second the mirror is fixed at 3 points in its peripheral zone. The analysis of high precision measurements prove the design.

* Work supported in part by INTAS grant 06-1000012-8781

HERA-B Dipole Magnet simulations for CBM

P. Akishin, V. Ivanov, and E. Litvinenko
LIT JINR, Dubna, Russia

As a result of the discussions at the Muon Workshop[1] and the Simulation Meeting in October 2006, the dipole magnet with a large gap from HERA-B experiment at DESY was proposed for muon measurements at CBM. The model of the magnet from HERA-B usable for "cbmroot" ("fairroot") framework [2] was created by LIT JINR group on the basis of the available technical drawing of the magnet.

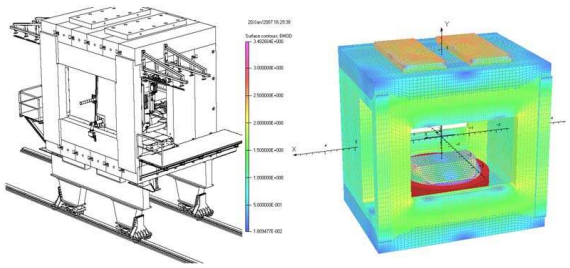

Figure 1: HERA-B magnet view (left) and its model for TOSCA (right)

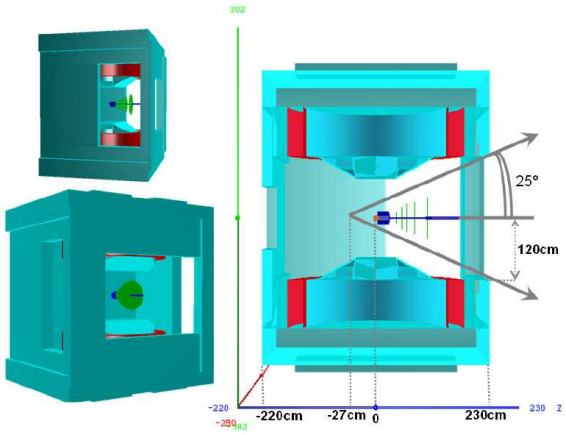

Figure 2: The magnet ("magnet_hera.geo") and STS detectors under cbmroot.

The magnetic field map for the recreated model of the magnet was calculated using TOSCA. Figure 1 (right image) shows the magnet geometry used for these calculations and the magnet view from HERA-B experiment (left picture). The same geometry was also implemented using a subset of GEANT geometry primitives that is compatible with cbmroot framework software ("magnet_hera.geo"). Figure 2 shows the perspective views of the magnet taken from GEANT transported data simulated under cbmroot together with STS detectors with a standard variant of their

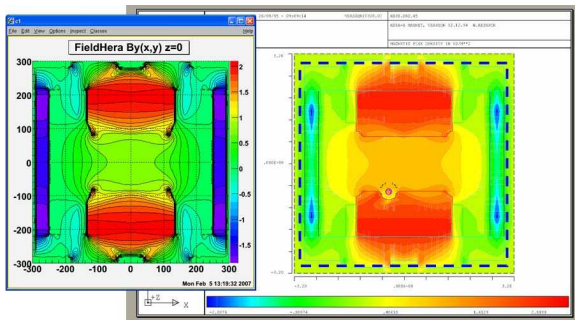

Figure 3: B_y(x,y,z=0) for implemented field map "FieldHera" (left) and corresponding picture from HERA-B (right).

geometry ("sts_standard.geo"). Figure 3 shows a satisfactory agreement of the field map "FieldHera" implemented for cbmroot with the available picture from HERA-B.

"FieldHera" (1.803 Tm)		
Magnet center	Last STS	Integral
27cm	100cm	0.668
27cm	182cm	1.005
"FieldHeraP" (1.915 Tm)		
Magnet center	Last STS	Integral
50cm	100cm	0.681
77cm	154cm	1.006

Table 1: Field Integral [Tm] from the target to the last STS detector of "Hera" and "HeraP" field maps for different magnet center and last STS detector positions

To achieve the required angular acceptance of 25 degrees it is necessary to locate the center of magnet not further than in 27 cm from the target, thus understating the field integral. In order to increase aperture, we developed a modified model of the magnet (geometry "magnet_hera_p.geo" and field map "FieldHeraP"), in which the size of the magnet along y axis was increased by 60 cm . Certainly, this will require changes in the walls of the magnet by means of the growth with the pieces of iron with a height of 60 cm. But then the magnet can be placed on the distance to 90 cm from the target without loss of the angular acceptance of the installation. The field integrals are shown in Table 1.

References

[1] http://www.gsi.de/documents/FOLDER-1161100002_e.html
[2] http://cbmroot.gsi.de/

HADES@SIS100

A.Kugler[1], J.A.Garzon[3], M.Golubeva[2], D.Gonzalez-Diaz[4], F.Guber[2], R.Holzmann[4], P.Tlusty[1]

[1]Nuclear Physics Institute, Czech Academy of Sciences, 25068 Rez, Czech.Republic; [2]Institute for Nuclear Research, Russian Academy of Science, Moscow, 117259 Moscow, Russia; [3]Departamento de Fisica de Particulas, University of Santiago de Compostela, 15706 Santiago de Compostela, Spain; [4]Gesellschaft für Schwerionenforschung (GSI), 64291 Darmstadt, Germany

While the CBM experiment at FAIR will be designed to study heavy-ion collisions above about 10 AGeV, the energy range from 2 – 10 AGeV, accessible also with the future accelerator facility, can be covered by an upgrade of the existing HADES setup. Therefore we carried out simulations of dilepton production in heavy-ion collisions at bombarding energies of about 8 AGeV as seen by the HADES detector, for details see [1].

The TOFINO subsystem of HADES, covering the azimuthal angles of $18^o < \theta < 45^o$ has a granularity equal to 4x6 modules only. We used the UrQMD code [2] to simulate the production of charged hadrons in the collision, resulting in a mean multiplicity of charged hadrons detected in the TOFINO acceptance as large as 80x6 for the most extreme conditions. Consequently, the TOFINO has to be replaced by a new subsystem with a much higher granularity. Such a subsystem based on RPC detector rods with widths in the range of 2-5 cm and different lengths is currently under construction. The resulting hadron occupancies of one rod for C+C@2AGeV increase by a factor of 16 when going to Au+Au@2AGeV (b=0-4 fm) and by an additional factor of 2 when going to Au+Au@8AGeV.

Finally, we simulated the full "dilepton cocktail". All meson sources were generated simultaneously with the proper weights per event using the PLUTO code (version 4_08), with realistic models of resonance production, as well as of the hadronic and electromagnetic decays. For ω and φ mesons, both Dalitz and direct decays were generated. To include into the simulation the HADES geometry, the generated events were filtered with acceptance matrices that take into account the momenta, azimuthal and polar angles of the leptons. The analysis of the generated events was performed with a smearing of the lepton momenta to take into account the detector resolution and with rejection of the closed pairs (a cut in opening angle of 9^o was applied to the lepton pairs). To be more specific, for beam energies of 1-2 AGeV, the meson production probabilities for π^0 and η were calculated according to C+C and Ca+Ca TAPS experimental data [3], and the probabilities for ω and φ were obtained from an m_t-scaling ansatz. For a beam energy of 8 AGeV the production probabilities of π^0 per participant were derived from the experimental data published in [4]. To get values for other mesons is not easy, because there are no experimental data for this energy. Therefore, the ratios for η, ω and φ mesons were obtained from a thermal model [5].

The resulting spectra for Au+Au collisions with b=0-8 fm (228 participants) are given in Fig. 1 and they correspond to 3.2 10^7 collisions at 8AGeV, respectively.

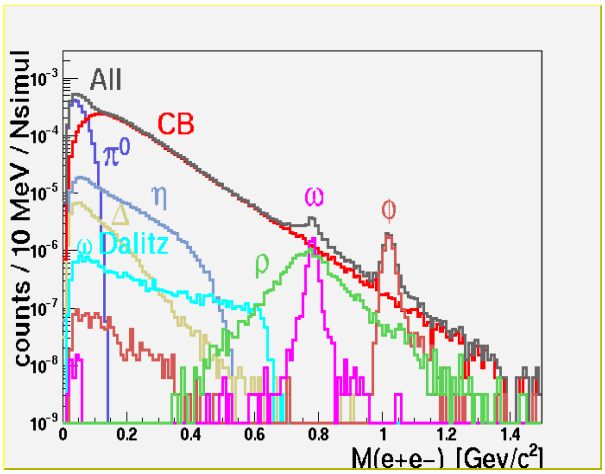

Figure 1: Simulated invariant-mass distribution of dilepton pairs per collision detected by HADES for Au+Au at 8 AGeV Fully simulated cocktail (black line) and combinatorial background (red line), as well as various cocktail components are shown.

To conclude, our simulations demonstrate that, in principle, HADES in its current configuration and after replacement of the TOFINO by a high granularity RPC wall is able to detect dileptons using beams up to an energy of 8 AGeV, which will become available at the new FAIR facility.

This work has been supported by GA AS CR IAA1048304 (Czech Republic), BMBF (Germany), MCYT FPA2000-2041-C02-02 and XUGA PGIDT02PXIC20605PN (Spain), INTAS-03-51-3208.

References

[1] A.Kugler et al. Proceedings of XLIV International winter meeting on Nuclear Physics, Bormio 2006, Vol.125,p.282-6
[2] S. Bass et al;. Prog. Part. Nucl. Phys. 41 (1998) 225
[3] R.Averbeck at al., TAPS collaboration, Z. Phys. A359 (1997) 65;
R. Averbeck at al., Phys. Rev. C67 (2003) 024903
[4] J.L.Klay et al. Phys. Rev. C68 (2003) 054905
[5] J. Cleymans and H. Satz, Z. Phys. C57 (1993) 135

Dielectron Detection Capabilities of HADES for Beam Energies accessible at FAIR

B. Bannier[1], F. Dohrmann[1], E. Grosse[1,2], B. Kämpfer[1], R. Kotte[1], L. Naumann[1], and J. Wüstenfeld[1]
[1]FZD, Dresden; [2]TU Dresden

For the FAIR project considerable updates of existing accelerator facilities at the GSI Darmstadt are projected. The available beam energies of the new SIS100 and SIS300 accelerators will be in the range of 2 AGeV to 45 AGeV. Experiments with both elementary probes as well as heavy-ions at beam energies $\leq$ 3.5 AGeV have been performed with the HADES detector at SIS18. The possible dielectron detection capabilities of HADES at the new facilities, focusing on Carbon–Carbon collisions at beam energies of $8 - 25$ AGeV were studied. Simulations were carried out using an event generator based on the state of the art relativistic transport code UrQMDv1.3p1 [1] together with a generic interface for additional decays simulated with the PLUTO phase space generator on top of UrQMD. In particular, this is used for implanting dielectron decay channels into UrQMD events. The dielectron sources considered are π^0, η, Δ^+, ω, ρ^0 and ϕ. A considerable source of background is photon conversion $\gamma \rightarrow e^+e^-$. Important sources of photons are the decays of π^0 and η mesons, therefore these decays have been processed independently of other sources to allow for a correct event structure. Based on this event generator dielectron spectra for 8 AGeV and 25 AGeV are shown in Fig. 1 taking into account only the geometrical acceptance of the HADES detector as it is currently installed. Tracking of particles through the magnetic field has not been included in these studies.

For both energies a peak in the ρ, ω mass region is visible, although the background situation at the higher energy deteriorates considerably. While the combinatorial background was found to be an important source of dielectrons, in our simulation distributions of like-sign pairs gave a good description of the combinatorial background. The yield of true pairs from $\omega \rightarrow e^+e^-$ decays was found to be above the combinatorial background in the respective invariant pair mass region. The like-sign method allows subtraction of the combinatorial background from spectra and the yield of true pairs from $\rho^0 \rightarrow e^+e^-$ is larger than the fluctuations of the combinatorial background. The ϕ meson yield found was too low compared to the expected ρ^0 yield in the respective invariant mass region to allow reliable studies. In summary, the simulations indicate that a determination of the yield of true pairs from particle decays in the $\rho - \omega$ mass region after one week of beam time seems feasible. Further investigations have to consider the HADES acceptance (possibly with modified hardware setups); tracking of the particles through the magnetic field and the detector material should be taken into account. This study [2] has to be seen in line with other studies [3,4] on this subject.

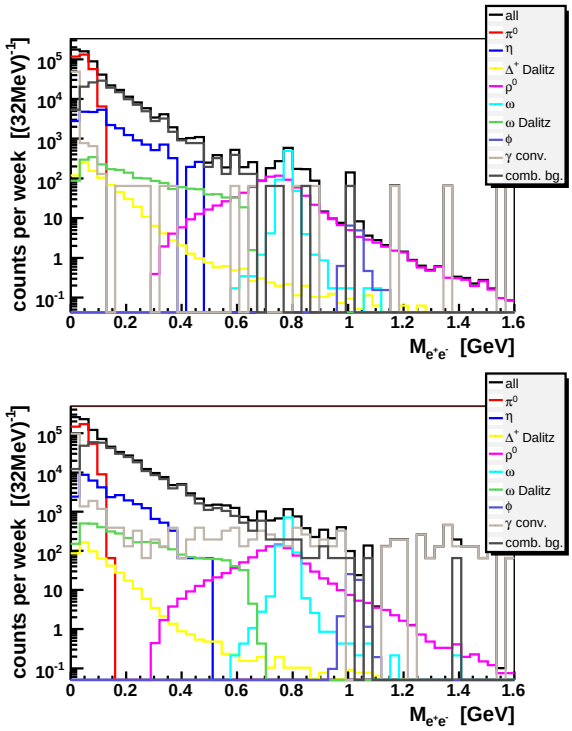

Fig. 1: Invariant mass spectra for central Carbon-Carbon collisions at beam energies of 8 AGeV (upper panel) and 25 AGeV (lower panel) after one week of beamtime. Pairs are created from all e^+ and e^- emitted into the geometrical HADES acceptance with momenta $p > 50$ MeV. Leptons from pairs with opening angles smaller than 9^o are excluded. Particle momenta have been convolved with a momentum dependent error following the procedure given in [5]. Details on how to subtract combinatorial background using the like-sign method are given in [2].

References

[1] http://www.th.physik.uni-frankfurt.de/∼urqmd
[2] B. Bannier, Diploma Thesis, Technische Universität Dresden, Sep. 2006
[3] T. Galatyuk and J. Stroth, CBM-PHYS-note-2006-001, internal report, GSI Darmstadt 2006
[4] A. Kugler, Talk at CBM meeting, GSI Darmstadt 2004; Proc. Nucl. Phys. Winter meeting, Bormio 2006
[5] R. Holzmann, HAFT: Hades Acceptance Filter for Theorists, internal report, GSI Darmstadt 2006, http://hades-wiki.gsi.de/cgi-bin/view/SimAna/HadesAcceptanceFilter

Results on timing properties of SCCVD diamond detectors for MIPs

M. Petrovici, M. Petriş, G. Caragheorgheopol, V. Simion, D. Moisă
National Institute for Physics and Nuclear Engineering, Bucharest, Romania
E. Berdermann, M. Ciobanu, A. Martemiyanov, M. Pomorski
Gesellschaft für Schwerionenforschung, Darmstadt, Germany

First encouraging results on timing performance of diamond detectors for MIPs were obtained using policrystal diamond detectors (PC) [1]. The timing properties of two single crystal diamond detectors (SCCVD-DD)with a thickness of 300 μm and 500 μm using a ^{90}Sr source and an applied electric field of $\sim$ 1 V/μm are presented in this report. The diamonds were placed in the collimated beam of beta particles, the reference signal being delivered by a NE102 plastic scintillator.

In the first measurements the signals delivered by the SCCVD-DD were amplified by fast amplifiers developed for multistrip multigap resistive plate counters (MSMGRPC) [2] and a FTA810L amplifier. The amplified signals of the SCCVD-DD and the signal of the plastic scintillator coupled with a phototube were split and processed for charge and timing information.

The start signals were delivered by the overlap coincidence between the signals of the diamond detector and the plastic scintillator. Fig.1 shows the charge distribuitions for the 300 μm thickness diamond detector (Fig.1a) and for the plastic scintillator (Fig.1b).

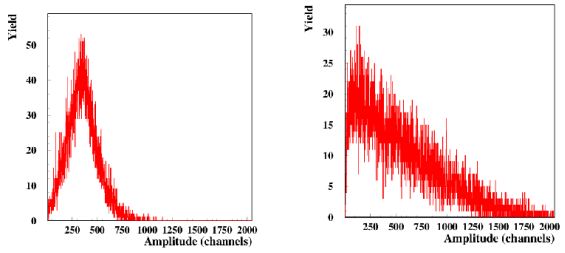

Figure 1: Charge distribution for: a) 300 μm diamond detector and b) plastic scintillator

The obtained time of flight spectrum after walk correction can be followed in Fig 2a. Subtracting the contribution of the plastic scintillator of 125 ps, measured between two identical plastic scintillators coupled to identical phototubes, a time resolution of 147 ps is obtained.

The time of flight spectrum obtained using the SCCVD-DD of 500 μm thickness and the same experimental setup is shown in Fig.2b. The time resolution under this condition, after subtracting the contribution of the reference detector, was 214ps. In the second part of the measurements the signals delivered by the SCCVD-DD were amplified by a charge sensitive preamplifier (CSA) with a 0.7 ns rise time. The rest of the experimental setup was the same. The results are presented in Fig.3.

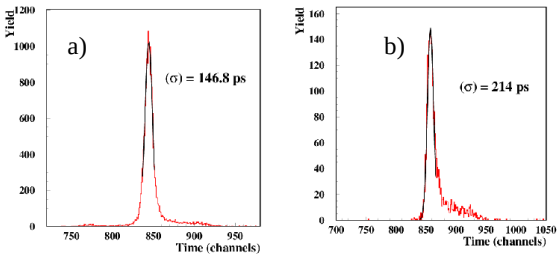

Figure 2: The time of flight spectra after walk correction: a) 300 μm and b)500 μm SCCVD-DD

The time resolution obtained using the SCCVD-DD of 300 μm thickness and a CSA with 0.7 ns rise time is 374 ps, while for SCCVD-DD of 500 μm thickness a time resolution of 1.14 ns is obtained.

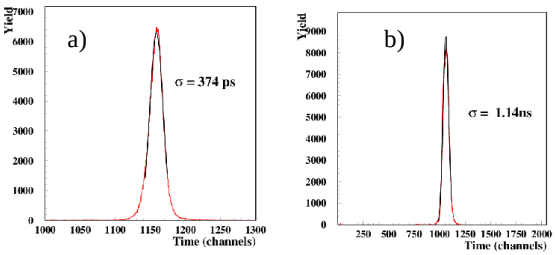

Figure 3: Time of flight spectra using charge sensitive preamplifier with 0.7 ns rise time: a) 300 μm abd b)500 μm SCCVD-DD

Based on the results presented in this report one could conclude that better results were obtained using the thinner detector for the same FEE used for the amplification of the signals delivered by the SCCVD-DD. Better performance in terms of time resolution gives the fast FEE electronics developed for MSMGRPC. Detailed efficiency studies and in-beam tests are in progress.

References

[1] M. Petrovici, E. Berdermann, M. Petriş, G. Caragheorgheopol, D. Moisă, NIPNE Scientific Report, 2001, p. 43

[2] M. Ciobanu, A. Schüttauf, E. Cordier, N. Herrmann, K.D. Hildenbrand, Y.J. Kim, Y. Leifels, M. Marquardt, M.Kis, P.Koczon, M. Petrovici, J. Weinert, X. Zhang, will be published

Achievements of CMOS Pixel Sensors for the CBM Micro-Vertex Detector

S.Amar-Youcef[1], A.Besson[2], G.Claus[2], M.Deveaux[1,2,3], A.Dorokhov[2], W.Dulinski[2], S.Heini[2], A.Himmi[2], K.Jaaskelainen[2], Ch.Müntz[1], F.Rami[2], J.Stroth[1], I.Valin[2], and M.Winter[2]

[1]J.W.Goethe Universität, Frankfurt; [2]IPHC and Université L.Pasteur, Strasbourg; [3]GSI, Darmstadt

It was already established that CMOS sensors provide the single point resolution and reduced material budget required for the ambitionned MVD vertexing performances. Achieving these performances in the CBM running conditions is however challenging, especially because of the required radiation tolerance and read-out speed. Important steps addressing these issues were made in 2006. Moreover, a new generation of real size sensors was fabricated, to be used for thinning and system integration studies [1].

Fast read-out architecture

The fast read-out architecture developped for the CBM MVD extrapolates from the MIMOSA-8 prototype, designed for the ILC vertex detector. The sensor includes correlated double sampling micro-circuits and discriminators, and delivers discriminated binary signals [2]. Its single point resolution was evaluated in Summer 2006 at the CERN-SPS. A resolution of $\lesssim 7\ \mu m$ was found, i.e. slightly better than the intrinsic resolution ($\sim 7.2\ \mu m$) reflecting the pixel pitch (25 μm). This result indicates that integrated ADCs may not be mandatory to get a single point resolution as small as $\sim 5\ \mu m$, provided the pixel pitch is kept small enough (typically $\lesssim 18\ \mu m$). This perspective coincides with the need for a small pitch in order to enhance the sensor tolerance to bulk damage, by reducing the distance the signal charges have to cross in order to reach a sensing diode.

MIMOSA-8 was manufactured in TSMC 0.25 technology, which features a $\lesssim 7\ \mu m$ thick epitaxial layer. The chip was translated in 2006 into the AMS 0.35 OPTO technology (MIMOSA-16), where the layer is $\sim 11\ \mu m$ thick. Besides a larger signal amplitude, MIMOSA-16 also includes other improvements: enhanced tolerance to ionising radiation (MIMOSA-15 pixel architecture [2]), as well as pixels incorporating high gain amplification micro-circuits.

Since it is not yet clear whether integrating an ADC at the end of each column may be avoided, various ADC architectures are being developed, in synergy with the ILC requirements. The first ADC prototypes (5-bit Wilkinson and 4-bit successive-approximation) designed at IPHC were submitted to fabrication in Autumn 2006. Prominent design challenges include compactness, aspect ratio, signal processing speed and power dissipation.

Radiation tolerance

Radiation tolerance studies started with MIMOSA-15 in 2005 [2] were complemented in 2006 with ~ 5 GeV/c e^- beam tests at DESY.

A sensor exposed to an integrated dose of ~ 1 MRad (obtained with a 10 keV X-Ray source) was observed to still exhibit a S/N ratio of 19 (it was 27 before irradiation), and a detection efficiency of ~ 99.9 % at a coolant temperature of -20°C (180 μs integration time). These performances validate the pixel architecture implemented against parasitic leakage current generated by ionising radiation.

MIMOSA-15 chips irradiated with 1 MeV neutrons were studied on the same beam. A sensor exposed to $\sim 2{\cdot}10^{12} n_{eq}/cm^2$ still exhibited a detection efficiency above 99 % at a coolant temperature of -20°C. For a fluence of $\sim 6{\cdot}10^{12} n_{eq}/cm^2$, the detection efficiency dropped to ~ 80 %. Given the available room from improvement, these results indicate that fluences $\gtrsim 10^{13} n_{eq}/cm^2$ per MVD layer are likely to be tolerable.

Improvements include pixel design optimisation and fabrication process choices which reduce the diffusion path of the signal electrons before reaching a sensing diode. Efforts were made in 2006 towards this goal, on the one hand by designing pixels featuring L-shaped sensing diodes and on the other hand by fabricating a sensor in a BiCMOS process featuring an epitaxial layer with a relatively high resistivity expected to allow for substantial depletion.

New generation of real size sensors

The most attractive fabrication technology characterised so far is the AMS-0.35 OPTO process. Excellent tracking performances were obtained with 5 consecutive small prototypes fabricated in this technology since late 2003, which was chosen for the sensors currently developed for short term tracking applications (STAR HFT, EUDET beam telescope). The latter triggered an engineering run in 2006, which was used to produce simultaneously a real size, multi-purpose sensor, intended to equip a first generation MVD demonstrator. The sensor, which features 256x256 pixels of 30 μm pitch, is read out in $\lesssim 1$ ms. It was fabricated in 2 different versions, one where the epitaxial layer is $\sim 11\ \mu m$ thick (default value) and one where it is expected to be $\gtrsim 16\ \mu m$ (new commercial option). The engineering run was also motivated by the possibility to study the fabrication yield and to have a stock of real size sensors available for thinning and system integration studies.

References

[1] M.Winter, "Status of CMOS sensor R&D", talk presented at the CBM collaboration meeting, Sept. 2005, GSI/Darmstadt;

[2] 2005 GSI Annual Report and references therein.

Layout studies of the CBM Silicon Tracking System

J. M. Heuser[1], R. Karabowicz[1], and E. Kryshen[2]
[1]GSI, Darmstadt, Germany; [2]St. Petersburg State Polytechnic University, Russia

The Silicon Tracking System (STS) is the central detector of the CBM experiment. It serves for track and momentum measurement of all charged particles produced in nuclear reactions at the target. Au+Au collisions at FAIR energies generate up to 1000 charged particles whose tracks have to be efficiently reconstructed with about 1% momentum resolution [1]. This task requires a low-mass silicon tracking detector system of high granularity. We are studying the layout of tracking stations made from thin micro-strip and pixel detectors, and their arrangement in a dipole magnetic field of 1 Tm bending power.

Detector Concept

The STS concept, schematically shown in Fig. 1, comprises 6 detector stations for the track measurement. Two stations may consist of LHC-type hybrid pixel detectors. Those are relatively thick and presumably require active cooling in the aperture, but contribute with unambiguous space points to the track finding where the track densities are high. For the remaining four stations, low-mass micro-strip detectors are considered to perform the track point measurement. The projective coordinate measurement of the sensors leads to a significant fraction of combinatorial or fake hits, a challenge to the reconstruction algorithms. However, the application of micro-strip sensors may lead to particularly low-mass stations if their power-consuming readout electronics can be placed outside of the STS aperture, a current R&D effort reported in [2] and [3]. For high-resolution vertex measurements, e.g. open charm detection, the STS is supported with a Micro-Vertex Detector (MVD) consisting of two very thin and fine-pitch MAPS pixel detector stations close to the target.

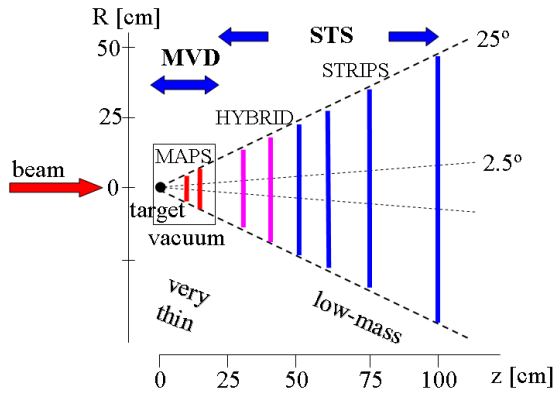

Figure 1: Schematics of the STS + MVD detector systems.

Performance Studies

We implemented the detector stations in the simulation framework CBMROOT as discs of silicon, with a thickness equivalent to the total average material expected from a real detector. During the hit digitization, a specific detector structure was projected onto the volumes. The hybrid pixel stations were segmented into 50×50 μm^2 pixels. The micro-strip stations were made from double-sided sensors segmented into strips of 50 μm pitch with a 15 degree stereo angle between front and back side. Central 25 GeV/nucleon Au+Au collisions from the URQMD generator were transported through the detector and reconstructed with a cellular automaton for track finding and a Kalman filter for track fitting [1]. Reconstruction efficiencies of about 97% (92%) for primary (all) tracks exceeding 1 GeV/c momentum, and a momentum resolution between 1% and 2% depending on the detector thickness (assessed in a parameter study, see Table 1) demonstrate the feasibility of the track measurement with the proposed detector concept.

		thin	standard	thick	thick-2	thick-3
MAPS	[μm Si]	2×150	2×150	2×150	2×150	2×150
Hybrid	[μm Si]	2×200	2×750	2×800	2×1000	2×1600
Strips	[μm Si]	4×200	4×400	4×800	4×1000	4×1600
total	[μm Si]	1500	3400	5100	6300	9900
total	[% X_0]	1.6	3.6	5.5	6.7	10.6
Δp/p	[%]	0.83	1.21	1.47	1.61	2.02

Table 1: Momentum resolution Δp/p as a function of the effective detector thickness.

Layout Iterations

Current performance studies investigate the effects of different strip lengths and stereo angles on the track reconstruction. We also study detector configurations where e.g. the hybrid pixel stations are replaced with pairs of micro-strip stations slightly rotated against each other. Next steps will focus on more complex and realistic implementations of the STS. This includes detailed geometrical models of the tracking stations, built from sensor wafers arranged into modular structures and mounted on mechanical supports.

References

[1] I. Kisel et al., *Event Reconstruction in the CBM Experiment*, this report
[2] J. M. Heuser et al., GSI document DOC-2006-Dec-19
[3] J. M. Heuser et al., *Development of Microstrip Sensors for the CBM Silicon Tracking System*, this report

Development of Microstrip Sensors for the CBM Silicon Tracking System

J. M. Heuser and Chr. J. Schmidt, GSI, Darmstadt, Germany

We have designed the first prototype of a silicon micro-strip sensor that can serve as a building block of detector modules for CBM's Silicon Tracking System.

Tracking Stations

The tracking stations are planar arrangements of micro-strip sensors, grouped into several modules of either the same or different length, that cover at given positions downstream of the target the fiducial area approximately between 2.5 and 25 degrees polar angle. Figure 1 visualizes this station concept with a vertical orientation of the modules and the long direction of the strips perpendicular to the bending plane of the magnet for best momentum measurement. The first and smallest station may be as close as 30 cm to the target. The last and largest station will be in about one meter distance from the target. One of the key requirements of the Silicon Tracking System is a low-mass design to achieve momentum measurement with about 1% resolution. Silicon micro-strip detectors are compatible with a low-mass design as the sensors themselves are thin. With an appropriate module structure, active readout electronics with its cooling requirements and material involved may be avoided in the aperture. The strongly inhomogeneous track density profile makes a sectorized module structure necessary. Close to the beam line, a module must comprise sensors with short strips. Longer strips, realized either on single wafers or by chaining two or more sensors, can be employed in the regions further outside. Those different "sectors" must be read out individually. This may be realized by routing the strips' analog signals from every sector through thin flat multi-line cables to front-end electronics at the periphery of the stations.

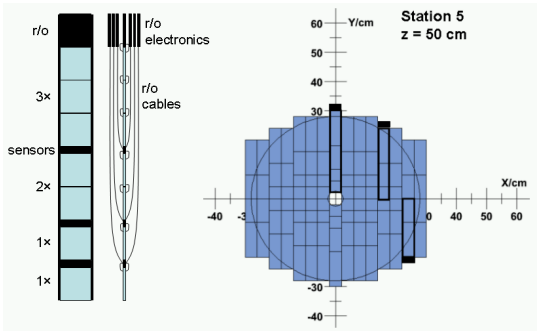

Figure 1: Silicon micro-strip sensors arranged into modules of different lengths building up a tracking station.

Sensor Design

We focused on a sensor compatible with this detector module structure. The design, shown in Fig. 2, addresses in particular connectivity issues. We intend to employ double-sided sensors with one strip orientation along the module's long axis, and a "stereo" direction on the second side. We strived to accomplish that both sensor sides can be contacted both at the top and the bottom edge. On the stereo side, this requires interconnections on a second metal layer between the strips of the two corner regions. This layout will enable us to chain several sensors, thus forming long strip sectors for the outer regions of the tracking stations. A staggered arrangement of the contact pads was applied allowing a wire-bonding scheme that conserves the correlation of neighbouring channels through the chain up to the readout electronics. Small stereo angles are preferred as unavoidable dead area on the sensor sides is kept small.

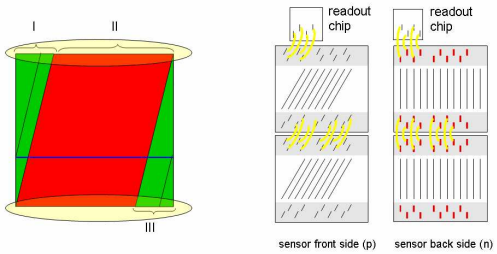

Figure 2: (Left) Schematics of the sensor's stereo side. (Right) Chained sensors and their interconnections.

Detector R&D

The first sensors, to be produced in 2007 [1], will have a thickness of 200–300 μm, are double-sided with 2×1024 AC-coupled strips of 50 μm pitch and feature a 15° stereo angle between front and back side. They will be utilized for the construction of a prototype detector module: an assembly of chained sensors, readout electronics [2] and mechanical support. Forthcoming prototypes will address radiation hardness, the minimization of inactive area near the edges, and will touch e. g. the biasing technique and the layout of the guard rings structure. The development of readout cables, made from fine-pitch aluminum traces on polyimide material for minimum material budget, is a particular important task. The capacitance of sensor and cable at the input of the front-end electronics must be small enough to achieve a sufficiently large signal-to-noise ratio.

References

[1] CiS Institut für Mikrosensorik gGmbH, Erfurt, Germany

[2] Chr. J. Schmidt et al., this report

Silicon Microstrip Sensor Prototypes for CBM

M. Merkin, D.Karmanov, N.Baranova
Skobeltsyn Institute of Nuclear Physics, Lomonosov Moscow State University

N.Egorov, S.Golubkov, A.Sidorov
Research Institute of Material Science and Technology, Zelenograd, Moscow

We have started to explore the design and the production of double-sided microstrip sensors for CBM's Silicon Tracking System, with focus on thin detectors and radiation tolerant design features.

Double-sided strip sensors: Thin, radiation hard

Silicon sensors are essentially not commercial products. Custom geometries and a variety of special requirements have to be taken into account for a given application.
For the CBM experiment, the challenge is to establish reliable technologies for the processing of both sides of thin silicon wafers. The goal is to manufacture low-mass double-sided sensors with long, fine-pitch charge collecting strips, laid out in a radiation tolerant design. There is very limited experience in the world on the production of double-sided radiation tolerant sensors.

R&D steps

For this project, High Reflectivity Wafers (HiREF®) from Wacker-Siltronic have been used. The planned R&D steps are:

(1) Sensor design and mask production:
   a. Single-sided test detectors with 50 µm strip pitch and DC or AC readout.
   b. Double-sided sensors with 50 µm strip pitch and 15º stereo angle between front-and back sides. Strips poly-silicon biased, AC-coupled readout.
(2) Production of 250 µm sensors.
(3) Optimization of the sensor design.
(4) Technology optimization of the production process.
(5) Production of 200 µm sensors.
(6) Detailed tests of the produced sensors.

First results from single-sided sensors

Two batches of test wafers have been processed in steps (1a) and (2) to qualify the 250 µm wafer material for the forthcoming production: One batch of sensors with 2 cm long single-sided DC strips of 50 µm pitch on 2 × 4 cm^2 area, and one batch with single-sided AC-coupled strips of the same design. Measurements with the DC strip sensors are shown in Fig.1. The IV-characteristics indicates good wafer material, with full depletion at around 100 V and high-voltage breakdown beyond 500 V. The leakage current for the given resistivity of 3 kOhm and the given thickness of 250 µm is reasonable: about 5 nA/strip. We can therefore proceed with the R&D steps as planned.

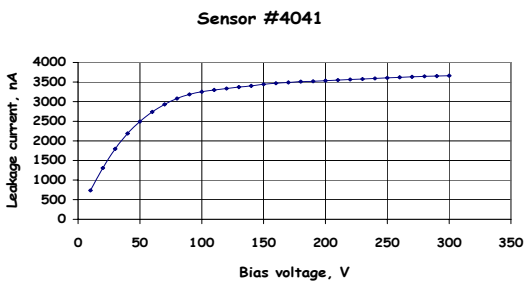

Figure 1: Current-voltage characteristics of a single-sided microstrip sensor on a HiREF® silicon wafer.

Design and production of double-sided sensor

The study of double-sided strip sensors matching the CBM specifications is in the center of our project. The design of a prototype sensor was recently completed (step 1b). Figures 2 and 3 show the corner regions of the N-side, and P-side. The stereo angle of the P-strips with respect to the N-strips is clearly seen, as well as the small DC probe pads and the double-row of larger AC readout pads. The design takes into account several features to enhance the radiation tolerance of the detector: Poly-silicon bias resistors on both the P and the N sides, P-stop implants between the strips on the N-side, and a multi-guard ring structure. The production masks have been fabricated. The complete set consists of 17 masks: 7 for the P-side, 9 for the N-side, and one additional mask for fiducial marks.
After full characterization of the test sensors, the production of double-sided microstrip sensor prototypes will be started with 250 µm wafers or thinner.

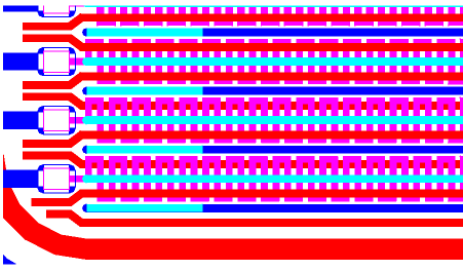

Figure 2: N-side design.

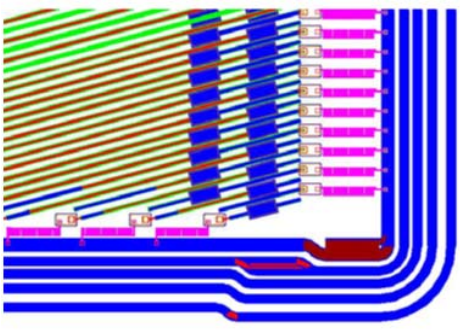

Figure 3: P-side design.

Prototype of the small diameter PMT for the RICH photo-detector plane

V.Brekhovskikh*, V.Dyatchenko*, V.Lapshin*, M.Medynsky*, V.Rykalin*, and S.Sadovsky*
* Institute for High Energy Physics, Protvino, 142281 Russia

The prototype of small diameter PMT FEU-Hive was produced in IHEP (Protvino) as the main option of the RICH UV photo-detector. This is a special small diameter photo-multiplier tube on the base of a resistive distributed dynode system with electrostatic focusing, bialkaline photo-cathode and tube with a glass window. The external diameter of the PMT FEU-Hive prototype is equal to 7.5 mm and the tube length is of the order of 100 mm. In total it was produced and studied more than 20 phototubes. One of the fully assemled PMT FEU-Hive is shown in Fig.1.

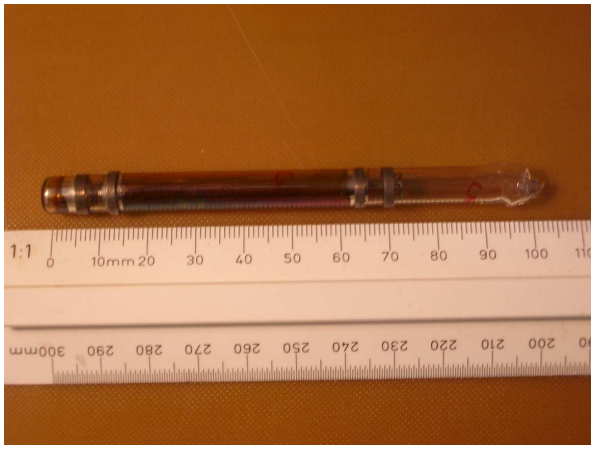

Figure 1: One of the PMT-Hive phototubes.

The phototubes were tested with the LED source at the special testbench. The basic measured parameters of the best produced FEU-Hive phototube are given in Table 1. As for PMT timing pulse shape, the typical single-photoelectron signals of FEU-Hive is shown in Fig2. One can see, that FEU-Hive is the sufficiently fast phototube to be effectively used in the RICH photodetector plane for the expected event rate.

External PMT diameter	7.8 mm
Photo-cathode diameter	6.5 mm
PMT length	100 mm
Photo-cathode:	K_2CsSb
Quantum efficiency, 410 nm	14 %
Nominal HV	1.5 kV
Amplification	$5x10^5$
Capacitance	10 pF
Power dissipation	0.25 mW
Dynamical charge range	3.0 pC
Noise current	5000 e/sec

Table 1: Parameters of the best PMT FEU-Hive.

The first data on operation of PMT-Hive with a WLS film on the photocathode window were obtained in a wide spectral region of Cherenkov irradiation excited by a ^{90}Sr radioactive source in a MgF_2 crystal of 5 mm thickness.

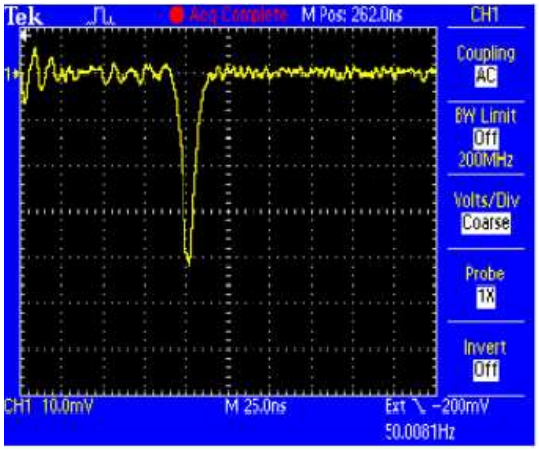

Figure 2: The typical single-photoelectron signals of PMT-Hive.

The edge of 90% transmission of this crystal corresponds to 130 nm and therefore crystal irradiation can simulate Cherenkov light in the CBM RICH detector. The WLS film based on a 15 μm teflon film with 20 μm layer of crystalline paratherphenyl on the upper surface was designed at IHEP with a special technology. The first results for the efficiency of WLS films, i.e. the average ratio signals from PMT-Hive with WLS films and without it, is equal to 1.85. The WLS efficiency measurements were perform in an atmosphere of technical nitrogen. But definitly the efficiency of WLS films should be better in the cases of high purity nitrogen or other gases transparent in the region of vacuum ultraviolet.

Thus, practically all measured characteristics of the FEU-Hive phototube correspond to the design goals of the CBM RICH photodector except for photo-cathode quantum efficiency. An increase of the quantum efficiency to the desired value, dicussed in CBM TSR, could be achieved with tuning of the mass production technology of the PMT FEU-HIVE having in mind the already obtained 24.4% photo-cathode for one of the produced phototubes.

Test of Transition Radiation Detectors for high rate environments

C. Garabatos[1], D. González-Díaz[1], A.Kalweit[2], F. Uhlig[1], and the CBM Collaboration
[1]GSI, Darmstadt, Germany; [2]TU Darmstadt, Darmstadt, Germany

Motivation

For the planned Compressed Baryonic Matter (CBM) experiment prototypes of Transition Radiation Detectors (TRD) were developed and tested. The TRD will be used for particle tracking and identification of high energy electrons and positrons for J/Ψ reconstruction.
Due to the fixed target geometry of the CBM experiment (see . Friese et al.,this report) particle rates of 100 kHz/cm^2 are expected for the innermost part of the first TRD station. At this rates a reduction of the effective gas gain of the TRD may appear due to build up of charge in the counting gas. Since the electron id is based on the signal amplitude, it is important for the TRD that the gain stays constant up to the highest expected particle rates. We present here results on this issue. The tested prototypes are very thin MWPC with an anode-cathode distance of only 3mm and a anode-wire pitch of 2mm with pad readout. This design is a compromise between the requirement of fast signals on the one hand and the necessity to absorb transition radiation photons on the other hand.

Setup

The measurements are performed using a X-ray tube to produce photons of an energy of 8keV which is calibrated using a ^{55}Fe source. The produced X-ray beam is collimated and attenuated with different sets of aluminum or nickel foils before entering the prototype. The size of the beam spot on the detector was measured to be 0.756 cm^2 using a Polaroid film. The gas gain is defined as

$$G = \frac{N_{e^-_{final}}}{N_{e^-_{primary}}} = \frac{I}{N_{e^-_{primary}} \cdot q_{e^-} \cdot R} \qquad (1)$$

where R is the absorbed photon rate in the detector, I the measured current and Ne the number of primary electrons produced by the X-ray photon. This number is taken from measured data [1].

Results

Figure 1 shows the measured gain as a function of the rate for a Xe-CO_2 mixture at different initial gains. The gain decreases with increasing rate due to the space-charge effect, which results in the screening of the electric field near the anode wire thus affecting the gain. The solid lines are a fit to the data using Mathieson's formula [2]

$$\ln(G/G_0)/G = KR \qquad (2)$$

where G_0 is the gain at zero rate and K is a constant which takes into account the chamber geometry and the gas properties.

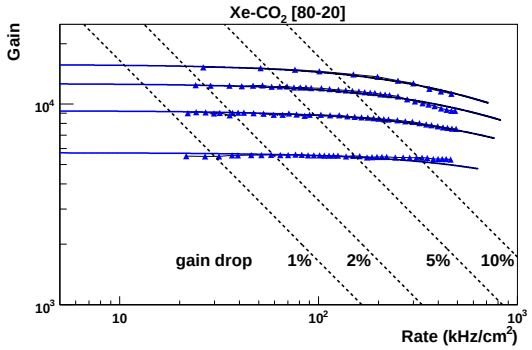

Figure 1: Gain as a function of the rate for measurements at different initial gains.

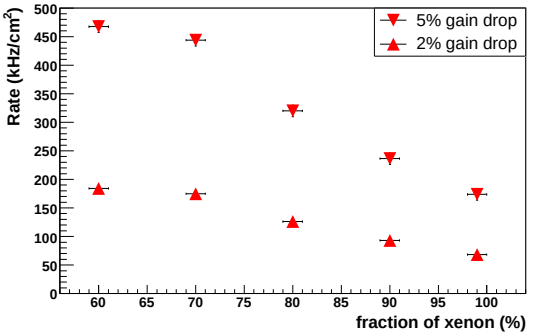

Figure 2: Rates at a gain drop of 2% and 5% and an initial gain of 5000.

Since the space-charge effect depends on the total charge in the chamber, the gain drop depends on both the initial gain and the rate. The dotted lines in Fig. 1 show constant gain drops as a function of the rate.

The energy loss of a traversing particle is smaller than the energy loss of a X-ray photon. Since in the CBM experiment the majority of particles passing the TRD will be minimum ionizing one has to calculate the rate of minimum ionizing particles which will produce the same energy loss than the X-ray photons in the test. This rates are shown in fig. 2 for different gas mixtures at an initial gain of 5000.

References

[1] F. Sauli, "Principles of operation of multiwire proportional and drift chambers", CERN 77-09 (1977) (Yellow report)

[2] E. Mathieson and G.C. Smith, Nucl. Instrum. Meth. A316 (1992) 246

Research and Development of fast TRD readout chambers

A. Andronic[2], V. Babkin[1], S. Chernenko[1], C. Garabatos[2], V. Golovatyuk[1], S. Razin[1], F. Uhlig[2],

H. K. Soltveit[3], Yu. Zanevsky[1], V. Zryuev[1]

[1]JINR Dubna, [2] GSI Darmstadt, [3]University of Heidelberg

We present the results of R&D obtained at the JINR for fast Transition Radiation Detector (TRD) prototypes. Several MWPC and GEM detectors with sensitive area 10 x 10 cm² were constructed and tested in a laboratory conditions and on the beam [1-3] to study a rate capability, position resolution and operational stability. The measurements were performed at GSI with secondary proton beams with momenta of 1,5 - 2,0 GeV/c. The rate was chosen by varying the extraction time of the primary beam from 1,5 to 10 seconds. To reach with the rate of up to ~ 400 kHz/cm² we chose as detectors the multiwire proportional chambers (MWPC) of 6 mm thickness, with anode wires of 20 µm diameter and the pitch of 2 mm. For an efficient absorption of TR, the counting gas is Xe-CO_2 [85-15]. The signals are readout on 2 raw from 16 pads of 5×20 mm² and amplified with a 16-channel ASIC preamplifier/shaper (designed in 0.35 µm CMOS technology) [4]. and sampled with a 25 MHz ADC (8 bit, nonlinear). Two identical chambers were tested with a different anode potential to compare the rate capability with differing gas amplification factor.

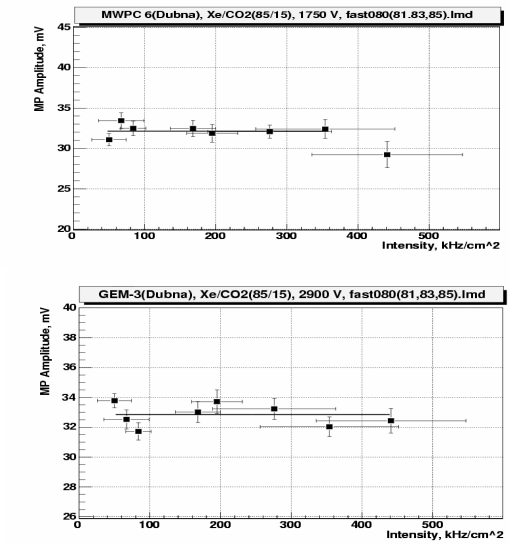

Fig 1. Rate dependence of the average signal for the MWPC (upper panel) and 3 stage GEM (lower panel)

From Fig.1 one can see that the MWPC with anode potential +1900 v shows practically no degradation of the signal amplitudes up to ~360 kHz/cm². The amplification factor of MWPC was < 10^4. Taking into account the high spatial resolution (< 200 µm) [5], high rate capability, and operational stability there is a good reason to believe that this detector meets all parameters needed for TRD CBM.

3-stage GEM with drift gap of 3 mm, 3 mm induction gap and 2 mm pitch of PCB readout plane was used during this test as a reference detector [1]. No degradation of amplitudes was obtained with this GEM detector up to ~450 kHz/cm². Another 2 stage GEM detector was constructed and tested at the JINR in a laboratory condition with Fe-55 source. It has one dimension readout board with the strips of 0,6 mm pitch and 10 cm length. The drift gap was 10 mm and 2 mm induction gap. The detector has operated with gas mixture of 85%Ar + 15%CO2. The amplification factor of the detector was about 3 x 10^3. The signal was readout to DAQ from the strips via the same 16-channels preamplifier/shaper [4] and ADC. During the test with 80 µm slit collimator a spatial resolution of 110 µm was obtained (fig.2), the distribution of fired strips number is shown in fig.2 as well.

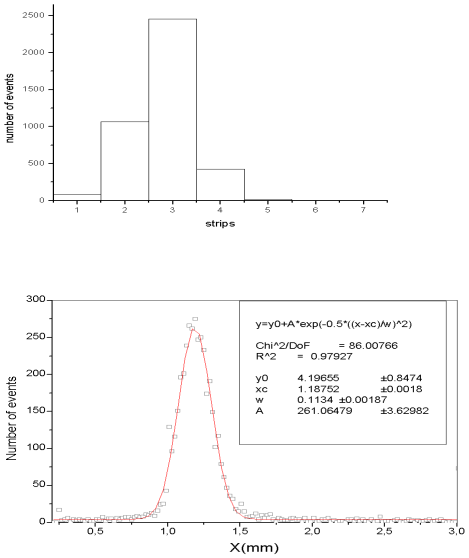

Fig.2. Distribution of fired strip numbers (upper panel) and spatial resolution (lower panel) of 2 stage GEM detector.

This work was partially supported by INTAS grant No: 03-54-4169. We would like to express our gratitude for the help to P. Braun- Munzinger, M. Petrovici, P. Senger, C. Schmidt, R. Simon, J. Wessels

References

[1] A. Andronic et al. “High rate performance of fast gaseous detectors”, GSI Annual Report 2004/2005-1

[2] A. Andronic et al. „ Electron/pion identification with fast TRD prototypes” GSI Annual Report 2006.

[3] M. Petrovici et al.„ High efficiency Transition Radiaition detector for high counting rate environment”, GSI Annual Report 2006.

[4] H.K. Soltveit, I. Rusanov and J. Stachel “Fast TRD Pre-Amplifier Shaper for the CBM Experiment”, GSI Annual Report 2005, p.72

[5] M. Petrovici et al. “Fast TRD-R&D status”, the report on CBM Coll. Meeting, 22 Sept. 2006, Strasbourg.

Electron/pion identification with fast TRD prototypes

A. Andronic[1], H. Appelshäuser[2], V. Babkin[3], P. Braun-Munzinger[1], V. Cătănescu[4], S. Chernenko[3], C. Garabatos[1], S. Golovatyuk[3], M. Hartig[2], J. Hehner[1], A. Herghelegiu[4], M. Kalisky[1], M. Klein-Bösing[5], D. Kresan[1], C. Lippmann[1], D. Miśkowiec[1], W. Niebur[1], D. Moisa[4], M. Petriş[4], M. Petrovici[4], A. Radu[4], C.J. Schmidt[1], V. Simion[4], R.S. Simon[1], I. Rusanov[6], H.K. Soltveit[6], J. Stachel[6], F. Uhlig[1], J.P. Wessels[5], A. Wilk[5], Yu. Zanevsky[3], and V. Zryuev[3]

[1]GSI, Darmstadt, Germany; [2]University of Frankfurt, Germany; [3]JINR Dubna, Russia; [4]NIPNE Bucharest, Romania; [5]University of Münster, Germany; [6]University of Heidelberg, Germany

We report results obtained in beam tests of fast Transition Radiation Detector (TRD) prototypes. Such a TRD, envisaged for electron/pion identification, is part of the setup of the CBM detector at FAIR [1]. To cope with the envisaged rates of up to 100 kHz/cm^2, we have chosen as detectors multi-wire proportional chambers (MWPCs) of 6 mm thickness, with anode wires of 20 μm diameter with a pitch of 2 and 3 mm. Transition radiation (TR) is produced in radiators composed of polypropylene foils of 20 μm thickness (d_1), regularly spaced by a distance (d_2) of either 200 or 500 μm, with the number of foils N_f of 220 or 120, respectively. For an efficient absorption of TR, the counting gas is Xe-CO_2 [85-15]. The signals are readout on pads of 8$\times$15 mm^2 and amplified with a 16-channel ASIC preamplifier/shaper especially designed in 0.35 μm CMOS technology. The signals are sampled with a 25 MHz ADC (8 bit, nonlinear). The measurements are performed at GSI with secondary beams with momenta of 1 and 1.5 GeV/c. Two segmented scintillator detectors are used for beam definition and for rate and time-of-flight measurements. Electrons are identified with respect to hadrons using a Pb-glass calorimeter and an air-filled Cherenkov detector. The beam profile is monitored using two Si-strip detectors. The MBS data acquisition system [2] is used.

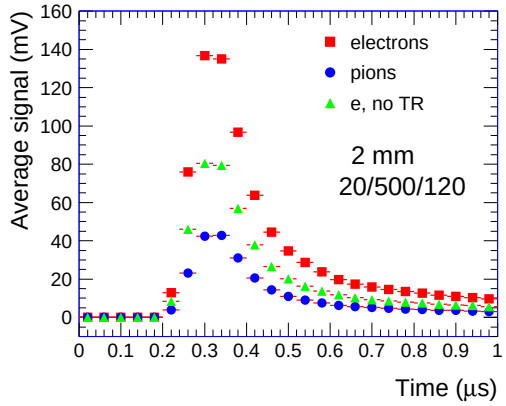

Figure 1: Average signals for pions and electrons.

An example of average signals is shown in Fig. 1 for the momentum of 1.5 GeV/c. The long tails are due to the slow-moving Xe ions created in the gas avalanche. The TR, produced only by very fast particles (γ >1000), is produced at this momentum only by electrons [3] and leads to a significant increase of the signal, which is essential for improving the electron/pion separation.

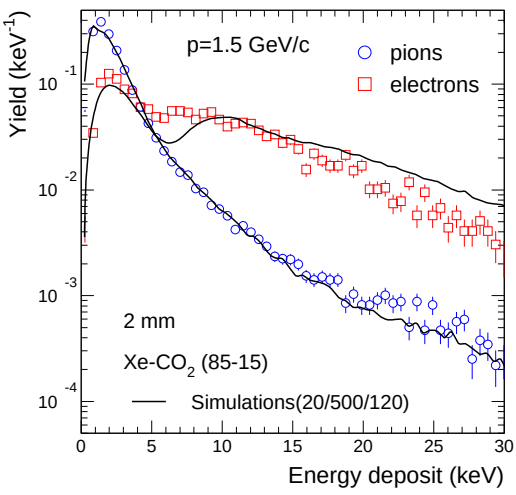

Figure 2: Measured charge spectra for pions and electrons of 1.5 GeV/c. The lines denote simulations.

In Fig. 2 we show the spectra of energy deposited in our detector for pions and electrons of 1.5 GeV/c. The Landau spectrum corresponding to the ionization energy loss (dE/dx) is, in case of electrons, complemented by the TR contribution, clearly visible in the spectrum around 10 keV. The absolute energy calibration has been done using the pion spectra with respect to simulations [4], shown in Fig. 2. These simulations reproduce very well the spectral shape for pions, but are describing the TR part only approximately. The measured TR appears to be softer than in the simulations.

The spectra measured with one layer (Fig. 2) allow us to simulate the electron identification capability of a TRD as a function of the number of layers. The results are shown in Fig. 3 for two momenta and for two radiators (characterized by $d_1/d_2/N_f$). An improvement in the e/π separation is seen at 1.5 GeV/c compared to 1 GeV/c due to the strong increase of the TR yield for electrons [3], which overcomes the relativistic rise of dE/dx of pions [4]. For higher mo-

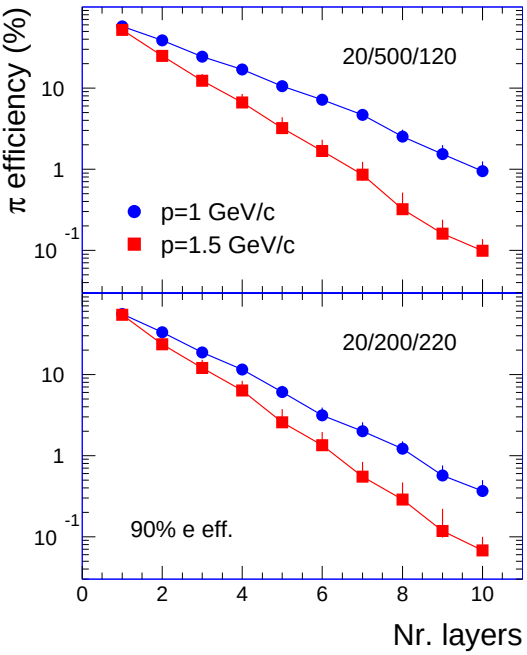

Figure 3: Extrapolated electron/pion identification performance as a function of the number of layers.

menta the e/π separation gradually degrades (a factor of 4 worse pion rejection is expected for 10 GeV/c [5]) due to the saturation of the TR yield beyond 2 GeV/c [3] and the pion dE/dx relativistic rise [4]. As seen in Fig. 3, the rejection power (expressed as π efficiency at 90% electron efficiency) is comparable for the two radiators for p=1.5 GeV/c and this is expected to be true also for higher momenta. The radiator with larger N_f is expected to produce a larger TR yield, but it appears that its smaller foil gap (d_2=200 μm) leads to a smaller TR yield per foil compared to the radiator with d_2=500 μm. This makes the latter option a more suited choice, both because a lighter radiator is prefered in a tracking TRD (as envisaged in CBM [1]) and because of easier manufacturing and less sensitivity to foil gap nonuniformities.

In Fig. 4 we show an example of the dependence on the measured energy deposit spectra for hadrons and electrons for different local rate values. From these results we could conclude that the effect of high rates appears as pile-up, not perfectly rejected through our segmented scintillator detectors, rather than producing a reduction of the signal, expected if space charge was present.

In Fig. 5 we present the rate dependence of the electron identification with respect to hadrons as measured with one layer at the momentum of 1.5 GeV/c. While the study of e/π^- separation could only be done at low rates (10 kHz/cm^2), the high rates are achieved with a positive beam. In this case, the beam content is dominated by the protons and, due to their larger energy loss, the electron separation is in this case clearly worse. The separation is not much

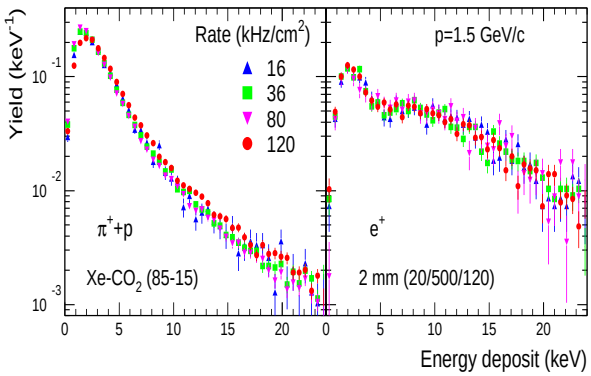

Figure 4: Energy deposit spectra for hadrons and electrons for different local rate values.

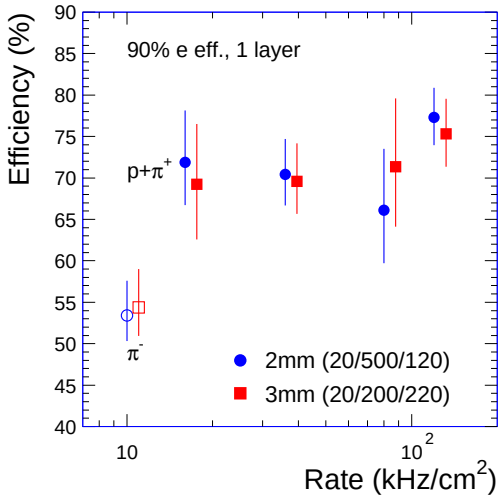

Figure 5: Rate dependence of the electron separation with respect to hadrons as measured with one layer.

influenced by rate, but a degradation occurs beyond 100 kHz/cm^2. Extrapolated to 10 layers this implies a reduction of the hadron rejection by a factor of about 3 at our highest rates. The trend is similar for the detectors with anode wire pitch of 2 and 3 mm.

This work is partially funded by the EU Integrated Infrastructure Initiative Project HADRON PHYSICS under Contract No. RII3-CT-2004-506078. We acknowledge the help from G. Augustinski, M. Ciobanu, N. Kurz and Y. Leifels.

References

[1] A. Andronic, Nucl. Instrum. Meth. A563 (2006) 349.

[2] H.G. Essel, N. Kurz, IEEE Trans. Nucl. Sci. 47 (2000) 337.

[3] A. Andronic et al., Nucl. Instrum. Meth. A558 (2006) 516.

[4] A. Andronic et al., Nucl. Instrum. Meth. A519 (2004) 508.

[5] R. Bailhache, C. Lippmann, Nucl. Instrum. Meth. A563 (2006) 310.

High efficiency Transition Radiation Detectors for high counting rate environments

M. Petrovici[1], M. Petriş[1], I. Berceanu[1], V. Simion[1], D. Moisă[1], A. Radu[1], D. Bartoş[1], V. Cătănescu[1], A. Herghelegiu[1], C. Măgureanu[1], M. Hoppe[2], A. Wilk[2], J.P. Wessels[2], A. Andronic[3], C. Garabatos[3], R. Simon[3], F. Uhlig[3]

[1]NIPNE-Bucharest, [2]University of Münster, [3]GSI-Darmstadt

One of the options currently considered for lepton identification with the CBM experiment [1] for FAIR is a shell of multiple layers of Transition Radiation Detectors (TRD).

Being a heavy-ion fixed target experiment in the energy range of 5-35 A·GeV the goal of CBM is to look for rare probes using the unique performance of FAIR in terms of high intensity heavy ion beams. This requires a high granularity TRD with good performance specifically engineered for a high counting rate environment. In this context, the optimization of the e/π rejection factor relative to the number of layers and electronic read-out channels is a challenging requirement. Various prototypes [2] based on Multiwire Proportional Chambers (MWPC) were designed, built and tested. Up to intensities of 100 kHz/cm^2, no major deterioration of their performance in terms of pulse height and position resolution has been observed.

However, this performance was reached at the expense of a low conversion efficiency for transition radiation in such a single layer MWPC based TRD. In order to circumvent this aspect, we designed and built several variants of a new prototype of TRD based on a double sided pad read-out electrode[3] with gas volumes on either side. Neglecting about 15% absorption in the central electrode, the double sided configuration is equivalent to a detector of 12 mm gas thickness, preserving the time response of the one of half the thickness [4].

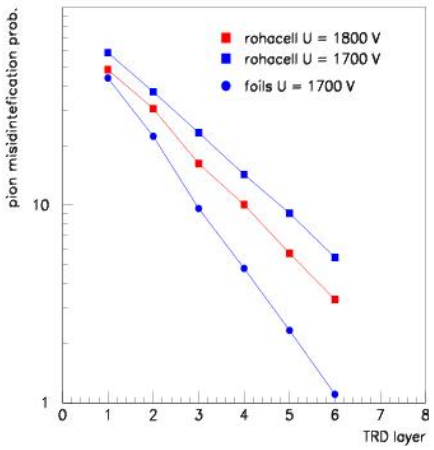

Figure 1: Pion efficiency at 90% electron efficiency at 1.5 GeV/c momentum as a function of number of layers

The prototype was tested in-beam at the SIS. The pion rejection factor was extracted using the likelihood on integrated energy deposit [5]. The pion efficiency at 90% electron efficiency at 1.5 GeV/c momentum as a function of number of layers for a Rohacell radiator is depicted in Fig. 1. The obtained pion efficiency for 6 layers is 3.32% for an anode voltage of 1800 V. For one run we used a polypropylene foil stack (120 foils, 20 μm thickness, 500 μm spacing) as radiator. For an anode voltage of 1700 V the obtained pion efficiency is (1.1%). The pion efficiency using Rohacell radiator at the same anode voltage is 5.43%, i.e. the regular foil radiator improves the pion rejection by almost a factor of five. If this improvement factor is applied to the measurement obtained at 1800 V anode voltage, a final pion efficiency of 0.67% is obtained for a 6 layer stack with a regular foil radiator.

Fig. 2 shows the pulse height distributions of pions and electrons, respectively for 26·10^3, 65·10^3, 110·10^3 and 220·10^3 particles/(s·cm^2) counting rate.

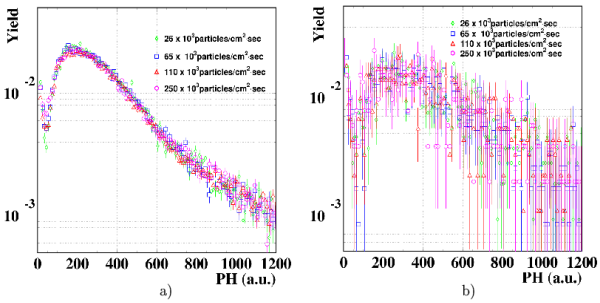

Figure 2: Pulse height distributions for a) protons and pions and b) electrons as a function of rate

Within experimental errors we conclude that these detectors preserve their pion efficiency performance up to counting rates of ∼200·10^3 particles/(s·cm^2).

Given the performance in terms of counting rate and pion efficiency this new principle of TRD commends itself as a viable solution for high counting rate environments. For a given pion efficiency and granularity it provides an optimum material budget at a reduced number of readout channels.

References

[1] CBM - Technical Status Report, 2005

[2] A. Andronic et al, GSI Ann. Rep. 2005-1, INSTMETH-33

[3] M. Petrovici et al. GSI Sci.Rep. 2006-1, p.67

[4] M. Petris et al,CBM Coll. Meet., March 9-12, 2005, GSI

[5] A.Büngener et al., Nucl. Instr. Meth. 214, 1983, p.261

Development of straw tubes for high rate capability application *

K. Davkov[1], V. Davkov[1], J. Marzec[2], V. Myalkovskiy[1], L. Naumann[3], V. Peshekhonov[1], A. Savenkov[1], D. Seliverstov[4], V. Tikhomirov[5], K. Viryasov[1], P. Wintz[6], K. Zaremba[1], and I. Zhukov[1]

[1]JINR Dubna, Russia; [2]University of Technology, Warszaw, Poland; [3]FZ Dresden-Rossendorf, Germany; [4]Institut of Nuclear Research, Gatchina, Russia; [5]Lebedev Institut, Moscow, Russia; [6]FZ Jülich, Germany

The construction of a large size straw tube particle tracking detector for the Compressed Baryonic Matter Experiment at FAIR is under consideration [1]. Drift chambers on the basis of thin-walled drift tubes (straws) have been widely used as tracking detectors in high rate environments [2,3,4]. In the inner part of the first CBM tracker station the expected hit density of charged particles for central Au+Au collisions at 25 AGeV amounts to $0.05/\mathrm{cm}^2$. To guarantee a sufficient efficiency of the tracking system, the occupancy of a single drift tube element should be below five percent and the active detector cross-section yields $1\,\mathrm{cm}^2$ for the expected hit density. To realise small area drift detectors long straw tubes with subdivided anodes of different length have been developed. The readout of a section should be independent of each other. Consequently it is possible to reduce the active cross-section of a straw tube to few cm^2. The low-mass inner straw elements and the technology of the multi-anode straw assembly have been devised and checked. A prototype of 19 straws with 57 readout channels has been manufactured. The straws are 500 mm long and 4 mm in diameter. The anodes are subdivided in two, three or four parts of different length. Fig. 1 shows a straw tube layout with four anode segments.

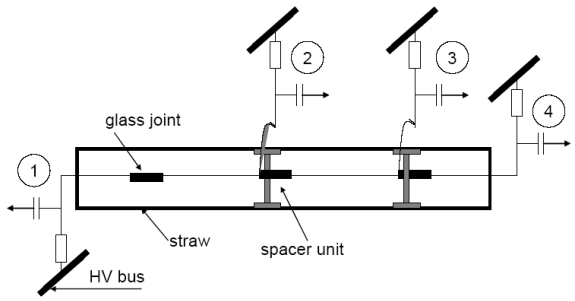

Figure 1: Schematical drawing of the straw tube design with four anodes.

Different readouts have been tested. The front-end readout of the outer anodes has been provided close to the end-plugs. For the inner sectors cables of 15 cm length connect the anode wires with the front-end electronics. In the threefold segmented anode the single glas joint has been removed to investigate the double-sided readout. The current sensitive preamplifiers with an input impedance of $300\,\Omega$ are connected to the anodes by a capacitive coupling of 200 pF. Each anode has been supplied with high voltage through a resistor of $1\,\mathrm{M}\Omega$. A gas mixture of Ar/CO_2 (70/30) at atmospheric pressure has been supplied through the two end-plugs of each straw. Collimated Gammas (^{55}Fe) irradiated the straws along the anodes with a width of 1 mm perpendicular to the wires. Fig. 2 shows the anode signal amplitude distribution in a threefold subdivided wire. The collimator was moved along the straw. The information from the inner sector is read out over the contact wire fed through the spacer supporting the capillary tube and the hole in the straw wall. To compare the signals going through the straw wall and the end plug, the readout of the right anode has a double-sided layout.

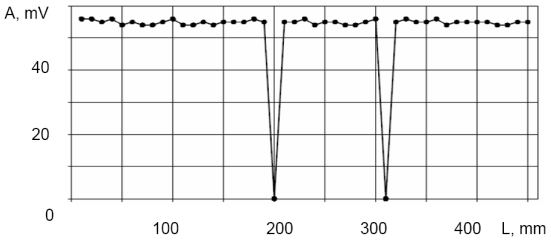

Figure 2: Amplitude distribution of the anode signals (A) along the threefold subdivided straw of 500 mm length (L).

The result shows, that detector inefficiencies are only evident in small regions of 7.2 mm length around the spacer units. The straws work stably, no discharges were observed between any construction elements placed inside the straws. The radiation length of the spacer amounts to 0.4 %. For minimum ionizing particles the rate capability amounts up to $4.5\,\mathrm{MHz/cm}^2$ in single straws of 4 mm in diameter with a gain of 5×10^4 [5].

References

[1] CBM Experiment, Techn. Status Report, GSI Darmstadt (2005)

[2] Y. Arai et al., NIM A381 (1996) 355

[3] ATLAS Inner Tracker Design Report, CERN/LHCC/97-16

[4] V. Bytchkov et al., Particles a. Nuclei, Letters N.2 (2002) 75

[5] I. Zhukov et al., JINR Preprint P13-2005-126

* Work supported by INTAS 03-54-5119

Progress in the CBM-TOF wall, R&D and simulation*

D. González-Díaz[1], E. Cordier[2], and A. Semak[3]
[1]GSI, Darmstadt, Germany; [2]Physikalisches Institut, Universität Heidelberg, Germany; [3]IHEP, Protvino, Russia

The CBM-TOF group aims at providing high π/k separation (more than 2-σ in the reconstructed mass) in Au+Au central collisions at 25 GeV/A, with a coverage of mid-rapidity by at least 1 unit in y and 1 GeV in p_T. These PId capabilities are needed for probing the QGP phase, through the study of such fundamental observables as the dynamical fluctuations of the kaon yield, kaon flow, hyperon production close to threshold and open charm.

Based on simulation, it was shown that the mentioned requirements can be satisfied by a tRPC (timing Resistive Plate Chamber) wall placed at 10 m distance from the target with 25-30° coverage in θ ($\sim$150 m^2), featuring a time resolution of 80 ps and an occupancy per cell below 5% ($\sim$ 60.000 cells). In order to cope with the high beam luminosity, the tRPC must handle rates up to 20 kHz/cm^2, while the FEE must process the very fast GHz signals from the tRPC at an interaction rate up to 10 MHz.

The CBM spectrometer benefits from the excellent overall PId capabilities of the TOF wall: for example, the π/e separation in time of flight is 3-σ for p=1.1 GeV, that provides extra π suppression (apart from that of RICH and TRD detectors) in view of di-electron spectroscopy.

Current R&D activities [1, 2, 3, 4, 5] focus on the development of high rate capability tRPCs, aiming at extending their working principle from few hundreds of Hz/cm^2 up to the required rate of 20 kHz/cm^2, for CBM usage. But also improvements on the description of the timing properties of the detector at high rates have been recently accomplished [6]. As a consequence of the latter, the idea that the deterioration of tRPC performances at high rates is mainly driven by the DC column resistivity ρd (resistivity times the resistive plate thickness per gap) is now more sound.

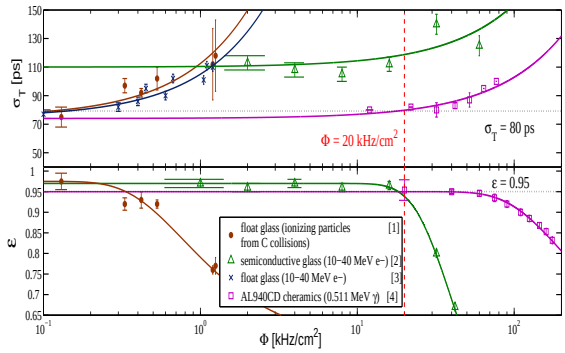

Figure 1: Compilation of different measurements.

A number of measurements was performed at different rates under different conditions: with ionizing particles from carbon collisions at GSI-SIS [1], with 10-40 MeV electrons at the ELBE LINAC [2, 3] and with γ sources [4]. Among the more promising candidates for the resistive plates of high rate tRPCs, semi-conductive glasses [2] and ceramics [4] must be mentioned, whereas the possibility of using warm thin glass deserves also consideration [5]. A compilation of results is shown in Figure 1, together with the dependence on rate Φ obtained in [6]:

$$\varepsilon \simeq \frac{\varepsilon_o}{1 + Ae^{-B/\Phi}}\ , \quad \sigma_T \simeq \sigma_o(1 + C\Phi) \qquad (1)$$

where ε_o, σ_o, A, B, C are obtained from the fit to data.

The current theoretical and experimental understanding of the detector has been used to better model the detector geometry and its response. Starting from the simulation of the gap response, a realistic description of the position resolution, inclined tracks and multiple hits have been provided for the first time. The studies performed after full tracking through CBM confirm the statements of paragraph 2 (see D. Kresan et al., this report) and open the path to a detailed comparison between pad and strip technologies that are currently existing for the tRPC readout. A first approach to the final mechanical structure has also been accomplished, where the distribution of the wall in towers looks by now the more suited solution, providing a high flexibility and a comfortable distribution of the weight (Figure 2).

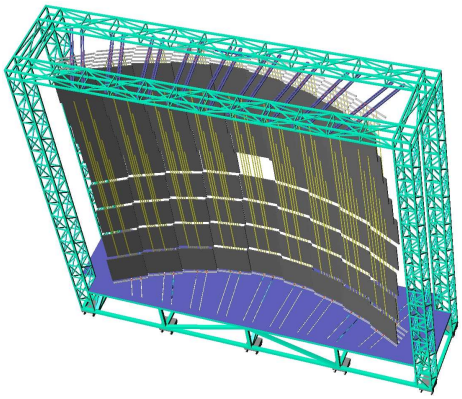

Figure 2: Front view of the TOF wall, divided into towers.

Details on the FEE, mostly focused on ASIC design, can be found in M. Ciobanu et al., in this report.

References

[1] H. Alvarez-Pol et al., NIM A, 535(2004)277.
[2] F. Dohrmann, talk at VIII CBM coll. meeting.
[3] R. Kotte et al. NIM A, 564(2006)155.
[4] L. Lopes et al., Nucl. Phys. B, (Proc. Suppl), 158(2006)66.
[5] P. Fonte et al., PoS(HEP2005)376.
[6] D. Gonzalez-Diaz et al., Nucl. Phys. B, (Proc. Suppl), 158(2006)111.

* Supported by JRA12 of EU/FP6 Hadronphysics (see annex), INTAS Ref. Nr. 03-54-3891 and German BMBF contract 06 HD190I.

Ceramic high-rate timing RPCs

L. Lopes[1], R. Ferreira Marques[1,2], P. Fonte[1,3], L. Hennetier[4], A. Pereira[1] and A.M. Sousa Correia[4]

[1]Laboratório de Instrumentação e Física Experimental de Partículas, Coimbra, Portugal, [2]Departamento de Física, Faculdade de Ciências e Tecnologia da Universidade de Coimbra, Coimbra, Portugal, [3]Instituto Superior de Engenharia de Coimbra, Coimbra, Portugal, [4]Centro Tecnológico da Ceramica e do Vidro, Coimbra, Portugal

Timing resistive plate chambers [1] are planar gaseous detectors made with a combination of metallic and resistive electrodes, which deliver a time resolution around 50 ps sigma (σ) and efficiency up to 99% for MIPs. This is currently the only practical technology envisaged for the CBM TOF Wall.

The counting rate capability of these detectors is mainly determined by the resistivity of the electrodes, which are typically made of glass with volume resistivity between 10^{12} and 10^{13} Ω·cm. This limits the maximum counting rate to around 2 kHz/cm^2 [2], which is insuficient for the central regions of CBM.

Here we report on the use of a ceramic commercial material with a measured resistivity of 10^9 Ω·cm and free from charge depletion effects [3]. The results establish the practical feasibility of accurate timing measurements with RPCs at rates up to 75 kHz/cm^2 - largelly suficient for aplication in CBM - while keeping a time resolution below 100 ps σ for 511 keV gamma rays. Full details may be found in [4].

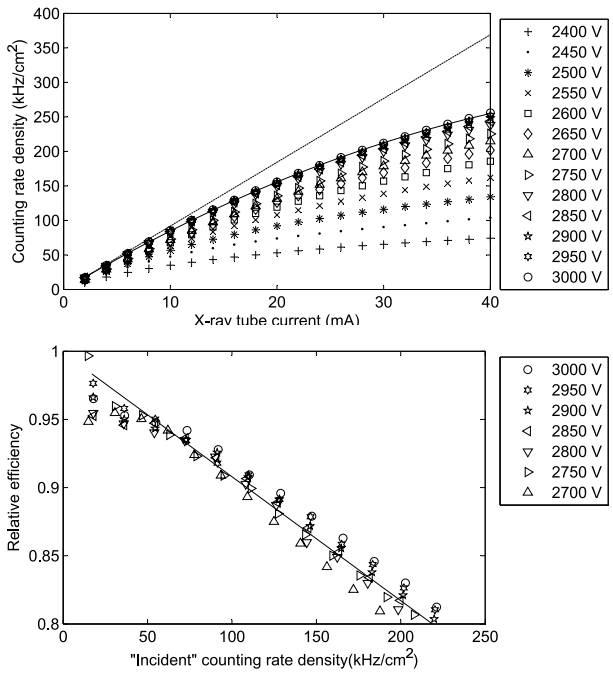

Figure 1: a) Counting rate density as a function of the X-ray tube current for a set of applied voltages. A fitting quadratic polynomial reproduces well the data (one example shown). b) The data points are normalized to the linear part of the fitting polynomial (the "incident" counting rate, also represented in a)), yielding the drop in relative efficiency that may be attributed to the counting rate. A general linear fit to these points shows a slope of 9% relative efficiency drop per 100 kHz/cm^2.

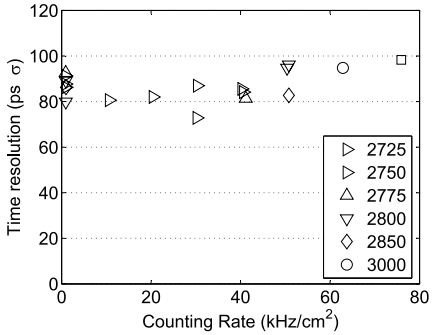

Figure 2: Time resolution as a function of the counting rate. Within the statistical fluctuations of the measurement, the time resolution remains essentially unchanged, around 90 ps σ, between 1 and 75 kHz/cm^2. The applied voltage was adjusted as the counting rate increased in order to compensate for voltage change across the ceramic.

The counting rate density as a function of the X-ray tube current for a set of applied voltages is shown in Fig. 1 a). For each voltage the data is well described by a quadratic polynomial. The relative sensitivity drop that may be attributed to the increasing counting rate (Fig. 1 b)) is estimated by normalizing the data points to the linear part of the fitting polynomial (the "incident" counting rate, also represented in a)). A linear fit to the set of the normalized points shows a slope of 9% relative sensitivity drop per 100 kHz/cm^2.

Time resolution results are shown in Fig. 2. Within the statistical fluctuations of the measurement (vertical spread of the points), the time resolution remains essentially unchanged around 90 ps σ, between 1 and 75 kHz/cm^2. Beyond this point the measurement becomes impossible owing to the predominance of random coincidences (see [5]).

It should be noted that the performance of timing RPCs in particle beams and with 511 keV photons has been compared and it was found that with photons the resolution is systematically worse.

This work was supported by the EU FP6 program via the contract RII3-CT-2003-506078 and by FCT and FEDER under project POCI/FP/63411/2005.

References

[1] Nucl. Instr. and Meth., A443 (2000) 201.
[2] Nucl. Instr. and Meth., A490 (2002) 58-70.
[3] AL-940CD charge-dissipative ceramics, Morgan Ceramics.
[4] Nucl. Phys. B - Proc. Sup., 158 (2006) 66-70, CBM-TOF-note-2006-001.
[5] Nucl. Instr. and Meth., in press (http://dx.doi.org/10.1016/j.nima.2006.10.245).

Testing the Performance of Timing MRPC Detectors at ELBE

F. Dohrmann, R. Kotte, L. Naumann, D. Stach, J. Wüstenfeld
Institut für Strahlenphysik, Forschungszentrum Dresden-Rossendorf

Multigap Resistive Plate Chambers (MRPCs) are potentially suited for cost-efficient large-area time-of-flight arrays needed for the identification of minimum ionizing particles (MIPs) in large-scale heavy-ion experiments [1-7]. Since the specific energy loss of 10 - 40 MeV electrons is quite similar to that of MIPs, a test setup is installed at the radiation source ELBE in Rossendorf where scattered electrons are used to mimic the behaviour of MIPs within RPC detectors. Furthermore, the high precision of the accelerator RF signal allows for a well defined time reference. Therefore, no high-resolution start counter requiring an additional pulse-height correction (time slewing) is necessary. Electrons from ELBE are scattered (quasi) elastically off a thin (18 μm) Al target. Passive (Pb shielding) and active collimation (various scintillation counters) defines a small solid angle and hence sufficient background suppression. The test detector is positioned 2 m away from the target at scattering angle of 45 degrees. For the layout of the experimental setup, see ref. [8].

Here, we present results obtained with a 20 cm long prototype of a symmetric Multistrip MRPC (central anode with 16 strips of 2.5 mm pitch, six gas gaps of 250 μm, eight float-glass plates of 1 mm) developed for the FOPI experiment at SIS/GSI [4-7]. Moreover, we tested two identical six-gap MRPCs (called IKH-MRPC), with four readout strips of 1 cm pitch and 7 cm length using the same float glass of high resistivity of $\sim 10^{12}\,\Omega$ cm. The IKH-MRPCs were built in the detector workshop of the Institute of Radiation Physics. The detectors were irradiated with 34 MeV electrons. The corresponding results are published recently [8].

The counters are operated with a gas mixture of 85 % $C_2H_2F_4$ + 10 % SF_6 + 5 % iso-C_4H_{10} at a flow of 1.8 l/h. Typical results of time resolution measurements are summarized in figs. 1 - 4. Reproducibility is achieved within ± 10 ps. Note that the given resolution values are corrected for the finite resolution of the time-to-digital-converter (TDC, here: CAEN V1290N) but not for any jitter of the RF signal and the front-end electronics (FEE, here: GSI development precursor with 4 channels, single-ended 50 Ω input, gain $\leq$ 250, bandwidth $\sim$ 1 GHz, threshold $\leq$ 100 mV [6, 7]).

The high-rate capability of MRPCs can be decisively improved by using low-resistivity glass. Thus, two four-gap MRPCs (called INR-MRPC) equipped with silicate glass plates showing a bulk resistivity of less than $10^{10}\,\Omega$ cm have been assembled at the Institute for High-Energy Physics and the Institute for Nuclear Research, Moscow, and successively tested at ELBE. Time resolutions of about 100 ps and efficiencies larger than 95% were obtained for rate densities up to 20 kHz/cm^2 (cf. fig. 5) meeting the demands of the CBM experiment planned at FAIR. These results will be published soon [9].

References

[1] P. Fonte et al., Nucl. Instr. Meth. A 443 (2000) 201
[2] P. Fonte et al., Nucl. Instr. Meth. A 449 (2000) 295
[3] A. Blanco et al., Nucl. Instr. Meth. A 485 (2002) 328
[4] M. Petrovici et al., Nucl. Instr. Meth. A 487 (2002) 337
[5] M. Petrovici et al., Nucl. Instr. Meth. A 508 (2003) 75
[6] A. Schüttauf, Nucl. Instr. Meth. A 533 (2004) 65
[7] A. Schüttauf, Nucl. Phys. B (Proc. S.) 158 (2006) 52
[8] R Kotte et al., Nucl. Instr. Meth. A 564 (2006) 155
[9] V. Ammosov et al., to be published in Nucl. Instr. Meth. A

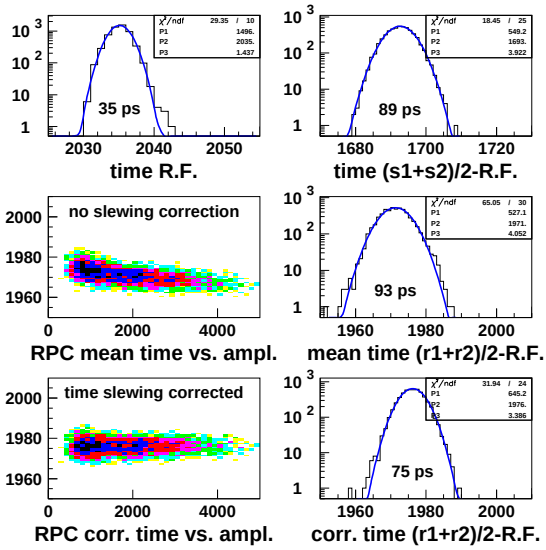

Fig. 1 *The time resolution, σ_t, of different measured quantities of the FOPI-MRPC prototype (full lines: Gaussian fits, TDC time slope 24.5 ps/ch). Upper left panel: The 13 MHz time reference signal of ELBE fed into two TDC channels (self-coincidence). For the resolution values given in the right side panels this TDC contribution is quadratically subtracted. Upper right: Mean timing $(t_{left}+t_{right})/2$ of a 2 x 2 cm^2 (5 mm thick) scintillator read out on two sides by XP2020 photo tubes. Middle (lower) left: Dependence of a similar mean timing of a RPC strip on integrated charge before (after) time slewing correction. The corresponding right panels show the projections onto the time axis. The RPC potential voltage was set to 8.2 kV and the corresponding rate was limited to 50 Hz/cm^2.*

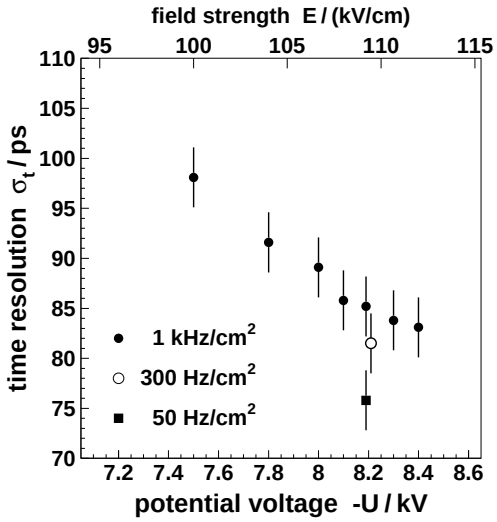

Fig. 2 *The time resolution vs. potential voltage applied to the FOPI-MRPC (bottom axis). The apparent field strength being the ratio of potential voltage over sum of gas gap sizes per detector half is provided as top axis. The various symbols indicate measurements taken at different count rates.*

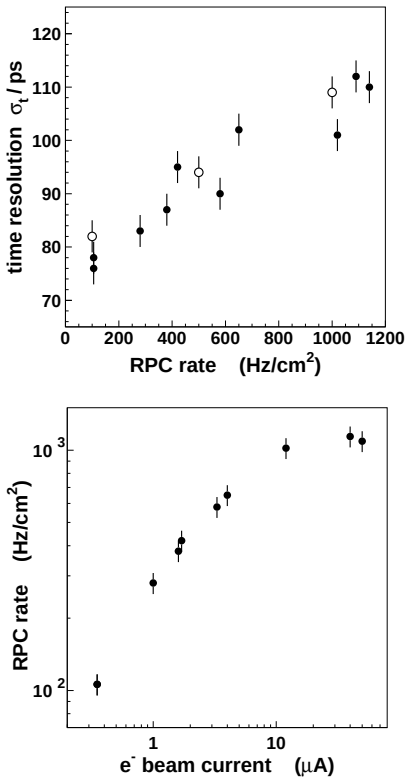

Fig. 3 *Upper panel: The time resolution vs. count rate of the FOPI-MRPC (full symbols) and of one of the IKH-MRPCs (open symbols). The apparent field strength was 110 kV/cm. lower panel: The count rate vs. primary e^- beam current of the FOPI-MRPC. A clear saturation effect due to signal degradation as result of the high glass resistivity is visible.*

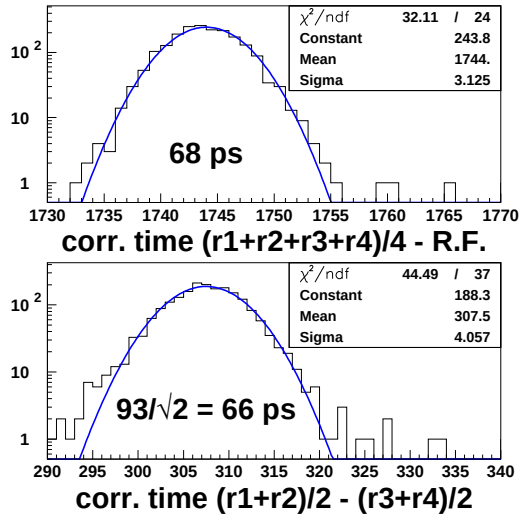

Fig. 4 *Upper panel: The mean timing w.r.t. the accelerator RF of four (time slewing corrected) signals from two strips of two identical IKH-MRPs. For the given resolution a 34 ps contribution of the TDC resolution is quadratically subtracted. Lower panel: The time resolution of the difference between the mean timing of two strips from different MRPCs.*

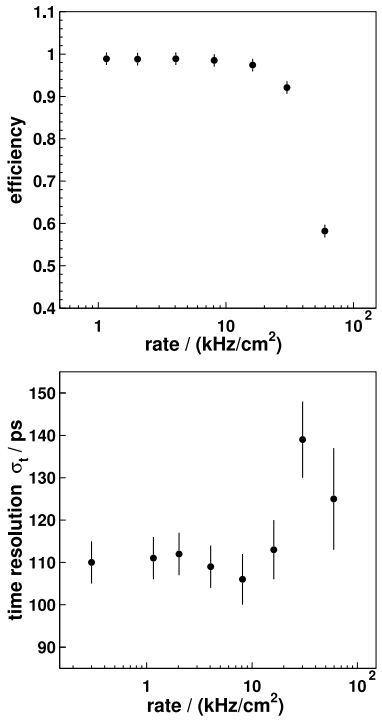

Fig. 5 *Efficiency (upper panel) and time resolution (lower panel) as a function of rate density for the INR-MRPC with low-resistivity silicate glass.*

High Counting Rate Position Sensitive Resistive Plate Counters

M. Petrovici, M. Petriş, V. Simion, D. Moisă, D. Bartoş, V. Cătănescu
National Institute for Physics and Nuclear Engineering, Bucharest, Romania
N. Herrmann
Physikalisches Institut der Universität, Heidelberg, Germany
M. Ciobanu, K.D. Hildenbrand, A. Schüttauf
Gesellschaft für Schwerionenforschung, Darmstadt, Germany

It is by now unanimously accepted that a high counting rate RPC could be obtained by decreasing the gap thickness and the resistivity of the glass electrodes. Decreasing the gap thickness requires an increased number of gaps, consequently a larger amount of material while a decrease of the resitivity by increasing the glass temperature implies a series of technical incoveninces for a large area subdetectors based on these type of counters. Obviously for a given number of gaps, their size and glass electrode thickness, the best alternative is to use lower resistivity glass electrodes. An other aspect which is worth to be considered for future applications of position sensitive RPCs is to replace the single ended readout structure with a differential readout. Results of preliminary tests using ^{60}Co source of a position sensitive RPC based on Pestov glass and the first differential readout prototype, ready to be tested in the near future, are presented in this report.

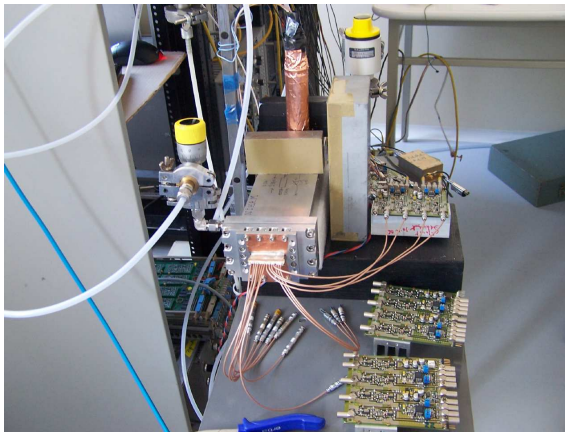

Figure 1: Experimental configuration used for radioactive source tests

A prototype of two times double-gap RPC in which the resistive electrodes are produced from Pestov glass of $\sim 10^{10}$ Ω·cm resitivity and the read-out of the induced fast signals done via stripe line intermediate electrode, the coresponding strips on the two sides being connected together [1], was designed and built. The gaps between these electrodes of 300 μm are realized by spacers made from fishing rod of such thickness. The read-out electrode, sandwiched by the two symmetric halves has 16 readout strip lines on each side with a pitch of 2.54 mm and a width of 1.1 mm, the corresponding strips on the two sides being connected together.

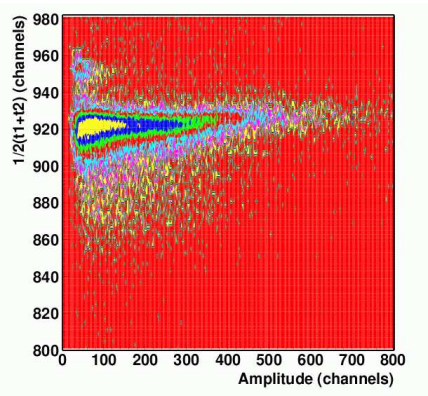

Figure 2: t_{sum}-amplitude correlation

The signals, are feed through lateral flanges of a rectangular, thin Al container. The inner structure is fixed on a special plexiglass plate which alignes the structure relative to the container. The results reported here have been obtained using a high voltage of 3.1 kV for each gap and a flow of standard gas mixture (85% $C_2F_4H_2$, 10% SF_6 and 5% C_4H_{10} (isobutane)) at normal pressure. Fig.1 shows the experimental configuration.

The signals delivered by the detector have been amplified by broad band fast amplifiers developed for similar RPCs based on comercial float glass used for FOPI TOF barrel [2]. CF4000 constant fractions have been used for timing. Time spectra have been obtained from γ - γ coincidence using ^{60}Co source, between the two ends of a middle stripe and a plastic scintillator (NE102) of cylindrical geometry (Φ = 25 mm and h=20 mm) coupled to a photomultiplier. The RPC amplitude - t_{sum} (t_{sum}=1/2(t_{left} + t_{right})) correlation is presented in Fig. 2.

A profile histogram of t_{sum} as a function of left-right time difference can be followed in Fig.3.

With a 3cm cut in the position in the region where the radioactive source was positioned, the time spectrum presented in Fig.4 is obtained.

A Gaussian fit gives σ=3 channels (one TDC2228A channel corresponds to 42 psec). Subtracting quadratically the contribution of the plastic scintillator measured in separate runs using 2 identical scintillators and phototubes, a $\sigma \leq$50 ps is obtained.

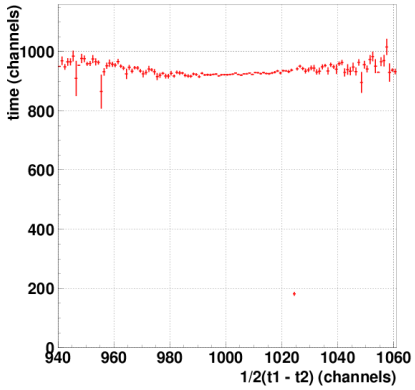

Figure 3: t_{sum} versus position along the counter

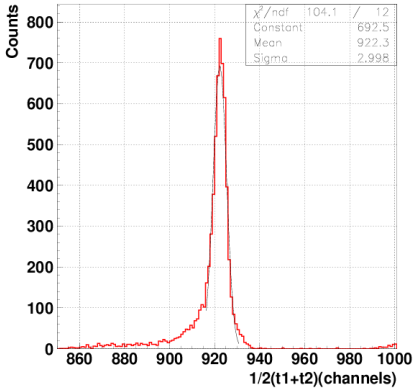

Figure 4: t_{sum} spectrum for a 3cm cut on the position in the region where the radioactive source was positioned

The results of these tests show that the counter has the requested performance in terms of time resolution. Studies of the counting rate performance will be done in the near future using MIPs at GSI Darmstadt.

A second prototype in which the cathode electrodes have identical strip line structure as the central electrode was realized and can be operated in a differential mode. A photo of the inner structure, housing box and flanges is presented in Fig.5.

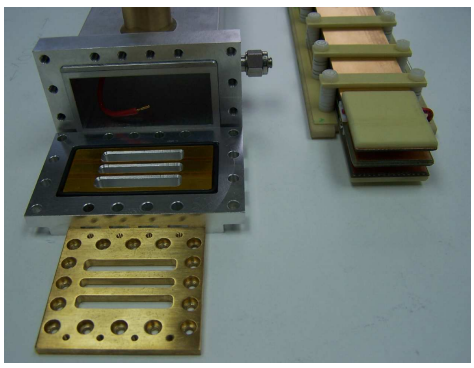

Figure 5: Inner structure, housing box and flanges of the diffrential, strip readout RPC prototype

The prototype was assembled, tested for tightness, introduced in the gas flow and is presently ready for tests using the ^{60}Co source.

References

[1] M. Petrovici, P. Braun-Munzinger, I. Cruceru, M. Duma, A. Gobbi, N. Herrmann, K.D. Hildenbrand, D. Moisa, M. Petriş, J. Schukraft, G. Stoicea, NIPNE Scientific Report 1999 pg. 59

M. Petrovici, N. Herrmann, K.D. Hildenbrand, G. Augustinski, M. Ciobanu, I. Cruceru, M. Duma, O.N.Hartmann, P. Koczon, T. Kress, M. Marquardt, D. Moisa, M. Petriş, C. Schroeder, V. Simion, G. Stoicea and J. Weinert, Nucl. Instr. Meth. 487A, 2002, 337

M. Petrovici, N. Herrmann, K.D. Hildenbrand, G. Augustinski, M. Ciobanu, I. Cruceru, M. Duma, O.N.Hartmann, P. Koczon, T. Kress, M. Marquardt, D. Moisa, M. Petriş, C. Schroeder, V. Simion, G. Stoicea and J. Weinert, Nucl. Instr. Meth. 508, 2003, 75

[2] A. Schüttauf, K.D. Hildenbrand, M. Ciobanu, E. Cordier, N. Herrmann, Y.J. Kim, M.Kis, P.Koczon, Y. Leifels, M. Petrovici, V. Simion, Nucl.Phys.B (proc. Suppl.) 158, 2006, 52

M. Ciobanu, A. Schüttauf, E. Cordier, N. Herrmann, K.D. Hildenbrand, Y.J. Kim, Y. Leifels, M. Marquardt, M.Kis, P.Koczon, M. Petrovici, J. Weinert, X. Zhang, will be published

Prototype of the fine-sampling electromagnetic calorimeter

G.Britvich, S.Chernichenko, Yu.Kharlov, V.Mochalov, P.Semenov, A.Soldatov, A.Soukhikh, M.Ukhanov, and V.Vasilchenko

Institute for High Energy Physics, Protvino, 142281 Russia

The electromagnetic calorimeter modules with fine sampling were constructed in IHEP. The module design were based on the electromagnetic calorimeter for the KOPIO experiment, with additional modification to the energy range of the CBM experiment. The modules were assembled from 380 alternating layers of lead and scintillator plates. Lead plates were doped by 3% of antomony to improve their rigidity. Scintillator plates were made of polysterene doped by 1.5% of paraterphenile. Scintillator was manufactured at the scintillator workshop of IHEP by the molding technology. Scintillation light was collected by the wave-length shifting fibers BCF-91A of diameter 1.2 mm. The fibers penetrated the modules in the longitudinal direction with the step of 9.3 mm forming the grid of 12×12 fibers per module. The physical properties of the modules are presented in the Table 1.

lead plate thickness	0.275 μm
scintillator plate thickness	1.5 mm
number of layers	380
effective radiation length, X_0	34 mm
total radiation length	$20X_0$
effective Moliere radius	59 mm
module size	$110 \times 110 \times 675$ mm^3
module weight	18 kg

Table 1: Physical properties of the module.

The matrix of 3×3 modules was manufactures and studied during the test beam run in December 2006. The scintillation light collected and re-emitted by the optical fibers was detected by the photomultipliers R5800 from Hamamatsu. The signal amplitude was measured by the 16-bit QDC. The matrix of modules was placed on the (x, y)-moving table controlled by a computer. The modules were exposed to a secondary beam of the beam line 2-B of the U70 accelerator in IHEP, Protvino. The beam had a mixed content of negative particles, mainly μ^-, π^- and e^- at momenta from 1 to 19 GeV/c. The electron component of the beam was used for the energy resolution measurements. The beam line 2-B (Fig.1) provided a beam particle tagging with a magnet spectrometer contained 4 drift chambers `DC1` – `DC4` and the dipole magnet `M` with a fixed bending angle of 55 mrad.

The modules were calibrated via exposing them to a 19-GeV/c beam. The best relative calibration coefficients were found by equalizing minimum ionizing particle (MIP) signals, while the absolute calibration was obtained by setting the total measured energy in the 3×3 matrix to 19 GeV. The measured energy spectrum in the ECAL prototype from the 19-GeV/c beam is illustrated by Fig.2 (left plot), the blow-up of the low energy range is shown on the right plot of this figure, where a clear MIP signal is seen.

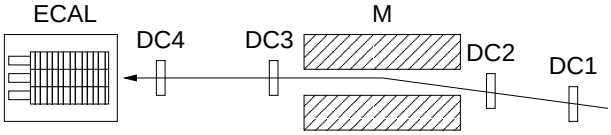

Figure 1: Experimental setup for ECAL modules studies.

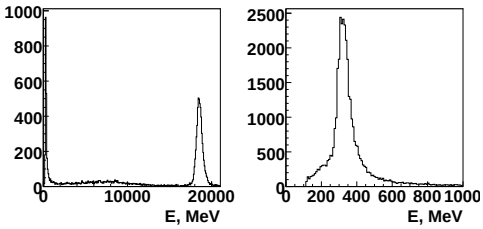

Figure 2: Measured energy from the 19-GeV/c beam.

After calibration, the ECAL prototype was exposed to beams at momenta 1, 2, 3.5, 5, 7, 10, 14 and 19 GeV/c, and the obtained energy resolutions at these energies are shown in Fig.3. The energy resolution of the fine-sampling calorimeter prototype is found to be extremely high compared to conventional sampling calorimeters, and, therefore, can be used for precise spectroscopy measurements of the neutral mesons and the photons.

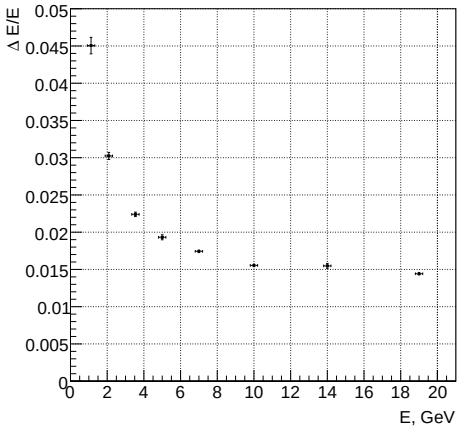

Figure 3: Measured energy resolution.

Simulation studies of calorimeter system. Preshower prototype. *

S. Belogurov[1], A. Golutvin[1], Y. Kharlov[2], S. Kiselev[1], D. Konstantinov[2], I. Korolko[1], V. Maiatski[1], K. Mikhailov[1], P. Polozov[1], M. Prokudin[1], G. Sharkov[1], and A. Stavinskiy[1]

[1]ITEP Moscow; [2]IHEP Protvino

Calorimeter software package in CBMROOT

A detailed simulation of a sampling calorimeter was developed within the standard CBM framework CBMROOT. To perform a detailed optimization of the calorimeter granularity the whole detector volume was divided in small 1×1 cm^2 stacks. This procedure allowed us to built a calorimeter with arbitrary transverse granularity at the hit producing stage with a single set of simulated with GEANT (FLUKA) events.

Standard algorithms for photon (electron) reconstruction were developed, tuned and tested. First of all we build simple 3×3 clusters around all hot calorimeter cells. On a next step we sum the energy depositions in the four hottest cluster cells applying a special energy and polar angle dependent calibration procedure to determine the momentum of incident particles. Finally we reconstruct the centre of gravity using the tabulated dependence of cluster asymmetry (in X and Y) as a function of $MC_{\rm truth}$ particle impact point. Energy asymmetry was determined as $A_X = (E_L - E_R)/E_{Tot}$ and $A_Y = (E_U - E_D)/E_{Tot}$. Algorithms for energy and impact point reconstruction were tuned for all possible calorimeter cell sizes.

Single-particle response

Using the software package described above we have studied the calorimeter response for single photons. The ECAL geometry from the CBM Technical Status Report was taken as a basic option for these simulations: sampling of the modules was 140 layers of 1 mm lead and 1 mm scintillator, the cell sizes were 3×3 cm^2, 6×6 cm^2, 12×12 cm^2. The stochastic term of the energy resolution was found to be 69 ± 2 MeV.

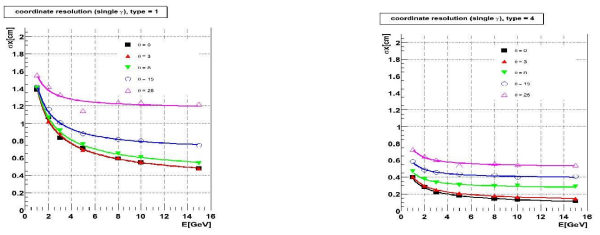

Figure 1: Spatial resolution in the CBMROOT simulation.

* Work supported by Federal agency of Russia for atomic energy, Federal agency of Russia for science and innovations and the Russian Foundation for Basic Research (grants 05-02-08096 and 06-08-01555) and by INTAS-05-111-4475, INTAS-05-111-5257, INTAS-03-54-6272.

The precision of impact point reconstruction was determined with the algorithm described in previous section. As a crosscheck we have developed a second algorithm which reconstructs the photon impact point coordinate through the first moment $x_{\rm rec} = \sum x_i w_i / \sum w_i$ where the sum is calculated over all cluster cells, x_i is the coordinate of the cell i, and w_i is the weight depending on the cell energy E_i and defined as $w_i = \max\left[0, w_0 + \log(E_i/E_{\rm tot})\right]$. The value of w_0 is obtained empirically to minimize the spatial resolution. Spatial resolution for different incident angles of incoming photons calculated for outer (12×12 cm^2, type 1) and inner (3×3 cm^2, type 4) cells is shown in Fig.1.

For inclined tracks the reconstructed position obtained with this procedure is systematically shifted. This shift, expressed as a difference between reconstructed coordinate $x_{\rm rec}$ and $MC_{\rm truth}$ coordinate, is proportional to the sinus of the incidence angle θ: $x_{\rm rec} - x_0 = t_{\rm eff} \sin\theta$. The slope $t_{\rm eff}$ is energy-dependent and can be interpreted as an effective shower depth in the calorimeter.

Energy reconstruction for different cells

The intrinsic energy resolution of the sampling calorimeter at CBM is considerably degraded by energy contributions from neighbor tracks. This effect depends obviously on calorimeter cell size. We performed a detailed study of photon reconstruction quality for all possible granularities of CBM calorimeter system.

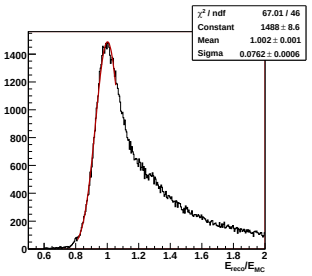

Figure 2: Reconstruction quality for 12×12 cm^2 cells.

Using the standard procedure we have reconstructed the energy of incoming photons and plotted the ratio E_{reco}/E_{MC}, which in ideal case should be a gaussian distribution with mean value 1.0. Energy contributions from neighbors result in a considerable right tail. The quality of γ reconstruction was defined as percentage of photons with E_{reco}/E_{MC} ratio lying within $\pm2\sigma$ around unity. Fig.2 demonstrates the reconstruction quality for low energy ($1 - 2$ GeV/c^2) photons hitting the outer region of

CBM calorimeter consisting of 12×12 cm^2 cells. Reconstruction quality degrades for larger cells, varying from 71% for 8×8 cm^2 cells to 49% 12×12 cm^2 cells.

Direct photons and their correlations

Measurement of photons (and reconstruction of π^0 and η mesons) with ECAL is important for realization of the CBM research program. Direct photons (i.e. not originating from decays) can be subdivided in prompt ones from initial hard processes with large p_t, photons from initial quark-gluon stage and from later hadronic interactions. Existing transport generators do not include direct photons [1]. Cross section for the main hadronic source (reactions $\pi\rho \rightarrow \pi\gamma$ and $\pi\pi \rightarrow \rho\gamma$) has been prepared by the ECAL group and implemented into the HSD transport code. Our estimations [1] have shown that with expected hight-intensity ion beams ($10^9/s$) the rate of prompt photons with $p_t > 2GeV/c$ would be $\sim 100/s$ for central $Au - Au$ collisions at $25AGeV$.

The momentum correlations of photons provide unique information on the reaction mechanism which is hardly accessible by all other means. The correlation strength parameter helps to determine the direct photon yield. The two-photon correlation function shown in Fig.3 was calculated with the source size parameter $r_0 = 5$ fm and different direct photon yields $d = N(\gamma_D)/N(\pi^0)$. The direct photons were generated according to the thermal-like momentum distribution $dN/dp \sim (p^2/E)\exp(-E/T_0)$ and mixed with 10^5 UrQMD events ($Au + Au$ at $25AGeV$). The two photon correlation function is a combination of the direct photon correlations ($R = 1 + \lambda \exp(-Q_{inv}^2 r_0^2)$) and residual correlations between photons from π^0 decays. For large values of direct photon fraction d one could observe a clear peak at small Q_{inv}. The height of this peak depends quadratically on parameter d. The height of the correlation function in $(\hbar/r_0 - m_{\pi_0})$ region of Q_{inv} depends on parameter d linearly and could be considered as an additional source of information on direct photon fraction.

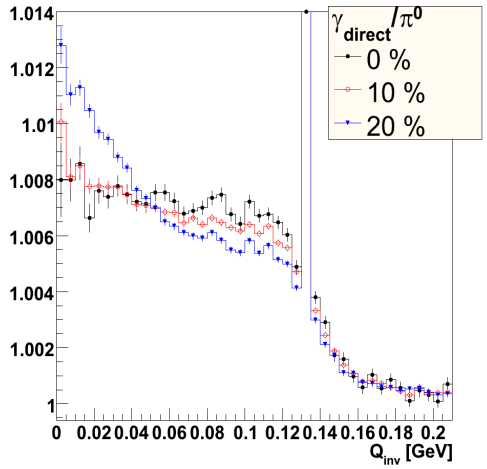

Figure 3: Two photon correlation function

Prototype of Preshower detector

Following the experience of ALICE TOF group [2] we have built and tested the prototype of CBM preshower detector based on scintillator-fiber system. Light registration was performed with Avalanche Photo-Diodes with Metal-Resistance-Semiconductor structure (MRS APDs) operated in the Geiger mode. These detectors were invented, designed and are currently produced in Moscow at Center of Perspective Technologies and Apparatus (CPTA) [3]. With moderate bias voltage of 50-60 V these detectors demonstrate intrinsic gain of up to 10^6. MRS APDs do not require special housing or fragile light transporting system and can be mounted directly inside scintillating plates, simplifying the construction of large detectors. Size of scintillating plates was set equal to $104 \times 104 \times 5$

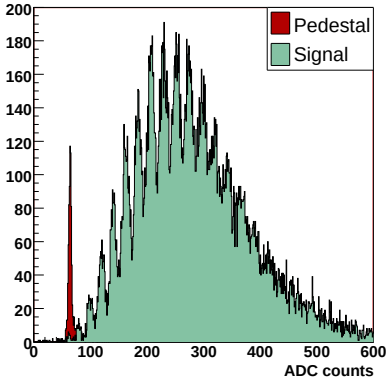

Figure 4: Amplitude spectrum from Preshower prototype.

mm^3 as dictated by ITEP beam test facility. Light collection inside plastic plate is performed by Kuraray Y11 wavelength-shifting (WLS) optical fiber (1mm in diameter) which was packed in narrow circular groove engraved on the plastic surface. One end of fiber piece is covered with reflecting foil, while the other is pressed to the sensitive surface of MRS APD. MRS APD signal amplification and control of bias voltage was done with special front-end electronic card. A typical amplitude distribution from minimum ionizing particles obtained during prototype beam tests is presented in Fig.4. A clear gap separates the trigger events from pedestals (particles missed the detector). An average light yield measured with 60 detectors equals 9-12 electrons/MIP. Increasing the thickness of scintillating tiles and filling fiber grooves with optical glue we would be able to increase the overall light output by factor 2.

References

[1] S.M. Kiselev, hep-ph/0701130

[2] A.Akindinov, G.Bondarenko, V.Golovin, et al. Nucl. Instr. And Meth. A539 (2005) 172.

[3] G.Bondarenko, V.Golovin, M.Tarasov, Patent for invention of Russia No. 2142175, 1999.

High resolution Projectile Spectator Detector

F. Guber[1], A. Ivashkin[1], A. Kurepin[1], A. Maevskaya[1], V. Katchanov[2]
[1]INR-Moscow, [2]IHEP-Protvino

The Projectile Spectator Detector (PSD) is meant to measure the number of non-interacting nucleons from a projectile nucleus in nucleus-nucleus collisions. This detector will be used at the CBM for the measurement of the collision centrality and for the study of event-by-event fluctuations to exclude the fluctuations of the number of participants. The PSD must have excellent energy resolution and transverse uniformity of this resolution. These requirements determined the choice of PSD as a full compensating modular lead-scintillator calorimeter. According to the experimental situation [1], [2], the expected energy resolution can reach $50\%/\sqrt{E(GeV)}$ with the constant term around zero. Calorimeter includes 12x9 array of the individual modules. The single module with front size 10x10 cm^2 consists of 60 lead/scintillator layers with the sampling ratio providing the compensating condition [3]. The readout scheme of PSD module ensures the longitudinal segmentation, good efficiency and uniformity of light collection. The light from WLS-fibers embedded in the round grooves in scintillator plates is readout by micropixel avalanche photodiodes, MAPDs coupled to the end of WLS-fiber. MAPDs [4] are avalanche photodiodes working in limited Geiger mode with the internal gain up to 10^6 and have no nuclear counting effect due to the pixel structure. The light from each 6 scintillator tiles is collected to one MAPD with active area 3x3 mm^2 and pixel density 10^4/mm^2. Such scheme provides independent signal readout from 10 longitudinal sections of a single module.

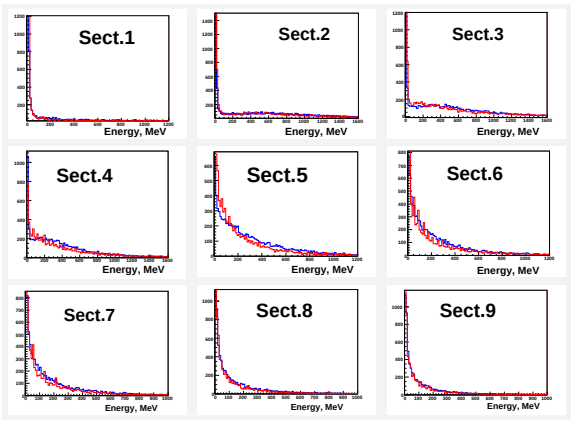

Figure 1: The energy spectra in different sections of PSD module. Red line - experimental distribution for 150 GeV pions, blue line - Monte Carlo simulation for 150 GeV pions.

In August, 2006 first beam test of PSD module prototype was performed in hadron beam at SPS, CERN. During the beam test the calibration of each readout channel was done with the muon beam. After the calibration, the energy deposition from the pions in each section was measured that reflects the longitudinal profile of the hadron shower. Fig. 1 presents the energy spectra in different sections of the PSD module. As seen, the shapes of the energy distributions are in good agreement with the MC predictions.

Fig. 2 shows the total deposited energy in the PSD module for a few beam energies. Here, the energy depositions in all sections were summed up with the appropriate normalization coefficients obtained from the calibration with muon beam. During the test the beam profile at the face of module had a definite spread that can be responsible for the slightly wider experimental distributions. The beam test reveals the reliable performance of the readout. To check the experimental energy resulution as the most crutical parameter of the calorimeter, the array of 9 modules is under construction now to be tested at hadron beam next year.

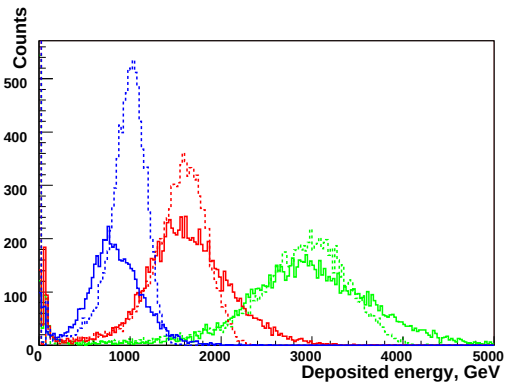

Figure 2: Summary spectra of deposited energies in PSD module for different pion beam energies. Solid line - experimental distributions, dashed line - MC predictions. Green lines - 150 GeV pion beam, red lines - 80 GeV, blue lines - 50 GeV.

References

[1] G.A. Alekseev et al., NIM A 461 (2001) 381-383.
[2] Y. Fujii, NIM A 453 (2000) 237-241.
[3] R. Wigmans, NIM A 259 (1987) 389-429.
[4] Z. Sadygov, NIM A 567 (2006) 70-73.

Towards high count rate, data driven Silicon strip readout electronics for CBM and other FAIR experiments*

C. J. Schmidt[1,2], K. Solvåg[1,3], G. Modzel[2], H. K. Soltveit[2], and S. Löchner[1]
[1]GSI, Darmstadt, Germany; [2]Phys. Inst., Heidelberg, Germany; [3]Inst. of Phys. and Techn., Bergen, Norway;

Introduction

CBM projects a large area multi station Silicon tracking station (STS) as one of its core detector systems. It will experience hit rates in the order of the ones targeted for LHC Silicon tracking systems. System- as well as physics-latencies impede the employment of complex tracking triggers like the one for open charm in a typical L1 trigger. No trigger information will be available in time to tag events of interest. Further, multi-event confluence in time must be considered typical rather than exceptional. This harsh environment not only poses tough demands on front-end detector and readout technology in terms of radiation hardness but also sets the stage to a novel, purely data driven readout architecture currently under development in the EU-FP6 project DETNI [1] targeting thermal neutron scattering applications [1]. Such asynchronous, non triggered, high rates and self sparsifying front-end readout architecture cast in Silicon as a microchip is the current choice to cope with the projected challenges. CBM and GSI closely cooperate with DETNI and engaged in evaluating the first DETNI prototype microchip n-XYTER at the GSI detector lab. These studies on the 128 channel chip will then allow the development of an adapted, radiation hard, dedicated CBM-XYTER chip for the CBM Silicon Tracker System. The good adaptation to Silicon strip detectors together with the non-specialized readout has generated great interest with several major FAIR projects that see in this architecture a promising choice to satisfy their particular needs.

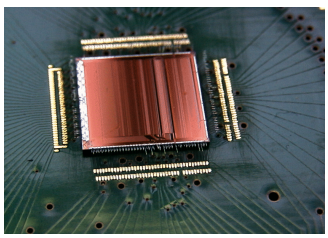

Figure 1: The n-XYTER chip

Data Driven Chip Architecture

The n-XYTER is a 128 channel front-end mixed-signal ASIC design. Each channel consists of a preamplifier and two parallel pulse shapers, a fast one for timing and a slow one for pulse height analysis. A discriminator on the fast channel will reset a peak detector on the slow channel in time that the signal height may be detected. Simultaneously it will trigger latching a time stamp with 1ns resolution that is used to tag the data. This asynchronous operation of the front-end together with the discriminator triggered data capture is termed in short as purely data driven front-end. For every channel, both, analogue pulse height and the digital time stamp, are then stored in FIFOs, where they will remain until readout. Data is read out of these FIFOs through a token ring structure, which will unprejudicedly read out whichever channel has data and skip non-hit channels. The chip is designed to be able to pump out data elements even at an average input rate of 32MHz, where momentary rates may statistically be fluctuating to even higher values. Each data element consists of a time stamp at 1ns resolution and an analogue pulse height to be digitized off chip.
The n-XYTER realization shows noise figures of between 850 and 1000 ENC on the fast channel (18 ns peaking time; depending upon polarity) at 30pF input capacitance, which is perfectly suited for MIP detection at standard Silicon thickness. The higher resolution slow channel with a peaking time of 140ns shows noise figures of about 600 ENC at 30pF input capacitance. The comparatively high capacitance targeted is at the expense of power. For the neutron application a non-issue, power is an important specification for a CBM version of the chip. A design to handle large capacitance specifications can either be used to handle longer strip detectors, otherwise it could be invested in long connecting wires from silicon to front-end allowing to remove necessary cooling infrastructure from within the detector.

Towards the CBM-XYTER

The n-XYTER is currently under careful investigation at the GSI detector lab. No flaws could be revealed so far. With the slow control operative, the architecture can now be explored in depth. After the current tests on isolated functionality, the chip will then be operated with an intelligent, more complex FPGA-based readout board. It will then finally be used to set up a Silicon strip detector test system. The analogue and digital tests as well as the detector system tests will be employed to formulate modifications that address the specific needs of CBM.

References

[1] NIM A, 568 (2006), 301-308

*Work supported by EU-FP6 HADRONPHYSICS (see Annex) and EU-FP6 NMI3 DETNI

[1]DETNI is a JRA of NMI-3 focussed upon neutron det. development

Development of a test system for n-XYTER ASICs

A. Czermak[1], P. Kuśmierski[2]
[1]Institute of Nuclear Physics (IFJ), PAN, Krakow, Poland; [2]Jagiellonian University, Krakow, Poland

We report on the progress at IFJ PAN with a readout system for comprehensive tests of the n-XYTER ASIC. The chip, developed by the DETNI Consortium and discussed in [1], will be used for prototype detector developments in the CBM experiment.

The SUCIMA DAQ board test system

The test system, which is based on the existing SUCIMA Imager Module [2], has been adapted to operate the chip and allows to perform a variety of laboratory measurements with the ASIC, eventually being connected to silicon detectors. A dedicated n-XYTER interface board has been designed that matches geometrically and electrically the SUCIMA data acquisition module. The SUCIMA board is shown in Fig. 1 mounted on top of an ASIC interface board carrying the 32-channel version of the 128-channel n-XYTER chip, called MSGCROC.

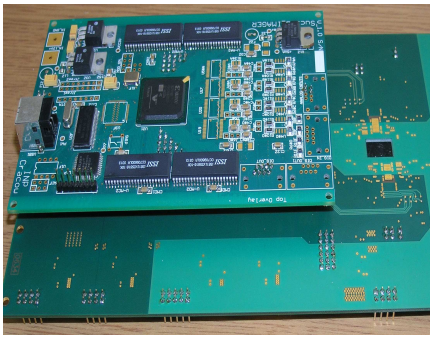

Figure 1: SUCIMA DAQ module on MSGCROC board.

First results from the MSGCROC chip

We have developed the VHDL programs for the basic FPGA logic on the DAQ board as well as the software for the Graphical User Interface. In collaboration with DETNI, the software has already been used for initial tests of the MSGCROC chip, including data storage, performance analysis and documentation of the test results. All measurements have been performed at nominal 3.3 V supply and nominal bias currents controlled by internal digital-to-analog converters. The internal bias reference currents, discrimination threshold voltage and various test modes in the ASIC are set via the SUCIMA board and the I^2C interface. Test results for trigger efficiency versus thresholds for different input charges are presented in Fig. 2, and pulse waveforms recorded at the output of the slow shaper (with gain set to 1) in Fig. 3.

The tests performed on the MSGCROC demonstrate correct functionality of all building blocks of the ASIC. The

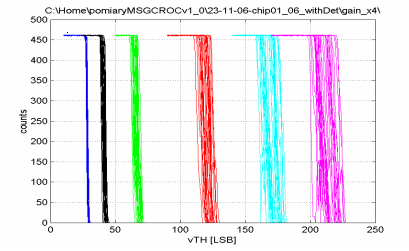

Figure 2: Trigger efficiencies (in arbitrary units) of all MGCROC channels for different test pulses, as a function of the adjusted threshold (in Volt).

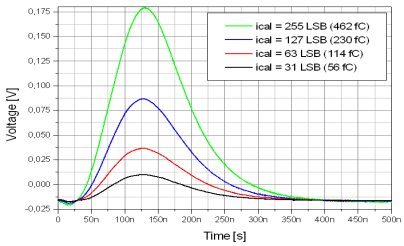

Figure 3: Pulse waveforms at the output of the slow shaper.

analogue parameters, i.e. gain, noise and also matching of these parameters are in agreement with the design specifications. The critical digital circuits responsible for data de-randomization and zero-suppressing token ring based readout have been tested at a lower clock frequency (64 MHz) than the nominal one (256 MHz). However, there are no indications that the ASIC should not perform correctly at higher clock frequencies.

Preparations for n-XYTER chip tests

In the near future, we will extend the test system to operate the 128-channel n-XYTER ASIC: Several interface boards have already been produced together with GSI. The Krakow group will populate these interface cards with components and will perform some initial tests. The boards will then be sent to GSI for mounting the n-XYTER chips. With the interface boards completed, both the n-XYTER designers and the SUCIMA DAQ team will work together on complete tests of the system and of the ASICs. Finally, two or three SUCIMA DAQ board based test systems will be available to interested CBM collaboration institutes, to explore the n-XYTER chip and its possible applications.

References

[1] Chr.J. Schmidt et al., this report

[2] A. Czermak et al., Proc. 8th ICATPP, Villa Olmo, Como, Italy, 6-10 October 2003.

Front End Electronic Building Blocks for CBM

T. Armbruster[1], M. Bruder[1], P. Fischer*[1], F. Giesen[1], V. Lindenstruth†[2], D. Muthers[3], I. Perić[1], D. Pietron[2], R. Tielert‡[3], and S. Tontisirin[3]

[1]University of Mannheim, Germany; [2]University of Heidelberg, Germany; [3]University of Kaiserlautern, Germany

Abstract

The CBM detectors require novel electronics for signal conditioning and data readout. A prototyping program has therefore been started to generate useful chip building blocks in the UMC $0.18\ \mu\mathrm{m}$ target technology. Examples of submitted structures are a fast ADC, clock/data recovery circuits, a content addressable memory, charge sensitive preamplifiers for micro strip detectors, a DAC and radiation hard circuits.

Introduction

CBM cannot use most of the Front End Electronics circuits which have been developed in the past for many particle physics experiments for two main reasons: The events at FAIR do not occur at well defined time intervals, and there will be no fast trigger to discard a large fraction of the data. All channels must therefore operate in a self-triggered mode. Time stamps must be added to all events. The data volume is very high due to a lack of the trigger. Various building blocks which will very likely be part of future designs have been designed and submitted in the chosen baseline technology, the UMC $0.18\,\mu\mathrm{m}$ CMOS process.

Design Overview

The most interesting designs are very briefly described here. For more information, please contact the authors.

Pipeline-ADC (Muthers, Tielert) The new iteration of the pipeline ADC family from Kaiserslautern features a high degree of flexibility in resolution, sampling rate and power dissipation. The chip has a serialized LVDS output and improved jitter performance. It is configurable between $10 - 12$ bits and offers a sampling rate of up to 100 MS/s. The measured power consumption is $34\,\mathrm{mW}$ at 12 bit when running at 50 MS/s.

Clock-Data Recovery (Tontisirin, Tielert) A clock and data recovery (CDR) circuit is required to provide a low jitter clock from the serial control data stream for the ADC and for time stamping. A 2-loop topology consisting of a clock data recovery and a clock jitter filter is used. The main CDR loop has an 1/4-rate phase frequency detector with wide frequency capture range and an intrinsic 1-to-4 data de-multiplexing. The clock jitter filter uses a low jitter LC-VCO with a small loop bandwidth. The two test chips operate at up to 2 Gb/s without the need for an external reference clock and off-chip loop component while dissipating $160\,\mathrm{mW}$. They deliver an output clock jitter of only $2.8\,\mathrm{ps\,(rms)}$. With an input ISI data jitter of $150\,\mathrm{ps\,(pp)}$, the output clock jitter is $4.6\,\mathrm{ps\,(rms)}$.

Charge Amplifier Prototypes (Armbruster, Pietron, Lindenstruth, Perić, Fischer) Low noise charge amplifiers are a central element for readout of silicon strip detectors and also for a possible backside readout of DEPFET sensors. Two designs have been worked out: The DEPFET backside readout (Pietron) evaluates different transistor layouts and their impact on noise and includes a synthesized digital block for time stamping. The CBM-XYTER test chip (Armbruster) focusses on the comparison of simulated vs. measured noise for various bandwidths and device sizes so that an optimal design (noise / power / speed) will be possible when detector parameters become known.

Content Addressable Memory Prototype (Giesen, Fischer) A content addressable memory is required for efficient address translation in the planned network communication system. The design has 512 entries of 2×18 bit. It uses a pipelined, low power architecture. The binary and ternary CAM cells have been measured to operate correctly at up to $300\,\mathrm{MHz}$ while consuming $40 - 80\,\mathrm{mA}$ (depending on the hit/miss pattern).

Radiation Hard Standard Cells (Bruder, Fischer) The modifications to the device extraction tool 'ASSURA' required to correctly recognize enclosed NMOS gates, as they are required for radiation hard design, have been implemented. Several normal and enclosed transistor test structures has been used for technology evaluation and for dc-modelling. A library containing the 14 most important digital cells has been layed out and the views required for automatic synthesis have been generated. Some simple digital designs haven been synthesized and routed automatically using this library. All designs are functional. This demonstrates that all tools for radiation hard chip design are now established.

12 Bit Current Mode DAC, IO Pads (Fischer) Some basic building blocks, like a 12 bit current mode DAC (LSB=$62\,\mathrm{nA}$, layout size $160 \times 200\,\mu\mathrm{m}^2$) and simple IO pads have been provided to the collaboration. The designs use separate supplies for analog and digital parts and triple wells for shielding. All designs have been submitted and their functionality has been verified successfully.

* peter.fischer@ti.uni-mannheim.de
† ti@kip.uni-heidelberg.de
‡ tielert@rhrk.uni-kl.de

Development of building blocks for data driven architecture for the CBM microstrip detectors

Eduard Atkin, Yuri Bocharov, Igor Ilyushchenko,
Alexander Klyuev, Alexey Silaev, Andrey Simakov, Alexander Smirnov
Department of Electronics, MEPhI

Alexander Voronin, Victor Ejov, Andrey Fedenko
SINP MSU

Derandomiser architecture building blocks

The analog derandomising architecture is expected to be a key one for CBM STS. For it therefore in 2006 there were designed and manufactured in the April 2006 run the several prototype blocks. Analog derandomizer block (4→2), the main idea of which was to develop a 4 channel fast analog FEE capable to process nanosecond signals deadtime-free by a fast cross-point switch and two output peak detectors.

ADC building blocks have been designed to study a set associative multiplex architecture. The technique is based upon a spatial locality of adjacent ionized strips. Among those there were: Op amp (fully differential folded cascode OTA with switch capacitor feedback) with: gain – 75 dB, unity GB – 145 MHz, SR – 160 V/μs, settling time – 1 ns, supply – 0,5 mA ; Sample-hold circuit, based on the OTA; Multiphase generator; Test radiation tolerant MOS structures.

A multipurpose test station for chips has been developed and used for lab tests.

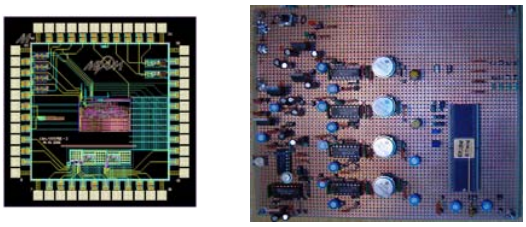

Fig.1 The derandomiser chip layout and the Test board with derandomiser chip

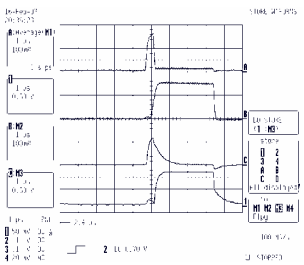

Fig.2 Response of the comparators and cross-point switch

The integrated charge sensitive amplifier

In the frames of the R&D work there has been developed and tested an integrated circuit of CSA as a critical block of front-end electronics, responsible for accurate matching of strip sensors of different pitch geometry (range of capacitances is up to 100pF) with read-out chain.

The charge-sensitive preamplifier schematics is based on a classical folded cascode architecture with an additional nonlinear feedback network. This solution allows to combine the well-known advantages of the charge preamplifier configuration in terms of gain stability with the possibility of detector leakage current compensation.

Specifications:

- Dynamic range of a few MIPs;
- Small signal – 7000 electrons per MIP;
- Detector (sensor) capacitance in the range 30-100 pF;
- Max capacitive load – 100 fF (on-chip load);
- Min load resistor – 10 kOhm;
- Low power consumption of about 1 mW/channel;
- Rise time (CSA output) – 10-200 ns;
- Signal-to-noise ratio better than 10 for 1 MIP;
- Number of channels – 8;
- Detector coupling:
  a) AC – capacitor is on the detector or
  b) DC – CSA built-in leakage current compensation
  It should be possible to read-out Si-strip signals in both AC- and DC- coupling modes without saturation. CSA should withstand a maximum sensor leakage (dark) current as high as 1 μA;
- Supply voltages – not more than ±3.3V (+1.8V typ.);
- Minimal package height or caseless;
- Minimal number of external components.

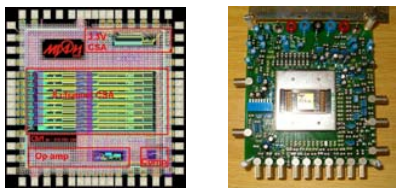

Fig.3 The CSA chip layout and the Test board with CSA chip

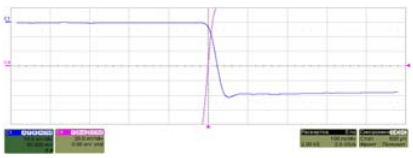

Fig.4 Response of the CSA

An ASIC based fast Preamplifier-Discriminator (PADI) for MRPCs *

M.Ciobanu[1,2], A.Schüttauf[1], E.Cordier[2], N.Herrmann[2], K.D.Hildenbrand[1], Y.J.Kim[1], M.Kiš[1], P.Koczon[1], Y.Leifels[1], X.Lopez[1], M.Marquardt[1], J.Weinert[1], and X.Zhang[1]

[1]GSI, Darmstadt, Germany; [2]Universität Heidelberg, Germany

The use of conventional integrated circuits to process primary RPC signals has reached its limit with designs like FOPI's 16 channel FEE5 [3]. To further reduce the price and power consumption per channel the natural way is a custom ASIC design. For this purpose the NINO architecture [1] used in the ALICE-ToF with its full differential structure offers a very attractive starting point for a new Preamplifier-Discriminator design.

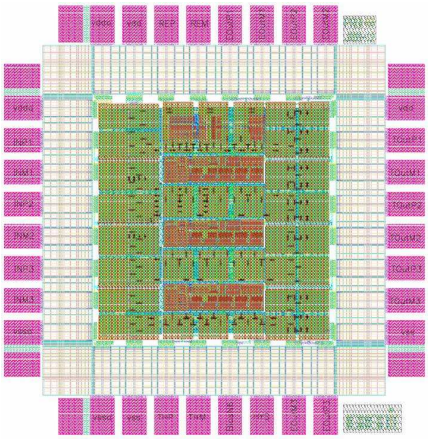

Figure 1: Asic Layout of the PADI chip with 3 channels

Taking into account the existing ideas of time measurements with fast gas detectors with up to 100000 channels within the CBM-detector at the FAIR-facility of GSI, we started to investigate, within the European project JRA-12, the development a new 4 channel PADI-ASIC in CMOS 0.18 μm technology. This chip has the following key parameters: fully differential, 50 Ω input impedance, LVDS compatible output, preamplifier gain G $\geq$ 200, preamplifier bandwidth $BW \geq$ 400 MHz, peaking time $t_P \leq$ 1ns, noise related to input $\sigma_n \leq 25\mu VRMS$, comparator gain $G \geq 200$, a DC feedback loop for offset and threshold stabilization and a threshold range related to the input of ΔU_{Thr} ~0.5-20 mV.

Based on these characteristics we designed a first version of the PADI-Chip (Fig. 1), with 3 channels in its first prototype. With the first delivered samples we have performed tests to check the basic functionality (connections, voltage, in/outputs of time and charge, thresholds). From these elementary tests we conclude that all channels are fully operational. Due to this very positive result we designed a PCB for the PADI-chip which is directly connected to our FOPI-digitizer TACQUILA3 [2].

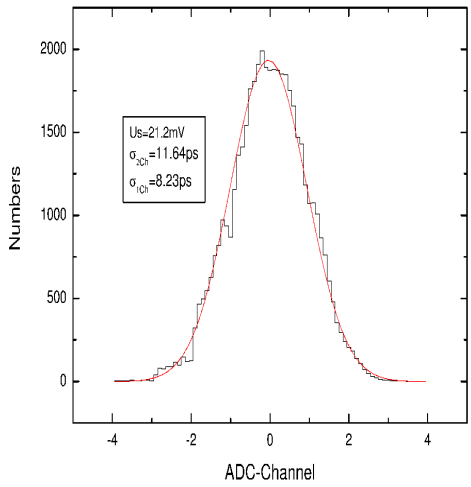

Figure 2: First timing measurement of the PADI-chip together with the TACQUILA-card. A time-resolution $\sigma_t \leq$ 10 ps has been reached for a single channel.

The combined setup (PADI-TACQUILA3) has a timing performance of $\sigma_t \leq$ 10 ps for pulser signals above 20 mV (see Fig 2.). In the following measurements we will map out the overall time resolution as a function of the amplitude. We will also compare time-over-threshold (ToT) to the direct charge measurement, to learn whether the ToT measurement is applicable for the walk correction.

References

[1] F.Anghinolfi, P.Jarron, A.N.Martemiyanov, E.Usenko, H.Wenninger, M.C.S.Williams and A.Zichichi
Nucl. Inst. and Methods A, Vol. 533, Issues 1-2, 1 November 2004, 183-187

[2] K.Koch, H.Hardel, R.Schulze, E.Badura and J.Hoffmann
IEEE Transactions on Nuclear Science, Vol. 52, No. 3, June 2005, 745-747

[3] M.Ciobanu [a,b], A.Schüttauf[a], E.Cordier[b], N.Herrmann[b], K.D.Hildenbrand[a],Y.J.Kim[a], Y.Leifels[a], M.Kis[a], P.Koczon[a], X.Lopez[a], M.Marquardt[a], M.Petrovici[c], J.Weinert[a],X.Zhang[a]
sub. to IEEE Transactions on Nuclear Science 2007

* work supported by JRA12 of EU/FP6 Hadronphysics (see annex), INTAS Ref.Nr. 03-54-3891 and German BMBF contract 06 HD190I.

PCI Express DMA Engine Design*

W. Gao[1], A. Kugel[1], R. Männer[1] and G. Marcus[1]
[1]Mannheim University, Germany

Abstract

DMA function is essential for the Active Buffer data transmission in CBM project. A DMA engine is developed on the PCI Express transaction layer and FPGA verification has been successfully done.

DMA Structure

The Active Buffer in the CBM experiment requires efficient data transmission between the host computer and the network. PCI Express is a good candidate for such applications [1]. For FPGA implementations, Xilinx Co. provides a logic core for the data link layer as well as the physical layer. [2] Accordingly a transaction layer DMA engine, 4 lanes, has been developed and well verified.

Virtual channel is the central idea to build such a DMA engine. In our design we use three channels (Figure 1), MRd, upstream DMA and downstream DMA. Although PCI Express has 15 types of TLPs, our design processes only 4 of them, MRd, MWr, CplD and Cpl. This sub-set of TLPs is the minimum requirement to do DMA as well as programmed I/O (PIO) transactions.

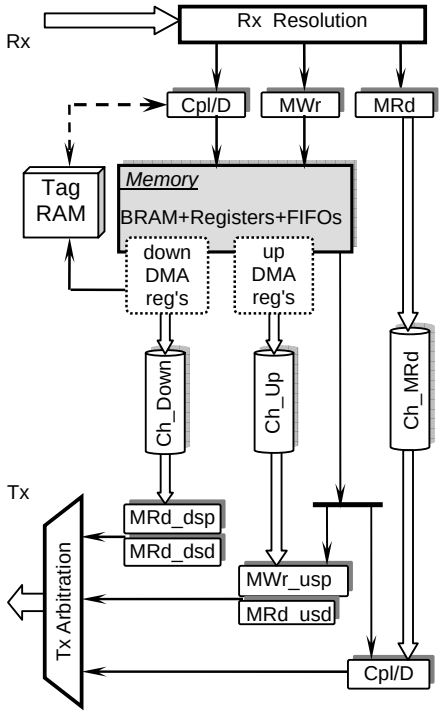

Figure 1: Block diagram of the top module.

There are 3 types of memories in this design, RAM (16kB), two FIFOs (each 32 DW in depth) and necessary registers. The two DMA channels can run parallel, which comes also out of the point-to-point advantage of PCI Express. Data in RAM and FIFOs can be accessed by DMA engine.

Concerning the property of PCI Express, reading operations are done in non-posted requests, identified by numbered tags (8 bits). So another block RAM is used for storage of tags information.

Incoming TLPs are directed into corresponding channels at the Rx port. At the Tx port, the output requests of different channels are arbitrated upon LRSF (least-recently-served-first) policy to obtain fairness and to avoid starvation.

DMA operation is managed in form of descriptors, which are a set of registers accessible to the upper-level applications. A DMA transfer is initiated by loading correct values into the necessary registers (source address, destination address, length, next descriptor address), and then, by writing a start command to the control register. Also, Busy/Done state is readable from registers in the DMA process.

Functional Verification

Fundamental system test with software has been done and expected functions are proved correct. Before the performance tests, strict simulation on the transaction layer has been done to find hidden bugs.

To do DMA simulation, a set of parameters are randomly chosen for every DMA transaction, including the address pair (host address and endpoint address), the byte count and the address for the next descriptor resident in the simulated host memory. Then, a downstream DMA is started; meanwhile the requested CplD TLPs are fed into the Rx port. After downstream DMA simulation is done, an upstream DMA of the mirrored set of parameters (source address and destination address exchanged) is started; meanwhile the outgoing MWr TLPs are checked at the Tx port and any error will be reported.

To do PIO simulation, an MWr TLP of random length is sent into the Rx port to a random address of the endpoint memory space, and then, an MRd TLP requesting the same combination of data (endpoint address and length) is sent. Afterwards, checking is done at the Tx port for CplD/Cpl TLP. If the outgoing data do not agree with the incoming ones, error is asserted.

These simulations continue running with the flow control signals also randomly given.

References

[1] PCI Express Base Specification. Rev. 1.0a
[2] Xilinx Co. LogiCORE™ PCI Express v3.3 User Guide. UG185. September 21, 2006

* Work supported by EU, FP6 HADRONPHYSICS.

Developments for a future DAQ framework DABC

J. Adamczewski[1], H.G. Essel[1], N. Kurz[1], and S. Linev[1]
[1]GSI, Darmstadt, Germany

Requirements and concept

The **D**ata **A**cquisition **B**ackbone **C**ore *DABC* will provide a general software framework for DAQ tasks over the next years. It serves as test bed for FAIR detector tests, readout components tests, data flow investigations (switched event building) and DAQ controls. Specifically, the system must be able to handle the large data bandwidth of experiments with self-triggered front-end electronics like CBM [1]. Additionally, it is necessary to integrate the current GSI standard data acquisition system MBS [2]. The huge installed MBS equipment cannot be replaced. Instead, MBS driven front-end components (readout) should be attachable as data sources to the new framework. The DABC replaces the MBS event building functionality.

The XDAQ C++ software framework [3] developed for the CMS experiment at CERN was chosen as base for the first implementation of DABC. It features:

Task management: One node may contain several *XDAQ Executives* (processes); each *Executive* may contain *XDAQ Applications* as threads. Each application may create additional threads (*workloops*).

Data transfer management: *Peer Transport* and *Messenger* interfaces.

Hardware integration: *Hardware Access Library*.

Control support: state machines; process variable *Infospaces*; message and error loggers; web server for each *Executive*.

Evaluation and testing

The developments so far concentrated on performance and functionality evaluations.

Data transport

Data transport on a fast switched network has been investigated on a small InfiniBand (IB) linux cluster installed at GSI in 2005. An XDAQ *Peer Transport* over IB was implemented based on the uDAPL library to check the performance of IB data transfer with the XDAQ I2O messaging mechanism. For package sizes $P \geq 15$ kByte the bandwidth B saturated at $\simeq 905$ MByte$/s$ to be compared with 955 MByte$/s$ for measurements with direct uDAPL. However, the rise of the $B(P)$ curve for small packages was less steep for the XDAQ transport, since this is ruled by the minimum transfer time τ_{min} ("latency" overhead of the framework), from $(\frac{dB}{dP})_{P\to 0} = \frac{1}{\tau_{min}}$. Depending on the benchmark set up, XDAQ showed values $\tau_{min} \simeq 10 \ldots 30$ μs, well exceeding the plain uDAPL latency of $\tau_{min} \simeq 4$ μs.

Hardware access

As general software interface to attach DAQ hardware like readout boards, XDAQ provides a *Hardware Access Library* package [3]. This defines base classes for user-space communication with boards on a bus (e.g. PCI or VME). We implemented HAL *BusAdapter* and *DeviceIdentifier* classes for a generic PCI/PCIe driver of the Mannheim FPGA group[1].

The new HAL classes were tested with the available GSI *PCIGTB2* board. It was possible to access the board from an XDAQ *Application*, setting up registers and reading/writing on the *PCIGTB2* internal memory. Although the tests showed that the general HAL interface is not sufficient for all cases, (e.g. DMA; exact i/o timing), it turned out that it is well possible to implement missing features as methods of the specific *HardwareDevice* class.

Control System

XDAQ offers a http server on each node to exchange control messages and monitoring data via SOAP protocol. We developed a simple prototype of a control GUI as JAVA application. However, every update of a monitored value requires an active http/SOAP request from the GUI.

An improved approach for monitoring consists in a "publisher-subscriber"-model, where each GUI registers to be updated automatically if a variable changes in the monitored application. DIM [4] is a well established protocol library for such a usage. We developed adapter classes to run a DIM server in the XDAQ *executive*. XDAQ infospace variables are exported as DIM services. Additionally, the XDAQ application state machine can be switched by DIM commands. The DIM server provides control access from any other DIM interfaced packages, like the Labview-DIM interface of the GSI CS-framework [5] for a test control GUI, or the EPICS DIM gateway currently under development at GSI (http://wiki.gsi.de/Epics).

References

[1] "CBM technical status report", GSI, January 2005, pp.235

[2] H.G. Essel and N. Kurz, "Multi Branch System homepage", http://daq.gsi.de

[3] J. Gutleber and L. Orsini, "XDAQ framework", http://xdaqwiki.cern.ch/index.php/Main_Page

[4] C. Gaspar, "Distribution Information Management system DIM", http://dim.web.cern.ch/dim/

[5] D. Beck and H.Brand, "The CS framework", https://sourceforge.net/projects/cs-framework/

[1]thanks to G. Marcus, H. Singpiel, and A. Kugel, Technische Informatik V, Universtät Mannheim

Infiniband cluster for Future DAQ

J. Adamczewski[1], H.G. Essel[1], and S. Linev[1]
[1]GSI, Darmstadt, Germany

Network requirements

The data acquisition for future experiments at FAIR requires a fast and relatively large network for event data transport from front-end electronics to the computing nodes where further event analysis can be performed. The CBM experiment, for example, produces about 1 TB/s of raw data rate, which should be switched in such event building network (B-Net). This requires to build a system with ∼1000 nodes, each connected to a network with 1 GB/s link performance.

Currently we are evaluating InfiniBand (IB) as probable candidate for B-Net in our first prototype of a Data Acquisition Backbone DABC (see in this report). A small test cluster of 4 nodes was installed at GSI in November 2005. Each node of that cluster is equipped with a Mellanox MHES18-XT InfiniBand Host Channel Adapter (HCA). The nominal data rate of such adapters is 1GB/s in full duplex mode.

InfiniBand software

All software required to configure and operate InfiniBand networks is collected in the OpenFabric Enterprise Distribution OFED (former OpenIB), developed by the OpenFabrics Alliance [1]. There are also software packages from hardware vendors (for instance IBGold from Mellanox), but mostly they contain the same components as the OFED package. Several user-level APIs were investigated and tested.

The low level **verbs API**, included in the OFED package as *libibverbs* library, provides direct access to InfiniBand HCA functionality from user space (so-called kernel bypass). It's most important functionality: non-blocking zero-copy data transfer, remote direct memory access (RDMA) and unreliable hardware multicast. Unfortunately, the **verbs API** is not well documented.

The user-level **direct access API (uDAPL)**, developed by the DAT collaborative [2] was inspired by IB functionality. Therefore it has many similarities with **verbs API**. Since **uDAPL** uses a peer-to-peer communication paradigm, multicast is not supported. There are several implementations of this APIs from different vendors, which are mostly compatible with each other.

Message passing interface (MPI) is widely used in the field of parallel computing. It defines an API for fast exchange of data between computing nodes. The MPI over InfiniBand Project - MVAPICH [3] provides non-blocking zero-copy data transfer, and in latest versions it even supports hardware IB multicast.

Benchmarking

A special test application was written to evaluate InfiniBand performance with all mentioned APIs. This test application is capable to generate different kinds of traffic patterns over InfiniBand. A time synchronization between nodes was implemented to perform time scheduled data transfers. Mostly the all-to-all traffic pattern was investigated, where each node transfers data to all other nodes according the round-robin schedule. The dependency of achieved data rates per node from packet size for different APIs is presented in table 1.

Buffer	1K	4K	16K	64K	256K
verbs	364	809	940	953	957
uDAPL	494	723	837	875	882
MPI	327	616	752	885	897

Table 1: Achieved data rates (in B/μs) in all-to-all tests

All APIs provide good performance and reach 900 B/μs for big packet sizes. While **verbs** has less API overhead, it reaches such data rate already at 8K buffer size.

Separately IB multicast was tested: **verbs** achieves 625 B/μs data rate with less than 0,01% packets lost; **MPI** only 350 B/μs, but this includes handshaking and retry when packets are lost.

Using a B-Net scheduled traffic pattern one achieves event building all-to-all traffic of 750 B/μs plus simultaneous transport multicast traffic from scheduler of 50 B/μs/node, and status traffic of 20 B/μs/node.

Future tests and developments

Our first tests show, that InfiniBand provides data rates as required for an event building network in future FAIR experiments. All investigated APIs potentially can be used in further developments of DAQ systems.

Because all our tests were performed on a small 4-nodes cluster, we cannot prove the scalability of our B-Net approach for systems with more than 100 nodes. Therefore further tests are planned in cooperation with the Forschungszentrum Karlsruhe, where several 32-nodes InfiniBand clusters are available.

References

[1] OpenFabrics Alliance website, http://www.openfabrics.org

[2] DAT Collaborative website, http://www.datcollaborative.org

[3] MPI over InfiniBand Project website, http://nowlab.cse.ohio-state.edu/projects/mpi-iba/

Workshops and Meetings 2006

- Muon Detection in the CBM Experiment, GSI, October 16-17, 2006
- 8th Collaboration Meeting, Strasbourg, September 20-22, 2006
- Symposium on the Physics of High Baryon Density, Strasbourg, September 19, 2006
- The Physics of High Baryon Density, held at ECT* Trento, 29 May - 2 June, 2006
- CBM Tracking Workshop, GSI, May 15 - 19, 2006
- CBM RICH Workshop, GSI, March 6-7, 2006
- 7th Collaboration Meeting, GSI, February 28 - March 3, 2006

CBM related publications 2006

- P. Senger, Compressed Baryonic Matter - Experiments at GSI and at FAIR, Proceedings of Helmholtz Summerschool on "Dense Matter In Heavy Ion Collisions and Astrophysics, August 2006, Dubna.
- P. Senger, The Compressed Baryonic Matter Experiment at FAIR, Proceedings of "Workshop Critical Point and the Onset of Deconfinement", Florence, July 3-6 2006.
- P. Senger, Strange particles and neutron stars - Experiments at GSI, Proceedings of "International Symposium on Heavy-Ion Physics", April 2-6, 2006, Frankfurt.
- J. Heuser et al., Development of a Silicon Tracking and Vertex detection System for the CBM Experiment at FAIR, Proceedings of the 15th International Workshop on Vertex Detectors (Vertex06), 25-29 September 2006, Perugia, Italy, to be published in Nucl. Instr. and Meth. A.
- C. Höhne, F. Rami, and P. Staszel, The Compressed Baryonic Matter experiment at FAIR, Nucl. Phys. News 16, 19 (2006).
- H. Essel, FutureDAQ for FAIR: On-line Event Selection, Proceedings of Computing in High Energy and Nuclear Physics, 13-17 February 2006, T.I.F.R. Mumbai, India, to be published.
- V. Friese, Strangeness and Charm in the CBM Experiment, Proceedings of Strangeness in Quark Matter 2006, Los Angeles, March 31, 2006, to be published in J. Phys. G.
- A.Kugler et al, "HADES@SIS100", Proceedings of XLIV International winter meeting on Nuclear Physics, Bormio 2006, Vol.125,p.282
- H.K. Soltveit, Preamplifier-shaper prototype for the Fast Transition Radiation Detector of the Compressed Baryonic Matter (CBM) experiment at FAIR, Proceedings of the 12th Workshop on Electronics for LHC and future Experiments, 25-29 September, 2006, Valencia, Spain
- R. Kotte et al., Testing timing RPC detectors at the Rossendorf electron linac ELBE, NIM A564 (2006) 155
- I. Kisel, Event reconstruction in the CBM experiment, NIM A566 (2006) 85
- A. Andronic, The TRD of the CBM experiment, NIM A563 (2006) 349
- V. Friese, The CBM experiment at GSI / FAIR, Nucl. Phys. A 774 (2006) 377
- J. Heuser et al., Requirements for the Silicon Tracking System of CBM, NIM A 568 (2006) 258
- H. Essel, FutureDAQ for CBM: On-line Event Selection, IEEE Trans. Nucl. Sci., vol. 53, no. 3, pp. 677-681
- S. Gorbunov and I. Kisel, Elastic net for standalone RICH ring Finding, NIM A559 (2006) 139

CBM Notes 2006

- S. Gorbunov, I. Kisel, Secondary Vertex Fit Based on the Kalman Filter, SOFT-note-2006-002
- L. Lopes et al., Ceramic high-rate timing RPCs, TOF-note-2006-001
- T. Galatyuk, J. Stroth, Strategies for Electron Pair Reconstruction in CBM PHYS-note-2006-001
- F. Guber et al., Very Forward Hadron Calorimeter for the CBM Experiment - Projectile Spectator Detector (PSD), PSD-note-2006-001
- S. Gorbunov, I. Kisel, Primary Vertex Fit Based on the Kalman Filter, SOFT-note-2006-001

List of CBM member institutions

- **Bergen**, Norway, **Department of Physics, University of Bergen**
- **Bhubaneswar**, India, **Institute of Physics**
- **Bucharest**, Romania, **National Institute for Physics and Nuclear Engineering**
- **Budapest**, Hungary, **Eötvös University**
- **Budapest**, Hungary, **KFKI**
- **Chandigarh**, India, **Department of Physics, Panjab University**
- **Coimbra**, Portugal, **LIP**
- **Darmstadt**, Germany, **GSI**
- **Dresden**, Germany, **FZD, Institut für Strahlenphysik**
- **Dubna**, Russia, **JINR-LHE**
- **Dubna**, Russia, **JINR-LPP**
- **Dubna**, Russia **JINR-LIT**
- **Frankfurt**, Germany, **Institut für Kernphysik, Universität Frankfurt**
- **Gatchina**, Russia, **PNPI**
- **Hefei**, China, **Department of Modern Physics, University of Science & Technology of China**
- **Heidelberg**, Germany, **Physikalisches Institut, Universität Heidelberg**
- **Heidelberg**, Germany, **Kirchhoff-Institut für Physik, Universität Heidelberg**
- **Kaiserslautern**, Germany, **Universität Kaiserslautern**
- **Katowice**, Poland, **University of Silesia**
- **Kharagpur**, India, **Department of Physics and Meteorology, Indian Institute of Technology**
- **Kolkata**, India, **High Energy Physics Division, Saha Institute of Nuclear Physics**
- **Kolkata**, India, **Variable Energy Cyclotron Centre**
- **Krakow**, Poland, **Jagiellonian University**
- **Kyiv**, Ukraine, **Taras Shevchenko National University of Kyiv**
- **Mannheim**, Germany, **Inst. of Computer Engineering, Universität Mannheim**
- **Moscow**, Russia, **Institute for Nuclear Research**
- **Moscow**, Russia, **ITEP**
- **Moscow**, Russia, **SINP, Moscow State University**
- **Moscow**, Russia, **Kurchatov Institute**
- **Moscow**, Russia, **MEPhi**
- **Münster**, Germany, **Institut für Kernphysik, Universität Münster**
- **Nikosia**, Cyprus, **Cyprus University**
- **Obninsk**, Russia, **Obninsk State University of Atomic Energy**
- **Prag**, Czech Republic, **Technical University**
- **Protvino**, Russia, **IHEP**
- **Pusan**, Korea, **Pusan National University**
- **Rez**, Czech Republic, **Czech Academy of Sciences**
- **Seoul**, Korea, **Korea University**
- **Split**, Croatia, **University of Split**
- **St. Petersburg**, Russia, **Khlopin Radium Institute (KRI)**
- **St. Petersburg**, Russia, **St. Petersburg State Polytechnic University**
- **Strasbourg**, France, **Institut Pluridisciplinaire Hubert Curien IN2P3-CNRS/ULP (IPHC)**
- **Varanasi**, India, **Department of Physics, Banaras Hindu University**
- **Warszawa**, Poland, **University, Nuclear Physics Division**
- **Wuhan**, China, **Institute of Particle Physics, Hua-zhong Normal University**
- **Zagreb**, Croatia, **Ruđjer Bošković Institute**

Contacts

CBM

Spokesperson:
Peter Senger *(p.senger@gsi.de)*

Technical coordinator:
Walter Müller *(w.f.j.mueller@gsi.de)*

Physics coordinator:
Volker Friese *(v.friese@gsi.de)*

Chairman of the Collaboration Board:
Mihai Petrovici *(mpetro@ifin.nipne.ro)*

Collaboration board

D. Röhrich, P.K. Sahu, M. Petrovici, F. Deak, G. Vesztergombi, M.M. Aggarwal, P. Fonte, J. Eschke, F. Dohrmann, A. Malakhov, V. Peshekhonov, V. Ivanov, J. Stroth, V. Samsonov, Jian Wu, N. Herrmann, V. Lindenstruth, R. Tielert, W. Zipper, A.K. Singh, Sukalyan Chattopadhyay, Subhasis Chattopadhyay, Z. Majka, I. Kadenko, R. Männer, A. Kurepin, A. Golutvin, M. Merkin, V. Manko, B. Bogdanovich, J. Wessels, H. Tsertos, V. Saveliev, V. Petracek, S. Sadovsky, In-Kwon Yoo, A. Kugler, Byungsik Hong, M. Dzelalija, Y. Murin, Y. Berdnikov, F. Rami, B.K. Singh, B. Sikora, Daicui Zhou, R.Caplar

Management board

Andrey Golutvin, Norbert Herrmann, Fouad Rami, Dieter Röhrich, Joachim Stroth, Johannes Wessels

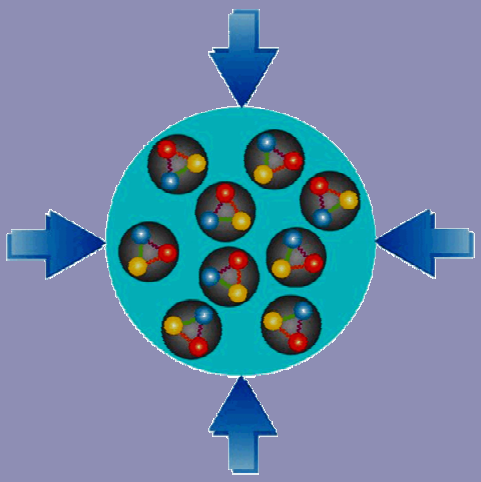

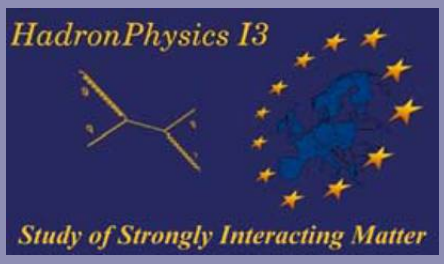

This work is supported by the EU Integrated Infrastructure Initiative Hadron-Physics Project (I3HP) under Contract number RII3-CT-2004-506078, by INTAS Ref. № 06-1000012-8729, -8778, -8781, -8810, -8914, and by the German Federal Ministry for Education and Research.